NTNU

Norwegian University of
Science and Technology

Study of Particle Resuspension by Impaction

Alexander Hammersgård

Norwegian University of Science and Technology
Department of Energy and Process Engineering

NTNU

Norwegian University
of Science and Technology

Department of Energy
and Process Engineering

EPT-M-2011-3

MASTER THESIS

for

Stud.techn. Alexander Hammersgård
Spring 2011

Study of Particle Resuspension by Impaction

Undersøkelse av partikkelmedrivning forårsaket av anslag

Background and objective.

Removal of microparticles from heat exchanger surfaces is important in heat recovery from waste gas processes. Particle build-up results in reduced heat transfer and increased pressure drop, cleaning of the surfaces are necessary. Passive cleaning without the use of external remedies can be accomplished by the flow aerodynamic (shear) forces and particle impaction forces.

Despite the practical significance of this, the particle removal mechanisms are still not well understood. This is partly because both the particle deposition processes and removal mechanisms may be are unique to a specific process and depends on many factors including particle size distribution, particle and heat transfer surface material, and flow and thermal conditions.

The overall goal of this study is to contribute to the improvement of the current level of knowledge of the particulate fouling and removal processes. Understanding these processes and mechanisms will aid in mitigating fouling during the design phase of heat exchangers and when it is in operation. This study will involve both analytical and numerical methods as well as experimental work.

The following questions shall be considered in this work:

1. Perform a literature study on particle removal by impaction on a solid wall or on already deposited particles. Available models shall be presented and discussed. Differences in the models shall be pointed out.
2. Based on the literature study, a model for particle impaction and possible rebound/removal shall be recommended for programming. Further, the recommended model shall be implemented into a suitable computer code. The model implementation, including all required sub-models shall be presented.
3. Calculations shall be performed using the programmed model on a set of operating conditions defined in cooperation with the Department. All required additional data and boundary conditions shall be described. The results shall be presented and discussed.

4. A test rig for the measurement of particulate fouling is under construction. The candidate shall participate in the calibration of the test rig and the initial experiments on the rig. All relevant experimental results shall be presented and discussed

5. Suggestions for further work shall be presented and discussed.

Within 14 days of receiving the written text on the master thesis, the candidate shall submit a research plan for his project to the department.

When the thesis is evaluated, emphasis is put on processing of the results, and that they are presented in tabular and/or graphic form in a clear manner, and that they are analyzed carefully.

The thesis should be formulated as a research report with summary both in English and Norwegian, conclusion, literature references, table of contents etc. During the preparation of the text, the candidate should make an effort to produce a well-structured and easily readable report. In order to ease the evaluation of the thesis, it is important that the cross-references are correct. In the making of the report, strong emphasis should be placed on both a thorough discussion of the results and an orderly presentation.

The candidate is requested to initiate and keep close contact with his/her academic supervisor(s) throughout the working period. The candidate must follow the rules and regulations of NTNU as well as passive directions given by the Department of Energy and Process Engineering.

Pursuant to "Regulations concerning the supplementary provisions to the technology study program/Master of Science" at NTNU §20, the Department reserves the permission to utilize all the results and data for teaching and research purposes as well as in future publications.

One – 1 complete original of the thesis shall be submitted to the authority that handed out the set subject. (A short summary including the author's name and the title of the thesis should also be submitted, for use as reference in journals (max. 1 page with double spacing)).
Two – 2 – copies of the thesis shall be submitted to the Department. Upon request, additional copies shall be submitted directly to research advisors/companies. A CD-ROM (Word format or corresponding) containing the thesis, and including the short summary, must also be submitted to the Department of Energy and Process Engineering

Department of Energy and Process Engineering, 15. February 2011

Olav Bolland
Department Head

Erling Næss
Academic Supervisor

Research Advisors:
Dr. Muyiwa Adaramola, post.doc, NTNU/EPT

ABSTRACT

This thesis discusses particle resuspension from surfaces caused by particle impaction. The thesis also focuses on particle transport and different transport mechanisms regarding different particle sizes. The transport mechanisms are important both for deposition and impaction, and thereby resuspension. An introductory to turbulent flows, which is important for particle transportation, is included. A comprehensive talk about particle-surface interface such as adhesion forces and elastic deformation is also given in the thesis. Regarding collisions theories, both qualitative and quantitative experiments and models will be presented, discussed and retested through a parameter study. Three models are selected among those presented, recommended for programming, and further implemented as MATLAB-scripts. These models cover a broad range of possible collisions; vertical, oblique and horizontal. A parameter study reviled the relative importance of different model parameters. The turbulent intensity was among the parameter studied.

Parallel to the literature survey and model programming, a test rig was build. The candidate participated in the startup period and did calibration experiments regarding the flow speed and flow rates at different fan speeds. In future studies a comprehensive particle fouling experiment will be carried out on this test rig. Suggestions to future studies are given at the end of the thesis.

SAMMENDRAG

(Norwegian abstract)

Denne oppgaven presenterer partikkel avrivning som følge av partikkel kollisjon. Oppgaven fokuserer også på partikkeltransport og ulike transportmekanismer for ulike partikkelstørrelser. Transportmekanismene er viktig for både avsetning og kollisjon, derav også medrivning. En introduksjon til turbulente strømninger, som er viktig for transport av partikler, er inkludert. En omfattende presentasjon om partikkel-vegg-kontakt om adhesjonkrefter og elastisk deformasjon vil også bli presentert i oppgaven. Vedrørende kollisjonsteorier, både kvalitative og kvantitative eksperimenter og modeller vil bli presentert, diskutert og retestet via en parameterstudie. Tre modeller er plukket ut blant de som er diskutert, foreslått for å programmeres og videre ble disse programmert i MATLAB-skripter. Disse tre modellene dekker et godt spekter av ulike kollisjoner; vertikale, vinklede og horisontale. En parameterstudie avdekker den relative betydningen av modellparametrene. Turbulent intensitet er en av disse parameterne.

Parallelt til litteraturstudiet og modellprogrammering, ble det bygget en test rig. Kandidaten deltok i oppstartsperioden av denne testriggen, hvor han gjorde kalibreringseksperimenter vedrørende strømningshastigheter og volumstrømninger for ulike viftehastigheter. Videre vil denne testriggen bli brukt til et omfattende foulingeksperiment. Forslag til videre arbeid er foreslått i slutten av oppgaven.

PREFACE

The work presented in this report is a result from the final semester of the Master of Science program within Energy and Environmental engineering at the Norwegian University of Science and Technology (NTNU). The work took place at the Department of Energy and Process Engineering and is one of two master theses dedicated to particle removal during the spring 2011.

The focus point in this thesis is particle removal by impaction. Existing theories, models and experimental results will be presented and discussed. An experimental part is presented in chapter 8. A wind tunnel, in which an upcoming fouling experiment is planned in the near time future, was calibrated.

A great thanks to professor Erling Næss and post.doc. Muyiwa Sam Adaramola for supervising me through this final semester. Weekly follow-ups, feed backs and constructive critique together with support and optimism have been very helpful during the semester. A special thanks to Fredrik Skaug Fadnes who is the author of the parallel master thesis, for each on-topic discussion which has given perspective and motivation to continuing the work. Last a great thanks to all friends and fellow students here at NTNU for many good times both inside and outside the Gløshaugen campus during these soon-to-end five years.

Trondheim 2011

Alexander Hammersgård

Contents

LIST OF FIGURES

LIST OF TABLES

Nomenclature

	Description	Unit	Introduced in equation
Roman letters			
A	Hamaker constant	J	(4.1)
a	Acceleration	m/s^2	(2.3)
a	Contact radius of particle	m	(4.6)
d	Diameter	m	
d_p	Particle diameter	m	
e	Coefficient of restitution		(5.16)
E	Young's modulus	Pa	(5.5)
F	Force	N	(2.3)
$\vec{g}$	Gravity constant	m/s^2	(2.5)
k	Thermal conductivity	W/mK	(2.8)
k	Turbulent kinetic energy	J	(2.26)
k_t , k_m	Mass transport coefficients	m/s	(3.1)
L_e	Separation distance		(4.1)
m	Mass	kg	(2.3)
$\dot{m}_d$	Mass deposition	kg/s	(3.1)
M	Moment	Nm	(5.36)
P	Pressure	Pa	(2.6)
R , r	Radius	m	(4.1)
R	Universal gas constant	J/kgK	(8.2)
S	Sticking probability		(5.1)
$t_{ejection}$	Ejection time	s	(5.34)
T	Temperature	K	(2.7)
T_{ij}	Total stress tensor	Pa	(2.30)
U , u	Velocity	m/s	(2.1)
u_τ	Friction velocity	m/s	
v	Poission ratio		(5.8)
V , v	Velocity	m/s	
V_d^+	Deposition velocity		(3.3)
W	Potential energy	J	(4.1)
Greek letters			
α, α_f	Relative approach, deformation	m	(5.4)
β	Diameter ratio, orifice plate		(8.3)

δ_{ij}	Kronecker delta		(2.26)
ε	Turbulent dissipation	m^2/s^3	(2.27)
θ	Velocity angle		(5.27)
η_{kol}	Kolmogorov's length scale	m	(3.6)
ρ	Density	kg/m^3	(2.4)
τ_{ij}	Stress tensor	Pa	(2.5)
τ_f	Relaxation time of eddy	s	(3.8)
τ_p	Relaxation time of particle	s	(3.9)
ϕ	Adhesion parameter		(5.2)
ϕ	Impaction angle		(5.27)
ϕ	Packing fraction		Model #3
μ	Dynamic viscosity	Ns/m^2	
υ	Kinematic viscosity	m^2/s	(2.6)
υ_T	Turbulent viscosity	m^2/s	(2.23)
σ	Surface energy	J/m^2	(4.5)
ω	Sensitivity		(7.1)

Non-dimensional symbols

Re	Reynold's number		
Sc	Schmidt number		(3.4)
St	Stokes number		(3.10)
R_f	Resuspension fraction		(5.56)

Symbols

$\rightarrow$	Vector		
'	Turbulent fluctuations		
$-$	Time averaging		Turbulence
+	Non dimensional		
c_p	Heat capacity	J/kgK	(2.8)
$\dfrac{\partial}{\partial x_j}, \dfrac{\partial}{\partial t}$	Spacial and time derivative	m^{-1}, s^{-1}	(2.6)
u^+	Nondimensional turbulent velocity	1	(2.34)
y^+	Wall coordinate/height	1	(2.34)
RMS	Root-mean-square		

1. INTRODUCTORY

1.1. BACKGROUND

Fouling of heat transfer equipment is an undesired problem because it reduces heat transfer and increases pressure drop. The metallurgical industry in Norway is a big consumer of electrical power, and huge energy savings are feasible by recycling waste gas from the melting furnaces. Unfortunately the waste gas contains dust of micrometrical size which deposit onto heat transfer surfaces. Eventually the layer of particles will insulate and thus reduce the heat transfer. The layer also adds roughness and shrinks flow area, and thereby increases the pressure drop too.

Cleaning of the equipment is therefore crucial to maximize heat recovery and minimize pressure losses. Experimental tests reveal that at some threshold velocity, the growth of particles is stopped and deposited particles removed from the surface. So called re-suspension is occurring until the surface is free of particle. The hypothesis is that particles let go of the surface whenever the local shear forces exceed the adhesion forces. Another hypothesis is that incoming particle which hits a deposited particle could set the target particle into motion. Which of these mechanisms dominate is still unknown, but both are dependent upon factors such as fluid velocity, turbulent intensity, material properties, fluid properties, temperature, temperature gradients, viscosity, impact angle and many others.

1.2. OBJECTIVES

Despite the experimental results, the actual mechanisms governing the deposition and removal are not well enough understood. Therefore the purpose of this study is to gain state of the art knowledge about particle resuspension by impaction. This knowledge will be helpful during the design phase of heat exchangers and during maintenance work of such equipment.

To obtain this knowledge the author will carry out a literature survey of existing models and theories. The reader will become familiar with the models, theories and the most importantly physics behind each model. Differences between the models will be pointed out. Based on this literature study the models, including all sub-models, will be implemented as suitable computer codes. The models should also be tested through a parameter study.

1.3. BUILDUP OF THIS THESIS

This thesis considers five main topics, all defined in the problem description. By systematically covering these points, the thesis covers the objectives defined in the previous chapter. Additional topics are also covered in the thesis, for instance an independent chapter about turbulence is included. The turbulence chapter is included because it gives a

physical description about the phenomena, which is helpful for both the reader and writer since almost all particle movement in flows is governed by turbulent forces. A discussion about what kind of fluid mechanisms that are capable of accelerate particles in other direction than the main stream, is given in chapter 3.5.

The thesis will also explain how different particle sizes are transported from the free stream and to the wall, and how they actually stick there. This is found in chapter 3.

In chapter 5 the literature study on particle impaction is summarized, and the literature study acts as the foundation for the rest of the thesis. Three different models are presented (chapter 5.5 and 5.7) and later implemented, and in addition more qualitative studied of particle impaction is given in chapter 5.2. Some of the results from the simulation study by Abd-Elhady are found in chapter 5.6, his model considers a single particle hitting a layer of particles and gives the threshold velocities associated with particle resuspension. Abd-Elhady's model was not implemented into MATLAB due to high computational time and the limited time set aside for this thesis.

Statistical turbulence is included in one of the implemented models, and a description of the procedure is given in chapter 5.7.3 together with the results.

The actual coding of the different models is presented in chapter 6, and the reader will find a parameter study in chapter 7. The parameter study covers point 3 in the problem description where it is written that calculations should be performed with a set of operating conditions defined by the Department. The results are discussed and analyzed through the sensitivity, which indicates *how important a certain parameter is regarding the threshold velocity.*

The experimental part of this work is reported in chapter 8. Here the reader will find a description of the wind tunnel-section and the results from the calibration work.

In chapter 9 to 10 a comprehensive discussion and conclusion for the whole work is given, and in chapter 11 possible further studies are suggested.

1.4. THE FOULING PROBLEM

In addition to being purely an academic challenge, there are consequences related to fouling which influence the economy for industrial facilities as well. For instance, worldwide fouling in general is responsible for 9.5 billion USD in increased operating expenses in oil refineries alone (Klaren D.G., 2005). Klaren's calculations are based on a crude oil price of 30 USD per barrel, and at the time of writing the crude is traded for 100 USD per barrel (June 2011). To quantify the global cost associated with fouling is difficult, if not impossible, but in Britain somewhere between 200 and 500 million pounds during 1978 is suggested in the literature (Temu, 1998). In 1978 Britain had a GDP of £$1.68 \cdot 10^{11}$ (Nationalmaster.com), in other words the fouling consumed 0,1-0,3% of the national GDP.

The technical consequences followed by fouling are reduced heat transfer and increased pressure drop. While the fouling layer builds up, the flow area decreases and triggers a higher flow velocity. The particles also add roughness which the fluid must overcome. Both increased velocity and friction cause increased pressure drop. The reduced heat transfer is caused by the insulating properties of the deposited layer.

There are environmental consequences too, such as increased CO_2 emissions. From the oil refineries described above, an increase of 88 million tons of CO_2 per annum is suggested as a reasonable number (Müller-Steinhagen, 2009),which is exactly the double of the total emissions caused by Norwegians onshore each year (Statistisk sentralbyrå & Klima- og forurensningsdirektoratet, 2010).

For these reasons the fouling problem has been a prioritized field of study ever since the mid 20th century. The goal is to reduce the impact of fouling and to control it. Totally removal of the problem is not possible because the driving forces behind the deposition and growth mechanisms are important in the processes themselves. For instance, it is not possible to remove oil from an oil refinery – but a lot of the fouling is a direct consequence of the presence of oil.

1.4.1. PARTICULATE FOULING

There are six major fouling categories and these are (Bott, 1994):

- Crystallization (e.g. calcium sulfate)
- Solidification (e.g. icing)
- Corroision
- Chemical (soot)
- Biological (e.g. bacteria and algae)
- Particulate

From these categories it is obvious that fouling is not strictly limited to industry alone. However, this thesis focuses on particulate fouling and resuspension. Particles are present in many types of industrial processes. Especially in metallurgical industries. From an alumina melting furnace, waste gas is recycled through heat exchangers because of its high temperature. Small alumina particles are transported to relative cold surfaces and will stick there, and if many particles repeat this sequence the fouling problem kicks in. How the particles are transported to the surfaces and why they stick will be described later.

The particles which cause these problems have sizes in the order of micrometers. But the particles have a wide size spread, from 1 μm to 50 μm. And different transport mechanisms are dominant for different sizes, e.g. the small particles are mainly transported by diffusion.

The results reported in this thesis however, are not limited to the metallurgical industry because particle resuspension is a phenomenon which is interesting for a many of topics; handling of toxic powders, exhaust and soot from all types of combustion engines, transmission of human bacteria, virus and diseases, and radioactive material. In 2011 a big earthquake outside Japan measuring 9 on the Richter scale ended with a tsunami which caused a blackout at a nuclear reactor onshore, witnessed that radioactive particles are a threat. After severe nuclear accidents, deposited radioactive material could resuspend from the primary cooling-circuit (Biasi et al., 2001). The difference between particlulate fouling in heat exchangers and nuclear reactor, is that resuspension is not wishful in the latter. And if resuspension is occurring it should be possible to predict the amount of released particles. Biasi et.al. (2001) wanted to highlight this issue, and they improved a existing resuspension models. Their work unfortunately did not include particle impaction, only removal by hydrodynamic forces, and is therefore not a very interesting report for this thesis. However, the reader should note that particulate fouling and resuspension is very important for many industrial and non-industrial topics indeed, and that knowledge about particle resuspension could be life- and environmentally important.

2. FLUID DYNAMICS AND HEAT TRANSFER

Before diving into the fouling issue in full, a description about the background physics for all heat exchangers and flow systems is in order. This chapter highlights the basics in fluid dynamics and heat transfer. Since an important part of fluid flows and heat transfer situations are turbulent, an introductory for turbulence is available in 2.2. Turbulence is a phenomenon which will be highlighted throughout this thesis, and the reader is advised to read this section carefully. There is also a "further reading"-section at the end of this chapter, and here you will find recommended literature for the different topics presented.

2.1. CONSERVATION EQUATIONS

Particles inside a fluid can deposit onto any surrounding surface, for instance a cylinder which crosses the flow. This is a well known situation in shell-and-tube heat exchangers. The suspended particles will follow the flow and be carried in whatever direction the fluid wish to go. It is obvious then, that fluid dynamics is important to the deposition process. The same argumentation can be used for particle collision.

So in the following text, the fundamental conservation equations in fluid dynamics and heat transfer will be presented.

2.1.1. CONSERVATION OF MASS

Velocities in heat exchangers are rarely high, therefore incompressible flow is a justified assumption. As long as the mach number is low (<0,3), the fluid will be incompressible. The conservation of mass is then given by

$$\nabla \vec{U} = 0 \tag{2.1}$$

or written in index notation

$$\frac{dU_j}{dx_j} = 0 \tag{2.2}$$

The conservation of mass is also known as *the continuity equation.*

5

2.1.2. CONSERVATION OF LINEAR MOMENTUM

This conservation equation is based on Newton's second law of motion

$$\vec{F} = m\vec{a} \qquad (2.3)$$

If the fluid is divided into cells of very small sizes, the mass is replaced by density. By acknowledging that the acceleration is the time derivative of velocity, one can rewrite eq. (2.3) to

$$\vec{F} = \rho \frac{D\vec{U}}{Dt} \qquad (2.4)$$

Where the left hand side is the sum of all body and surface forces, i.e. gravity, pressure and stresses for the most part.

$$\vec{F} = \rho \vec{g} + \nabla \vec{\tau}_{ij} \qquad (2.5)$$

In eq. (2.5) pressure is hidden inside the last term as a stress force. By further assuming that the density varies moderately with temperature and that the viscosity is constant, combining eq. (2.4) and (2.5) gives in index notation

$$\frac{\partial U_i}{\partial t} + U_j \frac{\partial U_i}{\partial x_j} = g_i - \frac{1}{\rho} \frac{\partial P}{\partial x_j} + \upsilon \frac{\partial}{\partial x_j} \left(\frac{\partial U_i}{\partial x_j} + \frac{\partial U_j}{\partial x_i} \right) \qquad (2.6)$$

Eq. (2.6) is better known as the Navier-Stokes equations. Note that this is actually three equation, one for each velocity direction, i.e. i=1,2,3.

2.1.3. CONSERVATION OF ENERGY

The conservation of energy is based upon that the change of energy inside a system (often called a control volume) which is the sum of work from external forces towards the system and heat which enters the system. When considering heat transfer only, and neglecting work, the conservation of energy can be written in its short form as

$$\rho c_p \frac{DT}{Dt} = k\nabla^2 T \qquad (2.7)$$

Constant thermal conductivity and incompressible flow are among the assumptions made in the derivation of eq. (2.7). The equation can be written out in a more neat index notation as

$$\frac{\partial T}{\partial t} + U_j \frac{\partial T}{\partial x_j} = \frac{k}{\rho c_p} \frac{\partial^2 T}{\partial x_j^2} \qquad (2.8)$$

The reader may recognize the physical constant in front of the last term as the thermal diffusivity.

2.2. TURBULENCE

Basic understanding about turbulence is important to understand how and why particles move once they are inside the fluid. Turbulent theory is complex, this chapter will only highlight the most important feature of the flow phenomena. In the literature though, which is full of details regarding turbulence, the reader may find more useful information which is left out here. See the further reading list at the end of this chapter for recommended literature.

Knowledge about turbulence is not limited to particle deposition and removal, or to fluid flow in a heat exchanger. Actually most flows in nature and industry applications are turbulent. For example the Gulf stream which carries warm tropical water to the western shores of Europe, could be characterized as a turbulent jet. A turbulent jet is a beam of fluid entering a relative calm fluid.

2.2.1. DEFINITION

The word *turbulence* is widely accepted as a word describing something irregular, unstable and unpredictable. The Oxford dictionary defines turbulence as "violent or unsteady movement of air or water, or some other fluid". The word turbulent indicate turbulence, and Webster's dictionary defines turbulent as "being in violent, agitation or commotion".

But these definitions are too general and insufficient for engineering purposes. In (Hinze, 1975) a more special definition about turbulence regarding fluid motion is given: "Turbulent fluid motion is an irregular condition of flow in which the various quantities show a random variation with time and space coordinates, so that statistically distinct average values can be discerned."

figure 1 illustrates the difference between a laminar and turbulent flow.
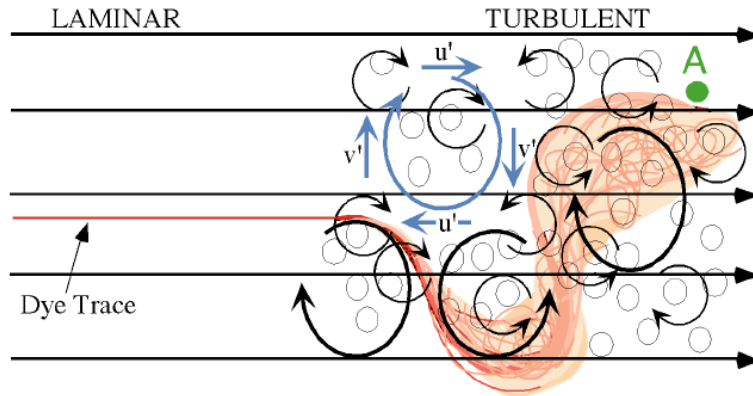
FIGURE 1-ILLUSTRATION OF A TURBULENT FLOW(MIT OPEN COURSEWARE, 2008)

To the left the flow is laminar and all streamlines are smooth and parallel. To the right the turbulent motion is governing the flow. The red line could represent a mass or particle beam, and this beam hits a big eddy and is forced downwards, at the same time a smaller eddy is forcing the beam upwards. The result is a split up of the beam and thus a good illustration of the diffusive nature of turbulence. (MIT open courseware, 2008)

It is hard to give a more exact definition because turbulence is indeed random both in time and space. But the definition by Hinze (1975) is useful because it gives a keyword about what to look for when doing analysis of turbulent flows: average values.

Time variation is hard to handle and makes the situation difficult to follow by any observer, therefore time integration of instantaneous values are the pathway to be able to give a description of a turbulent flow. Although the time variation is lost, the space variation is intact. This procedure is the basis for most CFD codes, and this trick will be used to find turbulent conservations equations.

2.2.2. TURBULENT CHARACTERISTICS

There are some characteristics which are unique and common to all turbulent flows. The mathematics are left out in this section, a more mathematical description of turbulence will follow right after this subchapter.

TABLE 1-TURBULENT CHARACTERISTICS (TENNEKES AND LUMLEY, 1972)

Turbulence is irregular	An exact mathematical description of local variables such as velocity, density, temperature or shear stresses, is not possible. Statistical description (e.g. time averaged) is the most reliable procedure to quantify the variables.
Turbulence is	Turbulence cause rapid mixing of momentum, heat and spicies. This is the reason that turbulent combustion is much more efficient than non-

8

diffusive	turbulent combustion; the fuel and oxygen are mixed and a complete combustion easier. The diffusive nature of turbulence is also important when considering heat transfer since turbulence will increase the advection. This diffusive nature will also distribute particles throughout for instance a channel section.
Turbulence is 3 dimensional	Due to the irregularity it is not possible to have a 2D flow which is turbulent. Turbulence is characterized by high levels of fluctuations and vorticity. It can be shown through the Navier-Stokes equations that the vorticity will decrease if the third dimension is absent. The reason is that the Vortex-stretching mechanism, which maintains the vorticity, is absent in 2D flows. To show this you will need to take the curl of the NS-equations and introduce the vorticity, which is given by the curl of the velocity. This exercise is given in Appendix 2 – Vortex stretching.
Turbulence has Reynolds numbers	Turbulence exists when the viscous forces are unable to dampen any randomness in the fluid. That is when the laminar flows become unstable. Small random fluctuations will grow and cause bigger, unpredictable fluctuations through the nonlinear terms in the Navier-Stokes equations. The Reynolds number represents the balance between inertia and viscous forces, and at high Reynolds numbers the viscous forces are suppressed compared to the inertia term. There is not a clear limit between laminar and turbulent flow, there are overlaps and transitional regimes where the flow is neither turbulent nor laminar.
Turbulence is dissipative	Without energy supply the turbulence will vanish. To illustrate this, imagine a stirred cup of coffee. In time the turbulence will die out, or, to put in a more technical, the turbulent energy will dissipate. The energy is lost from the turbulence and transformed into heat by viscous shear forces. The viscosity perform a deformation work upon very small fluid elements and eventually there is not enough turbulent energy to supply the random motions and vortexes, hence the turbulence vanishes.
Turbulence is continuous	The smallest scales in turbulence are big compared to molecular length scales. The relation between the mean free path and the Kolmogorov length scale, which is the smallest length scale regarding the turbulence itself, equals the Mach-number to the firth root of the Reynolds number, or

$$\frac{\text{mean free path}}{\text{kolmogorov}} = \frac{M}{\text{Re}^{1/4}}$$

	This relation is also known as the Knudsen number.
	The fact that turbulence is continuous is fortunate because then the Navier-stokes equations may be used without any modification.
	The turbulent time scales are also big compared to molecular collision time.
Turbulence is a flow condition	Sounds obvious, but all turbulence is a state of the flow. Turbulence is not a fluid property.

2.2.3. MATHEMATICAL DESCRIPTION

Description of turbulence is done through the Reynolds's decomposition. In words this means to set any instantaneous value (temperature, velocity, density, viscosity, conductivity etc.) equal to the average plus some fluctuating component, or

$$\xi = \bar{\xi} + \xi' \tag{2.9}$$

where the overbar is the average and 'dot' is the fluctuating part. None simplifications are done up to this point, an unknown value is only replaced by the sum of two other unknowns. Further the right hand side of equation (2.9) will be exploited.

A closer look at the properties of the decomposition is in order Let's take the (time-) average of eq. (2.9) and see what happens

$$\overline{\xi} = \overline{\bar{\xi} + \xi'} = \overline{\bar{\xi}} + \overline{\xi'} \tag{2.10}$$

Recognizing that "the average of an averaged value is the average itself", it is concluded that

$$\overline{\xi'} = 0 \tag{2.11}$$

Equation (2.11) is an important result, and will be used widely when deriving the turbulent conservation equations.

2.2.4. TURBULENT CONTINUITY EQUATION

Previously the conservation of mass and linear momentum equations were presented, now equation (2.9) will be introduced in these equations to see how the conservation equations behave for turbulent flows.

Inserting the Reynolds decomposition into the continuity equation, (2.2), gives

$$\frac{d}{dx_j}\left(\overline{u_j} + u_j'\right) = 0 \tag{2.12}$$

Taking the time average of (2.12) gives

$$\overline{\frac{d}{dx_j}\left(\overline{u_j} + u_j'\right)} = \frac{d}{dx_j}\left(\overline{\overline{u_j} + u_j'}\right) = 0 \tag{2.13}$$

By using equation (2.10) and (2.11) results in

$$\frac{d}{dx_j}\left(\overline{u_j}\right) = 0 \tag{2.14}$$

At first glance this result is probably not very interesting. The reason? Let's assume that there is no turbulence, i.e. the fluctuating component is zero, then equation (2.14) equals the continuity equation, (2.2). But, by subtracting equation (2.14) from equation (2.12), a rather unpredicted results pop

$$\frac{d}{dx_j}\left(u_j'\right) = 0 \tag{2.15}$$

It seems that the fluctuation *itself* respects the continuity equation. Physically this makes sense; luckily it is not hard to show this through the continuity equation.

2.2.5. RANS

RANS is short for Reynold's Average Navier-Stokes. This equation is derived by inserting a turbulent fluctuating component into the Navier-Stokes equation. The derivation will be presented here in short.

After inserting, the N-S-equation looks like

$$\frac{\partial(u_i + u_i')}{\partial t} + (u_j + u_j')\frac{\partial(u_i + u_i')}{\partial x_j} = -\frac{1}{\rho}\frac{\partial(\overline{P} + P')}{\partial x_j} + \upsilon\frac{\partial}{\partial x_j}\left(\frac{\partial(u_i + u_i')}{\partial x_j} + \frac{\partial(u_j + u_j')}{\partial x_i}\right) \tag{2.16}$$

11

The velocity may be put inside of the second term without changing the mathematics; this is justified through the continuity

And by introducing the shear

$$\tau_{ij} = \mu\left(\frac{\partial u_i}{\partial x_j} + \frac{\partial u_j}{\partial x_i}\right) \tag{2.17}$$

Equation (2.16) may be rewritten as

$$\rho\frac{\partial(u_i + u_i^{'})}{\partial t} + \rho\frac{\partial(u_j u_i + u_j u_i^{'} + u_i u_j^{'} + u_j^{'} u_i^{'})}{\partial x_j} = -\frac{\partial(\overline{P} + P^{'})}{\partial x_j} + \frac{\partial}{\partial x_j}\left(\overline{\tau_{ij}} + \tau_{ij}^{'}\right) \tag{2.18}$$

Taking the (time-) average of this, use eq. (2.11) for whatever its worth and assuming that the density can be moved inside the derivation hence it is a constant, the RANS-equation is derived

$$\frac{\partial}{\partial t}(\rho\overline{u_i}) + \frac{\partial}{\partial x_j}(\rho\overline{u_j u_i}) = -\frac{\partial\overline{P}}{\partial x_j} + \frac{\partial}{\partial x_j}\left(\overline{\tau_{ij}} - \rho\overline{u_j^{'} u_i^{'}}\right) \tag{2.19}$$

Which doesn't look very different from equation (2.6). But a completely new term has entered; The $\overline{u_j^{'} u_i^{'}}$ is known as the Reynold stresses and plays an important role in the turbulent momentum conservation equation. The problem is that nothing is known about the term other than it *acts* as a stress tensor and that it originates from the turbulence.

The new term is in other words just a new unknown in the set of equations, and there is no obvious correlation for it. This is known as the closure problem in turbulence.

2.2.6. TURBULENT HEAT TRANSFER

By doing the same exercise with equation (2.8) and replacing the instantaneous temperature with the average plus the fluctuating part, gives

$$\frac{\partial\overline{T} + T^{'}}{\partial t} + \frac{\partial(\overline{u_j} + u_j^{'})(\overline{T} + T^{'})}{\partial x_j} = \frac{k}{\rho c_p}\frac{\partial^2(\overline{T} + T^{'})}{\partial x_j^2} \tag{2.20}$$

Rearranging and taking the average, reduces equation (2.20) to

$$\frac{\partial\overline{T}}{\partial t} + \overline{u_j}\frac{\partial\overline{T}}{\partial x_j} = \frac{\partial}{\partial x_j}\left(\frac{k}{\rho c_p}\frac{\partial\overline{T}}{\partial x_j} - \overline{u_j^{'} T^{'}}\right) \tag{2.21}$$

The similarity between eq. (2.19) and (2.21) is the new term which comes from the fluctuating nature of the turbulence. $\overline{u_j'T'}$ appears as an additional heat flux caused by turbulence.

2.2.7. THE CLOSURE PROBLEM

Two new terms entered the conservation equations; $\overline{u_j'u_i'}$ in RANS and $\overline{u_j'T_i'}$ in the energy equation. How these should be modeled has been a discussed problem throughout the last century. Many models have been presented with varying accuracy. This is known as the closure problem of turbulence.

2.2.8. TURBULENT MODELING

It is not obvious how to model the Reynolds stresses, but a useful example is to look at a turbulent jet. The x-momentum equation for a turbulent jet is described by equation (2.22). A few assumptions are needed and equation (2.19) can be rewritten into (2.22). See (Tennekes and Lumley, 1972) for further details.

$$\overline{u}\frac{\partial \overline{u}}{\partial x} + \overline{v}\frac{\partial \overline{u}}{\partial y} = -\frac{\partial (\overline{u'v'})}{\partial y}$$

(2.22)

This equation gives some pinpoints for what to expect of the Reynolds stresses; the original idea was to define a turbulent viscosity (often called eddy viscosity) which related the stresses to the mean velocity (Andersson, 1988)

$$-\rho\overline{u'v'} = \rho\upsilon_T\frac{\partial \overline{u}}{\partial y}$$

(2.23)

Which gives

$$\overline{u}\frac{\partial \overline{u}}{\partial x} + \overline{v}\frac{\partial \overline{u}}{\partial y} = \frac{\partial}{\partial y}\left(\upsilon_T\frac{\partial \overline{u}}{\partial y}\right)$$

(2.24)

The next question is what the eddy viscosity is, and how it behaves. First of all, the eddy viscosity is not a fluid property but a flow variable related to the turbulence, and it varies in time and space. In 1877 Bossinesq assumed that the eddy viscosity could be a constant value, a rather primitive assumption since it only reduces a turbulent problem to a problem which is mathematically equivalent to a laminar one. It also gives a constant quantitative value to the turbulence, which of course is completely out of touch.

In equation (2.22) only one of the Reynolds stresses appears. However the Reynolds stresses, $\overline{u_j'u_i'}$, have a total of nine components in a 3D-flow, and as discussed previously all turbulent flows are 3D. These components are

$$
\begin{array}{ccc}
\overline{u'u'} & \overline{v'u'} & \overline{w'u'} \\
\overline{u'v'} & \overline{v'v'} & \overline{w'v'} \\
\overline{u'w'} & \overline{v'w'} & \overline{w'w'}
\end{array}
\tag{2.25}
$$

The further idea is to relate each of these stresses to some average velocity just the way it is done in (2.23). Bossinesq did this

$$
\overline{u_i'u_j'} = -\upsilon_T \left(\frac{\partial \overline{u_i}}{\partial x_j} + \frac{\partial \overline{u_j}}{\partial x_i} \right) + \frac{2}{3}\delta_{ij}k
\tag{2.26}
$$

Where $\delta_{ij} = 1$ if $j = i$ and zero for all others, $k = 0.5\overline{u_i'u_i'}$ is the turbulent kinetic energy.

But still the Reynolds stresses is an unclosed problem, because nothing is said about the eddy viscosity. Depending on the sophistication requested, zero-, one- or two-equation models are possibilities. A zero-equation model has zero transport-equations for the eddy viscosity; a one-equation model has one, etc. The k-ε is a two-equation model. And the eddy viscosity is related to k and ε through

$$
\upsilon_T = C \frac{k^2}{\varepsilon}
\tag{2.27}
$$

Where C is a model constant equal to 0,09 in the "standard k-ε-model" (Ertesvåg, 2000). To use this relation both k and ε needs to be known values for all position in the flow at all times, and this is achieved through two transport equations. One for k and one for ε. This requires additional computational time of course, but with modern computers the latter is no problem.

It is also possible to derive a transport equation for the Reynolds stresses itself, but the derivation ends up with a three order fluctuation which is extremely complex to handle both numerically and by modelling. The Reynolds stress equation is derived by subtracting the time averaged Navier-Stokes (or RANS) from the instantaneous equation for both the i*th* and j*th* dimension. Then the i*th* direction is multiplied with u_j' and vice versa, before doing another time averaging. (White, 2006). The derivation is left out here, but the procedure is explained in the literature, e.g. Ertesvåg (2000). Here the reader will also find a discussion regarding why or why not to use a transport equation for the Reynolds stresses.

By now the reader is probably wondering why all this discussion about turbulence is included; remember that turbulence is a common flow condition and almost all heat exchangers have turbulent flows inside them. It is obvious then, that turbulence also is important for particle transport, see chapter 3.5. But first let's have a look at turbulence close to the wall.

2.2.9. CLOSE TO THE WALL

Note that the RANS equation solves for the average velocities, but an unalterable rule in fluid dynamics is that all velocities will go to zero close to or at the wall. Better known as the no slip-condition.

$$u_i = \overline{u_i} + u_i'$$ (2.28)

Since the average velocity approaches zero as $y \to 0$, it means that the fluctuation must be zero at the wall too

$$u_i'(y=0) = 0$$ (2.29)

Let's take a look at the last term in eq. (2.19), for simplicity the term is repeated here

$$T_{ij} = \overline{\tau_{ij}} - \rho \overline{u_j' u_i'}$$ (2.30)

Where T_{ij} is the total stress tensor, if i=1 and j=2 this gives

$$T_{12} = \mu \left(\frac{\partial \overline{u}}{\partial y} + \underbrace{\frac{\partial \overline{v}}{\partial x}}_{=0} \right) - \rho \overline{u' v'}$$ (2.31)

The second term in the parenthesis is small compared to the first in a 1D boundary layer.

Equation (2.31) is the basis for the further analysis. The first question is what happens very close to the wall, and the second question is what happens a bit further away from the wall. What 'further away' means is at this point unclear, but will be explained later.

'At' the wall

- $\rho \overline{u' v'}$ can be ignored compared to $\mu \dfrac{\partial \overline{u}}{\partial y}$

- $T_{12} \approx \mu \dfrac{\partial \overline{u}}{\partial y} \approx T_{12}(0) \equiv \rho u_\tau^2 = const$. Where $u_\tau = \sqrt{\tau_w / \rho}$ is the friction velocity

15

This reduces eq. (2.31) to

$$\mu \frac{\partial \overline{u}}{\partial y} = \rho u_\tau^2 \qquad (2.32)$$

Integration gives

$$\frac{\overline{u}}{u_\tau} = \frac{u_\tau}{\upsilon} y \qquad (2.33)$$

And by introducing the nondimensional velocity and length scales $u^+ = \dfrac{\overline{u}}{u_\tau}$ and $y^+ = \dfrac{u_\tau y}{\upsilon}$ this gives

$$u^+ = y^+ \qquad (2.34)$$

Equation (2.34) is valid only in the very near region of the wall, where the turbulence is absent. This is called the viscous sublayer. Here the wall is 'near' enough to dampen any turbulent fluctuations, and this region is very thin. At $y^+ \approx 5-10$ equation (2.34) is no longer valid and the turbulent fluctuations become important. figure 2 shows the relative importance of the Reynolds stresses at different distances from the wall compared to the total shear stress
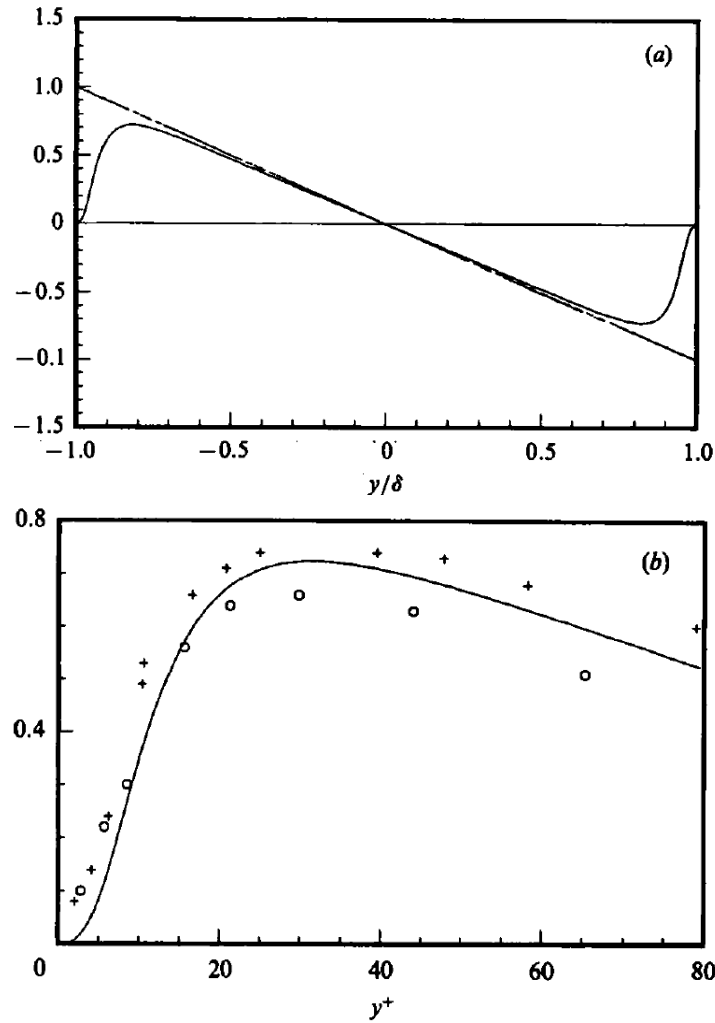
FIGURE 2-TOTAL SHEAR STRESS IN NEAR WALL TURBULENCE (KIM ET AL., 1987)

The top figure in figure 2 shows the total shear as a straight line and the relative importance of the Reynolds stresses, $-\overline{u'v'}$. The bottom figure shows how the Reynolds stresses behave close to the wall in wall coordinates. (Kim et al., 1987) Not that in this example there are two walls, therefore the Reynolds stresses decreases after y^+=40. Below y^+=10 the Reynolds stresses accounts for less than 20% of the total shear, hence the assumption of a viscous sublayer is justified.

By experiments (Andersson, 2010) the viscosity can be neglected outside the viscous sublayer, in other words the turbulent Reynolds stresses are large compared to viscous stresses. From figure 2 it is usual to assume that the Reynods stresses dominate when y^+>30. To get any further with equation (2.31) a dimensional analysis of the velocity gradient is needed.

$$\frac{\partial \overline{u}}{\partial y} \sim \frac{u_\tau}{y}$$

(2.35)

17

Doing a rather crude assumption and saying that these sides are equal, an expression for $\bar{u}$ is found.

$$\frac{\partial \bar{u}}{\partial y} = \frac{u_\tau}{Cy}$$ (2.36)

Integration gives

$$\frac{\bar{u}}{u_\tau} = u^+ = \frac{1}{C}\ln(y^+) + A$$ (2.37)

This is known as the logarithmic velocity profile. From experiments the constants in equation (2.37) has been found to be $C = 0.40$ and $A = 5.5$. (Ertesvåg, 2000)

The next question is how good this *law of the wall* model correspond to data measurements. This has been documented widely in the literature, which figure 3 illustrates
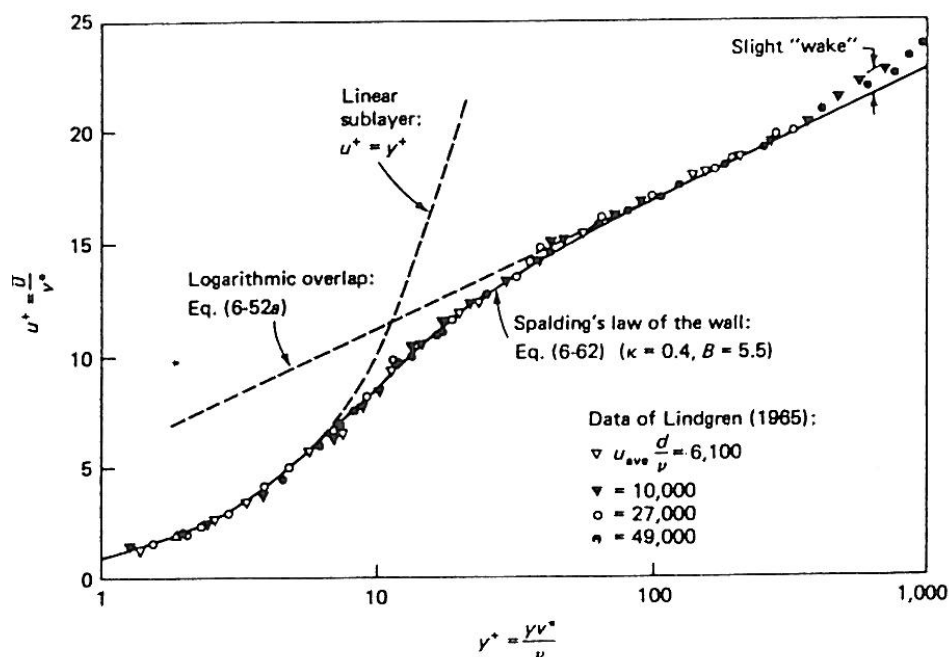
FIGURE 3-LAW OF THE WALL. THEORY AND EXPERIMENTS (ANDERSSON, 2010)

As can been seen from the figure, there is an overlapping layer from about $y^+ \cong 5$ `to $y^+ \cong 30$ where the measurements are much lower than both the linear and logarithmic expression. This is called the buffer layer, and in that area both viscous and turbulent stresses coexist.

Generally it is concluded that

$$u^+ = \min(y^+, 2.5\ln y^+ + 5.5)$$ (2.38)

18

2.3.   COMMENTS AND FURTHER READING

From the theory presented it is should be clear that the particles movement in a turbulent is rather complex. Flows are frequently turbulent, meaning they are random in time and space, and this will influence the particles inside. Since the focus of this thesis is on particles which resuspend due to an impacting particle, it is crucial to understand what velocities the incoming particle has in the time of impact.

Small attached particles will be inside the viscous sublayer and is therefore likely *not* to be affected by the outside turbulence in a significant way. An incoming particle needs to penetrate the sublayer, which will dampen and protect the attached particles underneath. If the incoming particle doesn't reach the target particles, or if it doesn't have enough momentum to penetrate the sublayer, a resuspension is impossible.

Çengel, Yunus A. Heat and mass transfer : fundamentals and applications. 4th ed. 2011
    Basic textbook

White, Frank. Fluid mechanics. 7th ed. 2011
    Basic textbook

White, Frank. Viscous fluid flow. 7th ed. 2011
    Extensive textbook covering creeping flows and turbulent transition

Tennekes & Lumley. A first course in turbulence. 1st ed. 1972
    Extensive textbook about turbulent physics

3. PARTICLE TRANSPORT TO THE WALL

This chapter will give an introduction to the deposition of particles onto a surface, i.e. how particles are transported from the bulk to the wall. How the particle actually sticks to the surface will be discussed later during the talk about adhesion forces.

This knowledge makes it possible to say something general about how any particle layer builds up. Some of the details are left out, so this chapter will only give the reader an overview of the mechanisms that are responsible for the transportation. It should be noted that particle deposition has been an important theme of study for many years, and a lot of papers are available if the reader is interested in more details. During the winter of 2011 the author did a literature survey about particle transportation (Hammersgård, 2011), and a lot of this work is based on the review paper by Ziskind (2006).

It is usual to separate big and small particles when discussing particle transport, because different transport mechanisms are responsible for the different sizes. Small particles tend to follow the fluid's streamlines and are unlikely to *hit* the surface by their own inertia, which is the case for bigger particles. Big inertia gives higher ability to follow a strait flight path, i.e. higher ability to resist change in direction. This is of course reflected in Newton's second law of motion. So if a big particle is sent on a collision course towards the wall, it will be able to penetrate the boundary layer and reach the wall.

3.1.   SMALL PARTICLES

Small particles are transported by diffusion, which requires a concentration gradient towards the wall. If a linear gradient-profile is assumed, the deposition caused by diffusion can be written as

$$\dot{m}_d = k_t (C_b - C_s) \tag{3.1}$$

Where k_t is the transport coefficient and C is the concentration, b and s indicate bulk and surface, respectively. The transport coefficient may be replaced by the mass transport coefficient, k_m, which is available through correlations in the literature concerning mass transport for forced convection. This approach shows good accuracy as long as the deposition rate is not too big (Epstein, 1983).

3.2. BIG PARTICLES

Big particles are not transported by diffusion. To understand why the reader is advised to read about what diffusion of mass is and the limits of this transport mechanism. A brief statement will be given though: diffusion is driven by random (molecular) motion, and when the particles become too big this effect decreases. It can be shown that the mass transport coefficient in equation (3.1) is proportional to the diameter to the power $-2/3$ (Epstein, 1988, Hammersgård, 2011). In other words, the diffusion transport decreases as the particles get bigger.

Big particles are transported by their own inertia, as stated above, and the transport rate can increase with orders of magnitude compared to diffusion transport. One theory is that turbulent random motions set particles into motion, and when the turbulent fluctuation disappear near the wall the particles will have enough inertia to reach the wall by themselves.

3.3. SIZE RANGES

Above a talk about big and small particles was given, but what is the size range? The usual way is to represent the size through a stopping distance. The stopping distance is the distance a particle travels if it is inserted with an initial velocity into a fluid. It is possible to set up a force balance and thereby calculate this distance, see for instance (Hammersgård, 2011).

By taking the stopping distance and dividing it by the initial velocity, the *relaxation time* appears. The relaxation time, t_p, is the common way to represent particle sizes. The relaxation time is unaffected by the initial velocity, and therefore constant for a specific particle diameter.

The relaxation time is made dimensionless by wall variables

$$t_p^+ = t_p \frac{u_*^2}{\upsilon} \tag{3.2}$$

Where u_* is the friction velocity and υ is the kinematic viscosity.

Small particles have relaxation time less than 0.2 and big particles larger than 20. In between the transport is partially diffusion and partially inertia.

The deposition velocity, which is equivalent to the deposition rate (Papavergos and Hedley, 1984), equals

22

$$V_d^+ = \begin{cases} 0.07 Sc^{-2/3} & t_p^+ < 0.2 \\ 3.5 \cdot 10^{-4} (t_p^+)^2 & 0.2 < t_p^+ < 20 \\ 0.18 & t_p^+ > 20 \end{cases} \qquad (3.3)$$

Where Sc is the Schmidt number

$$Sc = \frac{\upsilon}{D_B} \qquad (3.4)$$

And D_B is the Brownian diffusivity which is inverse to the particle diameter (Einstein, 1956)

$$D_B \propto d_p^{-1} \qquad (3.5)$$

Note that equation (3.3) is not continuous, this of course is due to uncertainty in the models. Note also that the deposition velocity is independent of the relaxation time for big particles. figure 4 compares equation (3.3) to experimental data, and it is concluded that, yes, they match.
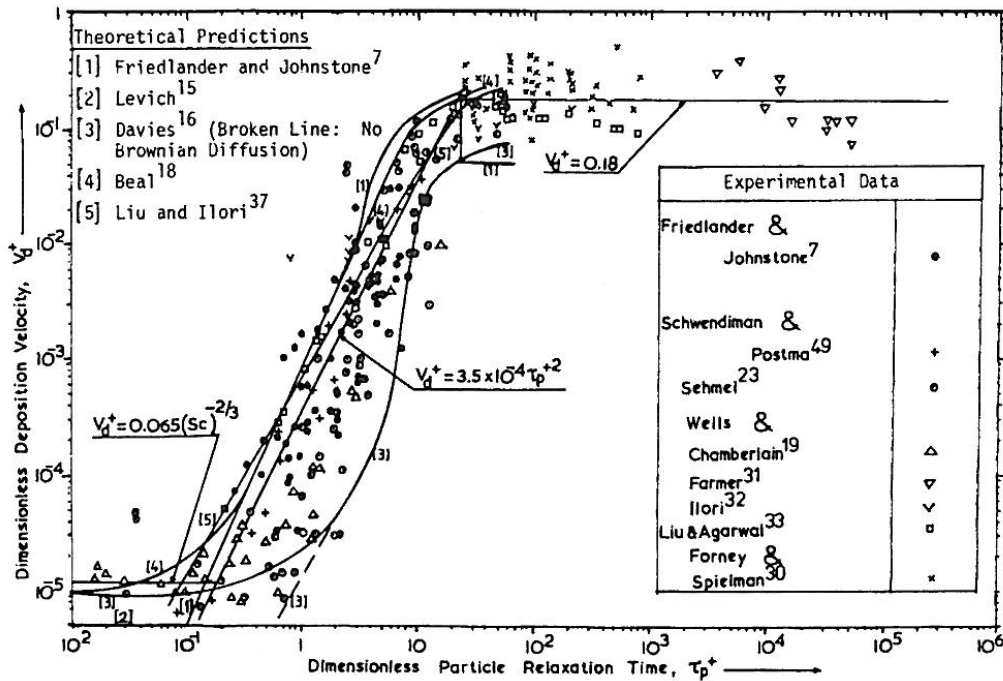
FIGURE 4-DEPOSITION VELOCITY FOR DIFFERENT PARTICLE RELAXTION TIMES (PAPAVERGOS AND HEDLEY, 1984)

23

3.4.   EFFECT OF ROUGHNESS, THERMOPHORESIS AND NON-SPHERICAL PARTICLES

The mechanisms discussed above are based on a flat non-roughed plate, spherical particles and no temperature gradients in the fluid.

Surface roughness increases the diffusion deposition rate. For the smallest particles a very rough surface can increase the deposition rate with 3 orders of magnitude (Guha, 2008). The roughness does not affect the deposition of bigger particles. The theory is that small particles are captured by surface cavities while bigger particles are not able to "hide" inside these.

A temperature gradient will give an increase in the Brownian motion in the direction of lower temperature. In other words a cold wall will attract while a hot wall will reject particles. The Brownian motion is only affecting the diffusion mechanism. For more details the reader is referred to Guha (2008). The temperature gradient-effect is commonly known as thermophoresis, and the importance of thermophoresis has been observed in industrial plants in Norway (Årdal). The experimental setup was three cross sectional tubes in a hot flue gas, the middle tube was cooled whereas the upper and lower was not. This resulted in a fouling growth only for the cooled tube (Næss, 2011).

The assumption about spherical particles is doubtful at best; Metallic (alumina) particles from furnaces are obviously not spheres, such particles are irregular in shape and size. The usual way to get around this issue is to introduce some hydrodynamic diameter, but experimental studies have revealed that this approach underestimate the deposition. For more details the reader is referred to Hammersgård (2011) where different experiments are presented and compared to theoretical measurements based on the hydrodynamic diameter-approach.

3.5.   PARTICLE TRANSPORT IN TURBULENT FLOWS

In this subchapter the attention will be focused on how particles are transported in turbulent flows. The question which is tried answered in this chapter is; from where is a particle accelerated if it reaches the wall?

In a moving fluid, particles of all sizes will experience a drag towards the direction of the flow, no question about that. But small fluctuations which exist in turbulent flows will, when some criteria are met, send particles on a collision course toward the channel walls. These fluctuations are called eddies. The eddies come in many sizes, the biggest have the same order of magnitude as the flow system itself (e.g. diameter of the pipe, width of a channel etc.) and the smallest are limited by the Reynolds number and viscosity; a high Reynolds

number gives more turbulence energy, and thereby the need of smaller eddies where the dissipation happens. The viscosity has the opposite effect of the Reynolds number. The smallest eddies are known as the Kolmogorov length scales, given by

$$\eta_{kol.} = \left(\frac{\upsilon^3}{\varepsilon} \right)^{1/4}$$

(3.6)

Where υ is kinematic viscosity and ε is the turbulent dissipation. The relation between the length of the large, l, and smallest eddies is

$$l/\eta_{kol.} = \mathrm{Re}^{3/4}$$

(3.7)

The large ones are approximately constant since they are given by external length scales, e.g. diameter. Thus the smallest will become smaller as the Reynolds number increases. As predicted. (Tennekes and Lumley, 1972)

In other words, a turbulent flow has a specter of eddy sizes. Not all of them are able to accelerate particles, though, because the smallest eddies spin around too fast and possesses too little momentum. While large eddies have too little velocity change and particles will be able to follow the eddy movement, in other words the inertia is too small. The conclusion is that there needs to be balance between the inertia of the particle and frequency of the eddy. This balance is quantified through the stokes number, Stk (Haugen, 2011).

Different definitions for the stokes number are available, but generally if $Stk \gg 1$ the inertia of the particle is too big for the flow to be able to deviate the flight path. For $Stk \ll 1$ the particles will follow the fluid perfectly. One definition is the ratio between the particle response time, or relaxation time, to the fluid relaxation time. The relaxation time of an eddy is here defined as the time duration for one loop:

$$\tau_f = \frac{d}{u^{'}}$$

(3.8)

Where d and $u^{'}$ is the diameter and fluctuating velocity of the eddy, respectively. The relaxation time of a single particle is defined as (Hammersgård, 2011)

$$\tau_p = \frac{\rho_p d_p^2}{18\mu}$$

(3.9)

The stokes number is then the ratio between equation (3.9) and (3.8)

$$St = \frac{\tau_p}{\tau_f}$$

(3.10)

25

The stokes number needs to be close to one, that way the balance between particle inertia and eddy frequency is intact, in other words $\tau_p \sim \tau_f$. Note that this is an order of magnitude relation and not an exact relation. Thus

$$d_p \sim \sqrt{\frac{d}{u'}\frac{18\mu}{\rho_p}} \tag{3.11}$$

A numerical example is air and alumina. An eddy of 1mm (=10^{-3}m) will be able to accelerate an alumina particle of about 10μm if a 10% turbulent intensity and an average velocity of 10m/s is assumed. The eddy is then roughly 100 times bigger than the particle. Equation (3.11) is a square root dependency, so if the eddy is 10 cm then the corresponding particle diameter is 109μm, or 1000 times smaller.

In figure 2 the turbulent intensity was shown to be a function of the distance to the wall. At the wall all turbulence and fluid motion is zero due to the no slip condition, the turbulence increases to its peak value a small distance away from the wall, lets name this distance L. The mean velocity is also zero at the wall, and increasing outwards. The viscous sub- and buffer layer is not included here for the sake of simplicity. The described situations is illustrated in figure 5
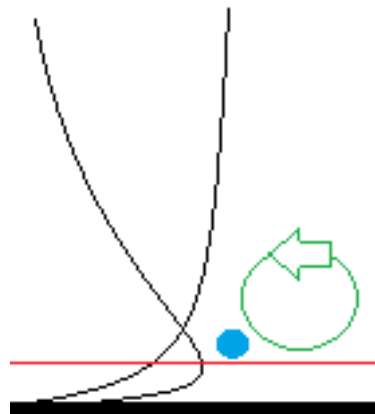
FIGURE 5-PARTICLE TRANSPORT NEAR THE WALL

figure 5 shows the velocity and turbulent intensity near the wall. Scales are unproportionale. An eddy is illustrated in green and the particle as a blue dot.

The red line is at height L from the wall. If the particle hits the wall, it has a relaxation time larger than the relaxation time of the layer below the red line. The latter is not a physical quantity, but may be understood as follows: it is the time an eddy uses to move the distance L. The eddy will vanish as it approaches the wall, so the particle needs to have enough momentum before approaching the wall.

Mathematical speaking the criteria is

$$\tau_p \geq \frac{L}{u'} \tag{3.12}$$

Since the relaxation time of the particle and eddy is same order of magnitude, as discussed above, it is implied that

$$\tau_f > \frac{L}{u_{RMS}} \tag{3.13}$$

Substituting equation (3.8) into (3.13) gives

$$\frac{d}{u'} > \frac{L}{u_{RMS}} \tag{3.14}$$

Further, the RMS value and fluctuating component have the same order of magnitude; see equation (5.47) and the definition of the RMS-value. This indicates that the diameter of the eddy needs to be larger than the distance L to the wall. Physically this doesn't add up since all eddies below the red line must be smaller than the distance. The concluding remark from this simple discussion is that the particles are accelerated relatively far away from the wall, i.e. from the outer region of the flow, where they are sent on a collision course. The eddies close to the wall are too small to accelerate the particles.

4. SURFACE-SURFACE INTERACTIONS

Contact between surfaces gives rise to adhesion forces. The adhesion force is caused by van der Waals forces, but electrostatic forces between macroscopic bodies are also important in some situations. The electrostatic forces are important for the deposition process as well, e.g. a three orders of magnitude (10^3) increase in the deposition velocity has been observed when electrostatic forces dominate (Guha, 2008). However electrostatic forces are neglected in this thesis and the interested reader is referred to Guha (2008), Ziskind (2006) and references therein.

Before the expression for the adhesion force between a sphere and a plane wall is presented, some theory to support this expression is in order. The van der Waals forces are assumed additive meaning that they do not influence each other (see a discussion about this assumption in chapter 4.1) and that the total force is given as the sum of all the small forces. The surface-to-surface interaction is characterized by what is known as the Hamaker constant. The Hamaker constant gives the potential energy between two bodies, and for both solids and liquids the value of the Hamaker constant is in the range $(0.4-4)\cdot10^{-19}\,\text{J}$ (Ziskind, 2006).

The potential energy between a sphere and a smooth surface is

$$W = -Ar_p\big/6L_e \tag{4.1}$$

Where A is the Hamaker constant between them, r_p the sphere radius and L_e the separation distance. The energy is the force times the distance, or the integral of the force over the distance. Derivation of equation (4.1) gives the force

$$F = -Ar_p\big/12L_e^2 \tag{4.2}$$

If the sphere and surface consists of two different materials, the Hamaker constant is given by

$$A_{12} = \sqrt{A_{11}A_{22}} \tag{4.3}$$

Where A_{jj} is the Hamaker constant for one material. Equation (4.3) is only valid for vacuum, and if there are some fluid between material 1 and 2 the Hamaker constant is

$$A_{132} = (\sqrt{A_{11}} - \sqrt{A_{33}})(\sqrt{A_{22}} - \sqrt{A_{33}}) \tag{4.4}$$

To avoid the difficulties related to find the Hamaker constant for all types of surface, it is much more convenient to use the surface energy. The surface energy is not easily available either, but it is more common to use the surface energy when modeling adhesion (Ziskind,

2006). But note that the Hamaker constant is a fundamental physical property for a specific material, whereas the surface energy is situation dependent.

According to the JKR-theory, the force between a sphere and a plane wall is

$$F_{a,JKR} = 3\pi\sigma r_p \qquad\qquad (4.5)$$

Where σ is the surface energy.

Because all materials are elastic, the adhesion forces will cause deformation and create an area of contact. Elasticity is beautifully illustrated in figure 6 where a golf ball is photographed with high speed photography when it hits a hard wall. An elastic deformation is characterized by that the original shape is intact after a collision, in other words the deformation is reversible. An elastic deformation conserves the energy also, and it is analogous to a perfect spring.
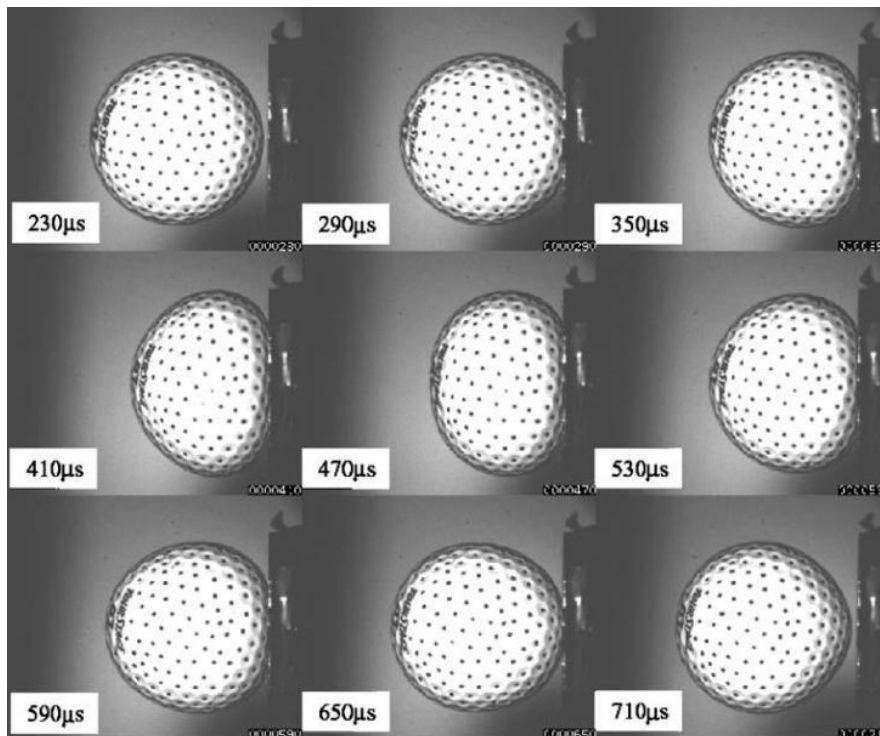
FIGURE 6-GOLF BALL ELASTIC DEFORMATION (GOLFWRX.COM, 2011)

Between the 290μs-frame to 650μs-frame the ball is squeezed towards the wall due its own inertia. The force causing the contact area in this example is the impact force from the wall, not the adhesion force. But this is a neat analogy to understand how the contact area between a particle and a wall appears. figure 6 also illustrates an elastic deformation very well.

The JKR theory gives an expression for the contact area for a resting particle. If the particle is assumed spherical, the radius of the contact area is

$$a = \left(\frac{6\pi\sigma r_p^2}{K} \right)^{1/3}$$

<div align="right">(4.6)</div>

Where K is a material property which includes the Young's modulus of elasticity and Poission ratio. This constant is discussed in more details in equation (5.8).

4.1.   THE ASSUMPTION THAT VAN DER WAALS-FORCES ARE ADDITATIVE

Hamaker assumed that molecular forces are additive and did not interact with each other. The force between two solid bodies is given by equation (4.2) alone; but remember that the Hamaker constant relies on whatever lies between the bodies. Imagine a large sphere, for instance, surrounded by liquid film, which hits a layer of small particles. Beneath the layer there is a solid surface which the particle experiences an attraction force towards. The situation is illustrated in figure 7.
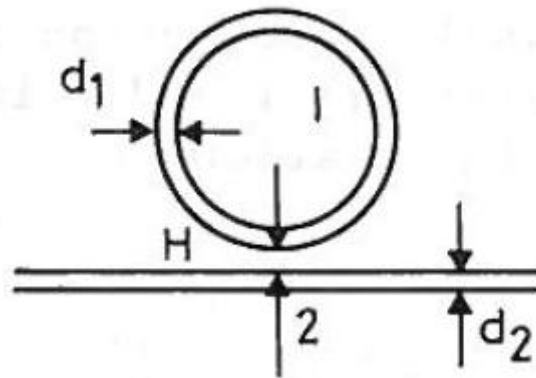
FIGURE 7-THIN LAYER INFLUENCE ON ADHESION FORCES (VISSER, 1988)

On figure 7 the separation distance is noted H, the thin layer d_2 and the liquid film d_1. The liquid film will vanish if the particle reaches the deposited layer, but as Visser (1988) writes, if the thickness d_2 is bigger than the separation distance H, the force between body 1 and 2 are given by the material properties of the layer and not by the properties of material 2. In other words; if the separation distance is large the molecule-molecule interactions between body 1 and 2 are influenced by the third party molecules in between.

5. PARTICLE RESUSPENSION BY IMPACTION

As mentioned in the introductory part a foulded heat exchanger may be cleaned by increasing the flow speed. Attached particles will resuspend at some threshold velocity, and the hypothesis is that the resuspension is caused by

- Shear stresses which rips the particles of the surface
- Incoming particle have a sand blasting effect on the surface
- A combination of these

In this chapter models and theories on particle removal by impaction will be presented and discussed. Some of the theories are qualitative and applies only for that particular case, but interesting observations and knowledge is possible to bring along from these theories as well. More quantitative theories will also be presented, and some of these will be implemented into MATLAB.

Based on these models a parameter study will be carried out.

5.1. PARTICLE ATTACHMENT

In chapter 3 a discussion about how the particles are transported to the wall by either diffusion or inertia, depending on their size, was presented. But how the particles actually attach to the wall other than presenting the adhesion forces, were left out. This is because the mechanisms are fairly complicated.

A common assumption is that if a particle hits the wall it will either bounce off or come to rest at the place of impact. The two outcomes are balanced by a statistical parameter known as the sticking probability. In 1978 a paper was published by S.K. Beal in which this parameter was examined. He argued that small particles have a high sticking probability because they can be captured by small irregularities on the surface, and that this effect decreased as the particles get bigger. The effect of increased surface roughness onto the deposition of small particles was discussed in chapter 3.4. Beal (1978) scaled the sticking probability to the stopping distance and came up with the following relation (Beal, 1978)

$$
\begin{aligned}
S &= 1 & s_p^+ &< 4.5 \\
S &= (4.5 / s_p^+)^3 & s_p^+ &> 4.5
\end{aligned}
$$

(5.1)

Where S is the sticking probability.

Equation (5.1) is based on experimental data and the least square method.

Later research has shown that the assumption about bounce off or stick on impact gives a simplified picture. In 2007 J.S. Marshall carried out a discrete-element-method calculation where he inserted microparticles (10 µm) into a 2D channel flow. The flow was laminar. He also introduced a parameter, ϕ, which was the ratio between a particle's adhesion force (actually the surface energy, but they are equivalent. See equation (4.5)) and kinetic energy of the particle (Marshall, 2007)

$$\phi = \frac{\sigma}{\rho_p U^2 r_p}$$
<div align="right">(5.2)</div>

And by varying this parameter the calculations showed that particles tend to accumulate near the wall. A plot across the channel shows this effect.
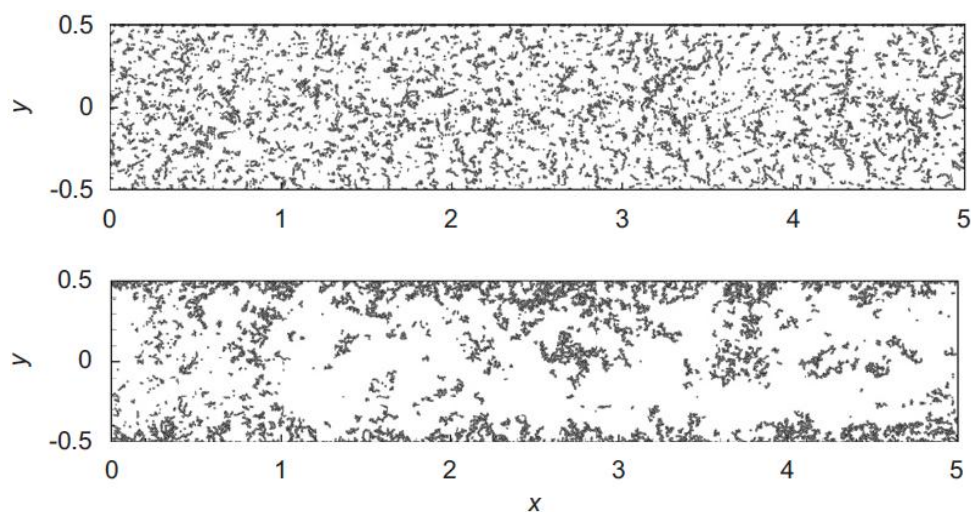
FIGURE 8-PARTICLE POSITION FOR DIFFERENT ADHESION PARAMETERS, Φ=1,5 (TOP) AND Φ=150 (BOTTOM) (MARSHALL, 2007)

From these figures Marshall found that the classical assumption about a single particle attach to the wall with some sticking probability is a simplification. He found that only in rare occasions a single particle actually collides with the wall; it is much more common that before impact the particles aggregate, and these aggregates either attach directly to the wall or other already attached aggregates. Larger particles however have a better ability to collide as single particles.

Another assumption that Marshall characterizes as weak is the assumption that a particle becomes frozen if it attaches to the wall. He argues that when an aggregate hits the wall, deformation, bending and break-off are processes which affects the deposition. Such mechanisms are also the ones which limit the deposition and eventually force the fouling layer to reach an asymptotic value, he writes.

An interesting note in Marshall's conclusion is that when a particle resuspend or is lifted away from the wall, the detachment is not related directly to fluid forces, but "*rather to*

collision and adhesion forces to a passing particle or aggregate". This justifies the hypothesis about particle resuspension by impaction.

5.2.   BIG PARTICLE IMPACTION – QUALITATIVE STUDY

As pointed out a number of times, the smallest particles are the ones that follow the streamlines easiest. They have too little inertia. Deposition of small particles is therefore through diffusion alone and not by impaction.

A paper by Eames and Dalziel (2000) describes what happens when a big particle hits a dusty layer. In their experiment a large particle with diameter radius 20mm was pushed towards a wall, covered by particles in the size range of 100-150µm. The impacting particle is too big to represent the particles in industrial applications, typically 1-50µm, but the paper illustrates that impaction is capable of resuspend deposited particles. In other words the background hypothesis of this work is possible.

Eames and Dalziel (2000) reported that it was not only the impaction itself which was responsible for the resuspension, but the vortexes which followed behind it. figure 9 shows these vortexes.
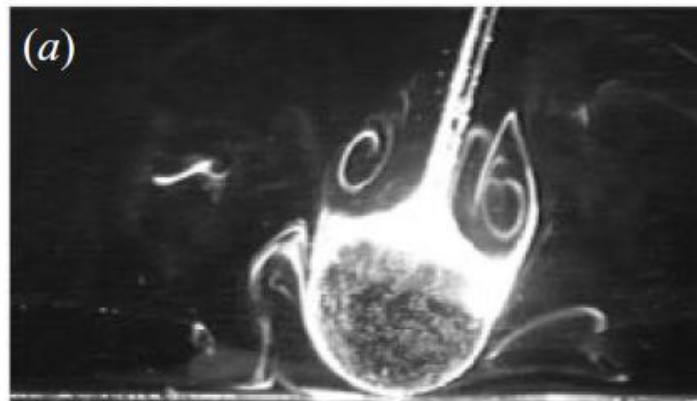
FIGURE 9-INCOMING PARTICLE AND VORTEX (EAMES AND DALZIEL, 2000)

The fluid is water which is about 1000 times denser than air. Upon impact the vortexes will continuo towards the wall a make high velocity gradients above the dust. These gradients will generate lift on the deposited dust particles. If the lift exceeds the gravitational and adhesive forces, the particles will resuspend. The vortexes are also pressed outwards from the place of impact. figure 10 below gives a time laps picture which describes this

35
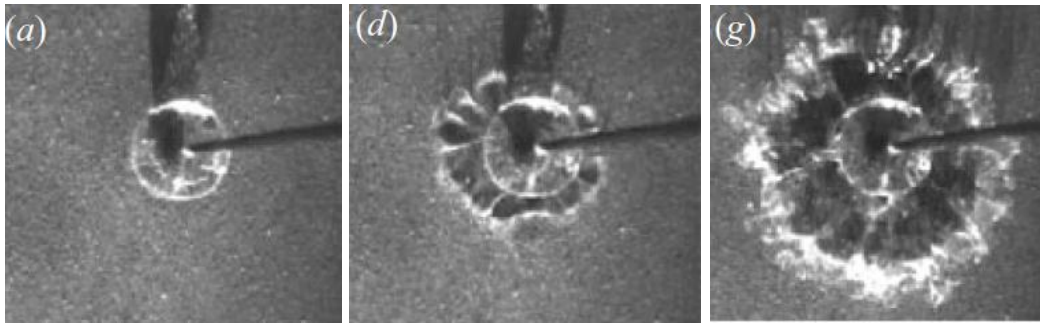
FIGURE 10-A SPHERE IMPACTION A DUST LAYER (EAMES AND DALZIEL, 2000)

Some qualitative conclusions were drawn by Eames (2000):

- Big impacting particles are capable of resuspend deposited particles
- Big impacting particles will carry along vortexes which may trigger secondary resuspension as the vortexes spreads out after impact

The experiment by Eames and Dalziel (2000) did mostly focus on the resuspension caused by the vortexes. These are of course a secondary consequence caused by the impacting sphere. In heat exchangers the impacting particles are much smaller (maximum 100µm), i.e. 200 times smaller than the 20mm sphere used in the experiment by Eames (2000). To generate the vortexes behind these smaller particles requires a larger velocity. Vortexes start to form when the Reynolds number based on the particle diameter is >35. This is known from theory by Kármán. (White, 2011a).

In air at 100˚C this would require that

$$\text{Re}_p = \frac{\rho u d}{\mu} \rightarrow ud = \frac{\mu}{\rho}\text{Re}_p \approx \frac{35}{43365} \qquad (5.3)$$

With a diameter of 100µm this gives 8 m/s. Such speeds are possible in heat exchangers, but remember that this is the *limit* at which vortexes are generated. Higher velocities are needed in order to generate strong vortex structures. Secondly, 100µm particles are, when considering flue gas from alumina furnaces, rare. Particles one order of magnitude smaller, typically 10µm, is more feasible and then the required velocity is increased further.

This result is a bit disappointing because now the only way an impacting particle can cause resuspension is that the impact itself is strong enough to break the adhesion forces between attached particles and the surface.

But the experiment by Eames and Dalziel is not worthless because it makes a starting point for further studies. What the reader should note is that, no, the vortexes generated by impacting particles are not able to resuspend attached particles because the incoming particles are too small and vortexes probably too weak if they exist. But there have been done similar experiments with a particle jet with smaller particles. In 1991 Walter John et.al.

36

published results from a particle jet which caused resuspension. The attached particles were $8.6\,\mu m$ diameter on average and the impacting particles were $3\,\mu m$ on average. The jet had a velocity of 40 m/s, or a Reynods number of about 10 based on the particle diameter. Their hypothesis was that resuspension by particle impaction is more effective than hydrodynamic forces alone because particles have at least 1000 times the density of air. The figure 11 below illustrates their results.
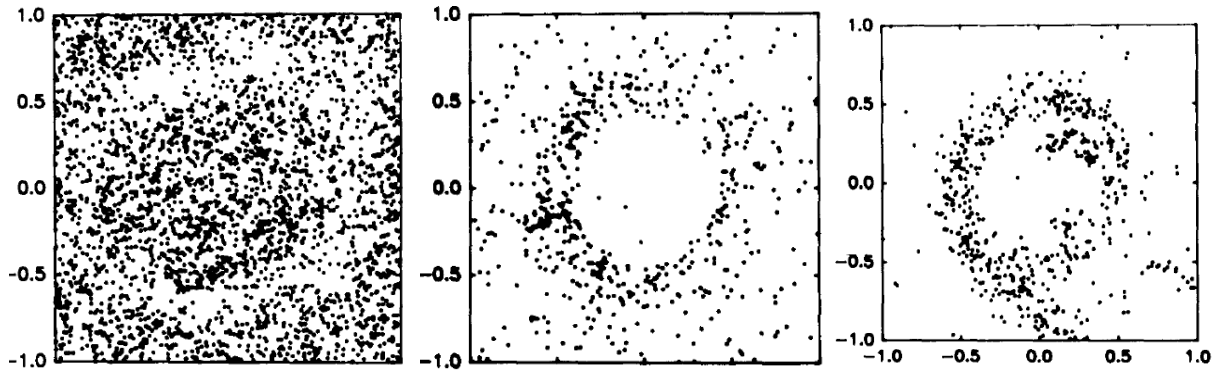
FIGURE 11-DEPOSITED PARTICLES ON A SURFACE AFTER EXPOSED TO A PARTICLE JET (JOHN ET AL., 1991)

The left picture is after exposure to a jet free of partile, while the middle and the right are after exposure to a particle jet; 3μm for 4.5 minutes (middle), 3μm for 15 minutes (right). Both all jets had 40 m/s average velocity.(John et al., 1991)

Comparing the left picture in figure 11 to the two others, it is clear that the particle jet is much more efficient when it comes to cleaning the surface. The particles are too small to have large vortex structures, so the resuspension is due to impaction alone.

The next discussion is about how momentum is transferred between two colliding particles.

5.3. ELASTIC AND PLASTIC DEFORMATION

Elastic collision was already discussed in chapter 4 where the golf ball collided with the wall.

When a particle hits a surface the kinetic energy is transferred into elastic deformation and plastic deformation. Elastic deformation is reversible such that both the particle and the target surface restore their original shapes after the bodies separate. Plastic deformation is nonreversible and the deformation during a collision is maintained. (Xu and Willeke, 1993)

The collision theory is designed such that when two bodies collide the first deformation to take place is elastic deformation. If the impact velocity is above a certain limit, an elastic stress limit is exceeded and the plastic deformation starts. The energy stored in the elastic deformation may be regained, but the energy causing plastic deformation is converted into heat. (Xu and Willeke, 1993)

5.4.   ADHESIVE ELASTIC SPHERES

In the following text it is assumed purely elastic deformation, and the adhesive forces between the elastic sphere and the target surface is included. The objective is to uncover the exit velocity if the particle rebound, or the minimum velocity for rebound. The latter is the velocity at the particle just escape the adhesion forces, and is often called the threshold velocity or sticking velocity. Plastic deformation is neglected because it will make the mathematics unnecessary complicated.

The procedure is also described in more details in the literature (Thornton and Ning, 1998), in Thornton and Ning's paper the reader will find the corresponding discussion for plastic deformation too.

For adhesive elastic spheres the JRK-theory gives a relation for the force between the bodies and the relative approach, α

$$\frac{\alpha}{\alpha_f} = \frac{3\left(\dfrac{F}{F_c}\right)+2\pm2\left(1+\dfrac{F}{F_c}\right)^{1/2}}{3^{2/3}\left(\dfrac{F}{F_c}+2\pm2\left(1+\dfrac{F}{F_c}\right)^{1/2}\right)^{1/3}} \tag{5.4}$$

The relative approach is a measure of the deformation, and is zero at the beginning of the deformation. In equation (5.4) α_f and F_c is given by

$$\alpha_f = \left(\frac{3F_c^2}{16R^*E^{*2}}\right)^{1/3} \tag{5.5}$$

And

$$F_c = \frac{3}{2}\pi\sigma R^* \tag{5.6}$$

Recognize equation (5.6) as the adhesion force from equation (4.5). σ is the surface energy between the two bodies and R^* and E^* are

$$\frac{1}{R^*} = \frac{1}{R_1} + \frac{1}{R_2} \tag{5.7}$$

$$\frac{1}{E^*} = \frac{1-v_1^2}{E_1} + \frac{1-v_2^2}{E_2} \tag{5.8}$$

where v and E is the poission ratio and youngs modulus, respectively.

When two bodies make contact, a contact force is suddenly established between This force is (Thornton and Ning, 1998)

$$F = -\frac{8}{9}F_c \qquad (5.9)$$

This value is also found through equation (5.4) by setting the relative approach to zero, i.e. $\alpha = 0$

Imagine now a sphere with a velocity towards a plane wall. Just upon impact the adhesion force is actually directed in the same direction as the velocity. But as deformation begins, the direction of the force is turned against the velocity direction. The velocity is reduced and at some point the deformation is at its maximum, point B in figure 12, and at the same time the velocity reach zero.

Since this is an elastic deformation, all the kinetic energy before impact is stored and "recyclable". When the deformation is completely reversed and the sphere has no deformation, i.e. point A in figure 12, the force acting on the sphere is negative compared to the velocity – the force is pulling it back.

This force is now pulling the sphere in the direction of the wall, i.e. slowing it down. And the velocity at this instant must be big enough to overcome this force. The velocity just happens to be equal the incoming velocity – remember it is a elastic deformation, and this is what is know as the threshold velocity; which velocity is needed for the particle to not stick, that is to exceed the adhesion force?

Thornton (1998) summarizes the collision sequence in figure 12.
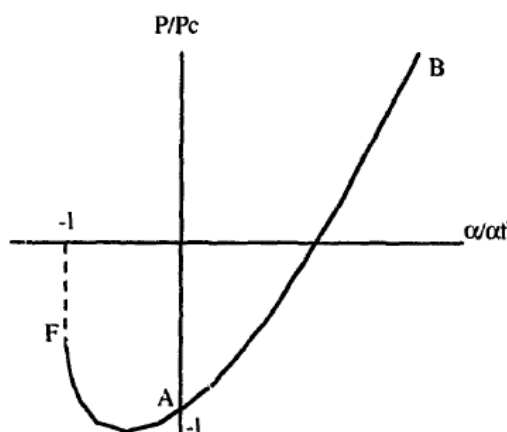
FIGURE 12-FORCE-DISPLACEMENT FOR ADHESIVE ELASTIC SPHERES (THORNTON AND NING, 1998)

To escape the wall, some of the kinetic energy is lost in order to separate the sphere and the wall. This work is noted W_S, and is given by the integral between $-1 < \alpha/\alpha_c < 0$.

The author of the JKR-theory suggested that

$$W_S = 7.58 \left(\frac{\sigma^5 R^{*4}}{E^{*2}} \right)^{1/3}$$

(5.10)

However it is possible to integrate (5.10) from 0 to $-\alpha_f$ to get an more exact expression for W_S (Thornton and Ning, 1998)

$$W_S = \int_0^{\alpha_f} F d\alpha = 7.09 \left(\frac{\sigma^5 R^{*4}}{E^{*2}} \right)^{1/3}$$

(5.11)

Based on this it is possible to put up an energy balance to calculate the rebound velocity.

$$\begin{pmatrix} \text{incoming kinetic} \\ \text{energy} \end{pmatrix} - \begin{pmatrix} \text{exiting kinetic} \\ \text{energy} \end{pmatrix} = \begin{pmatrix} \text{lost} \\ \text{energy} \end{pmatrix}$$

(5.12)

Which gives

$$m^* (V_i^2 - V_r^2) = 2 \cdot W_S$$

(5.13)

Where m^* follows the same correlation as equation (5.7).

Equation (5.13) gives the threshold velocity by setting $V_r = 0$. Combining equation (5.11) and (5.13) gives

$$V_i = V_{threshold} = \sqrt{\frac{2 \cdot 7.09}{m^*} \left(\frac{\sigma^5 R^{*4}}{E^{*2}} \right)^{1/6}}$$

(5.14)

If the incoming particle is a sphere and the target a plane wall, then $R^* = R$ and $m^* = m$. Further, if the sphere has uniform density, equation (5.14) gives (Thornton and Ning, 1998)

$$V_{threshold} = 1.84 \left(\frac{\sigma^5}{\rho^3 R^5 E^{*2}} \right)^{1/6}$$

(5.15)

Rebound occurs if the incoming velocity is greater than the threshold velocity. It is usual to define a coefficient of restitution given by

$$e = \sqrt{1 - \left(\frac{V_{treshold}}{V_i} \right)^2}$$

(5.16)

Further, if the incoming velocity is larger than the threshold velocity, the rebound velocity is

$$V_r = \left(V_i^2 - 3.38 \left(\frac{\sigma^5}{\rho^3 R^5 E^{*2}} \right)^{1/3} \right)^{1/2}$$ (5.17)

These equations only apply for a single object hitting another, and equation (5.15) to (5.17) are valid for spheres colliding with a plane wall only. Next, what happens when one sphere hits another sphere which is already attached to a plane wall?

5.5. ADHESIVE ELASTIC SPHERE-SPHERE-SURFACE COLLISION

In this chapter two different collision models will be presented:

      1. Perpendicular (centre-centre) collision

      2. Off centre-collision.

The first one is a vertical collision model and the mechanism is that momentum is transferred from the incoming particle vertically to the target particle. The only possible resuspension is pure lift off. The second model is an oblique collision and momentum is transferred vertically and horizontally. The resuspension are most likely to happen by rolling, and that happens when the collision moment exceeds the adhesive moment.

5.5.1. PERPENDICULAR COLLISION

The first collision is also known as a momentum-energy collision (Temu, 1998). The incoming particle hits the target particle with a velocity perpendicular to the wall. The impaction takes place at the top of the target particle, no rolling moment is induced. Momentum is transferred to the target particle through deformation, in figure 13 this is illustrated in frame E where the contact area is increased compared to the equilibrium state in frame A. This additional deformation will eventually force the particle to move away from the wall, and if the energy stored in the deformation is greater than the particle-surface energy, separation occurs. Note that both particles are assumed pure elastic. It is possible to take plastic deformation into account as well, but this would complicate the mathematics to an extent outside the scope of this thesis. And elastic deformation is sufficient to illustrate the basic mechanisms. In further work however, plastic deformation should be considered.

41
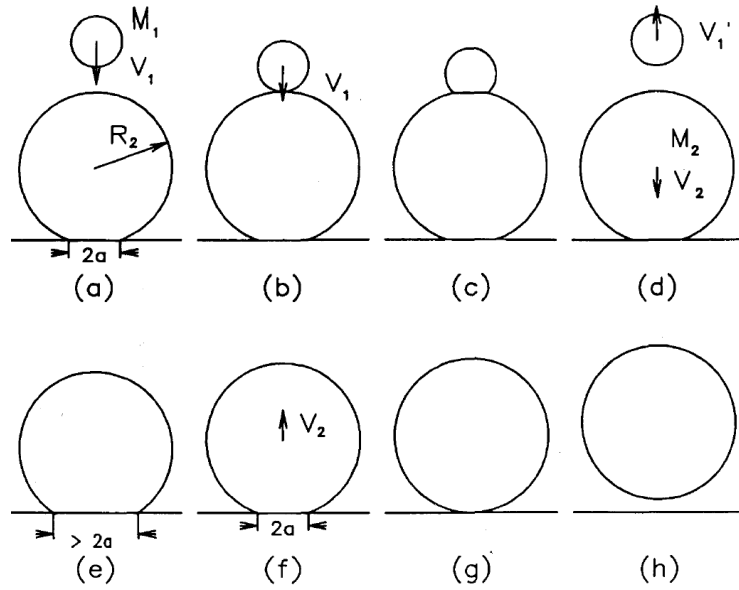
FIGURE 13-PERPENDICULAR COLLISION (JOHN AND SETHI, 1993)

The incoming particle hits the target particle at the top (B), is being deformed (C) and resuspended (D). The target particle is squeezed towards the wall (E) and the deformation will be reversed and result in a vertical velocity away from the wall (F). At frame (G) and (H) the deformation has reached zero and the target particle has escaped the adhesion forces. (John and Sethi, 1993)

Now depending on the level of sophistication it is possible to set up an energy balance for each particle. All the energy lost by the incoming particle in the collision is transferred to the target particle, so no energy is lost other than to overcome surface energies.

First step is to put up an energy balance for each particle

$$\begin{pmatrix} \text{incoming kinetic} \\ \text{energy} \end{pmatrix}_1 - \begin{pmatrix} \text{exiting kinetic} \\ \text{energy} \end{pmatrix}_1 = \begin{pmatrix} \text{lost} \\ \text{energy} \end{pmatrix}_1 \qquad (5.18)$$

$$\begin{pmatrix} \text{transferred} \\ \text{energy} \end{pmatrix}_2 - \begin{pmatrix} \text{exiting kinetic} \\ \text{energy} \end{pmatrix}_2 = \begin{pmatrix} \text{lost} \\ \text{energy} \end{pmatrix}_2 \qquad (5.19)$$

In the further analysis the only interest is the energy required to separate particle 2 (target) from the wall. Therefore the exiting kinetic energy for particle 2 is set to zero. The energy balance for particle 1 is

$$m_{12}^*(V_{1i}^2 - V_{1r}^2) = 2 \cdot W_{1S} = 14.18 \left(\frac{\sigma_{12}^5 R_{12}^{*4}}{E_{12}^{*2}} \right)^{1/3} \qquad (5.20)$$

V_{1r} is given by equation (5.17). Pay attention when doing calculations with this expression because the right hand side equals twice the losses. Note also that this equation is valid if and only if

$$m_{12}^* V_{1i}^2 > 14.18 \left(\frac{\sigma_{12}^5 R_{12}^{*4}}{E_{12}^{*2}} \right)^{1/3} \tag{5.21}$$

Since otherwise the incoming energy from particle 1 is not sufficient to overcome the surface energy between particle 1 and 2, in other words particle 1 sticks. This is of course not wanted since it adds particles to the fouling layer.

To carry out the energy balance for particle 1 is not that straight forward as equation (5.20) indicates because it assumes knowledge abouth the surface energy between the two particles, poission ratios and youngs modulus-constants. The two latter are material constants and easily available in tables, but the surface energy is rarely available. It is possible to calculate it though, John et.al. (1993) suggests that the surface energy between two surfaces is calculated by

$$\sigma_{12} = 2(\sigma_1 \sigma_2)^{1/2} \tag{5.22}$$

Which is the same correlation as for the Hamaker constant, see equation (4.3).

σ_i is the surface energy for each particle surface, and σ_{12} is the surface energy between them. Sadly the accuracy in equation (5.22) is discussable because often the surface energy for each material is unknown which forces the use ad hoc assumptions (John and Sethi, 1993)

Fortunately there is a trick to get around this problem: From classical physics the linear momentum is always conserved during a collision. This helps to calculate the velocity of particle 2 after the collision. John et.al. (1993) did this momentum balance. They found the velocity of the target particle after collision to be

$$V_2 = \left(\frac{2m_1}{m_1 + m_2} \right) V_1 \tag{5.23}$$

Which actually is a perfect inelastic collision. Why John et.al. (1993) chose to do this type of momentum balance was not explained in the paper, they could have chosen another type of collision. But their approach did correspond to experimental values.

The kinetic energy of the target particle in frame D in figure 13 is then

$$\frac{1}{2} m_2 V_2^2 = \frac{1}{2} m_2 \left(\frac{2m_1}{m_1 + m_2} \right)^2 V_1^2 \tag{5.24}$$

43

The target particle will be deformed according to this velocity. This is illustrated in frame E to H in figure 13. Principally this is equivalent to the situation with a sphere hitting a plane wall in the previous chapter. Setting up the energy balance and putting the rebound velocity to zero, equation (5.14) gives the threshold velocity

$$V_{threshold} = 1.84 \left(\frac{\sigma^5}{\rho^3 R^5 E^{*2}} \right)^{1/6}$$

(5.25)

Which is identical to equation (5.15) of course. In equation (5.25) the sphere diameters and densities are equal. In other words $V_1 = V_2$ after the collision according to equation (5.23).

The next task is if the two colliding spheres have different diameter. For derivation of the equation see *Appendix 1 – Threshold velocity for different size particles*, but the result is

$$V_{1T} = 0.92 \left(1 + \frac{R_2^3}{R_1^3} \frac{\rho_2}{\rho_1} \right) \left(\frac{\sigma^5}{\rho_2^3 R_2^5 E^{*2}} \right)^{1/6}$$

(5.26)

Note that this is the threshold velocity for particle 1 in order to separate particle 2.

John et.al. (1993) gives the same equation, but in their paper the constant 0.92 is replaced by 1.63. The writer thinks this is due to a minor error in John et.al. derivation, and the reader is invited to go through *Appendix 1 – Threshold velocity for different size particles* to see the stepwise derivation.

John et.al. (1993) did some calculations with equation (5.26) with the following data:

TABLE 2-PHYSICAL PROPERTIES FROM THE ORIGINAL PAPER (JOHN AND SETHI, 1993)

$R_1 = 1.5 \mu m \quad R_1 = 4.3 \mu m$,

$\sigma = 80.9 \, erg/cm^2$ (1 erg = 10^{-7} J),

$\rho = 1.35 \, g/cm^3$ for both particles,

$k_p = 2.42 \cdot 10^{-11} cm^2 / dyne$,

$k_s = 1.43 \cdot 10^{-11} cm^2 / dyne$

This lead to a threshold velocity of 3.9 m/s.

5.5.2. OFF CENTRE COLLISION

The second impaction model is the off centre collision. The resuspension starts with so called inceptive motion which is discussed by John et.al. (1993) and referred articles therein. Three incipient motions were identified: sliding, rolling and lift off. The assumption is that once one of these motions are initiated, the particle will be dislodged and resuspended. In further studies this assumption should be investigated, as it is a common assumption in many of the references used in this thesis.

Previous work has shown that rolling is the easiest motion to initiate (Ibrahim et al., 2003). Ibrahim et.al. (2003) reported that rolling happens at velocities one order of magnitude below the velocities associated with sliding and lift off.

In the paper by John et.al. (1991) a momentum balance was presented in order to find the critical force needed to initiate rotation about the contact radius. The critical force needed is

$$F_{cr} = \frac{\mp F_{ad}}{(R/a)\cos\theta \pm \sin\theta + (R/a)\sin(\phi-\theta)} \tag{5.27}$$

Where the top sign indicates rotation about point C and the lower sign about B on figure 14.
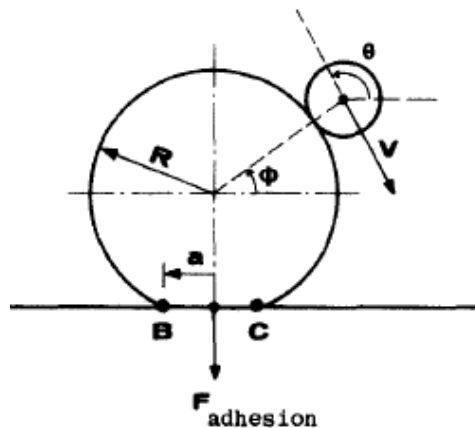
FIGURE 14-OFF CENTRE/OBLIQUE COLLISION (JOHN ET AL., 1991)

The force developed during a collision is calculated from the impulse required to stop the incoming particle, or

$$F_{impulse} = \frac{mv}{\Delta t} \tag{5.28}$$

Where m and v is the mass and velocity of the incoming particle, respectively, and Δt is the particle stopping time. John et.al. (1991) reports that the force developed during a collision is about 23 times bigger than the critical force in equation (5.27). This implies that any

impaction would lead to resuspension, however their experiment included a particle jet with very high velocities (40 m/s) and such velocities are not representative for heat exchangers.

The next question is what velocities are needed to separate the resting particle from the surface. The collision force needs to equal the critical force, equation (5.27). In John et.al. (1993) the analysis is given, and they presents two extreme cases.

1. The particles don't slip (infinite friction)
2. The particles slips (no friction)

The contact time, or stopping time, in equation (5.28) is determined by the velocity component along the line of centers, i.e. the line which connects the two particle centers

$$\Delta t = 4.02(2\rho k_p)^{0.4} \frac{R_1 R_2}{R_1 + R_2}(-V_1 \cos(\phi+\theta))^{-1/5} \tag{5.29}$$

Where $k_p = (1-\upsilon_p^2)/\pi E_p$ according to (John and Sethi, 1993) and υ and E is the poission ratio and Young's modulus, respectively, and the subscript p indicates the particle. R is the radius, and particle 1 indicates the incoming particle. ϕ and θ are the angles which determine the angle of impact and velocity, respectively, see figure 15 below. The contact time, equation (5.29), is based on the Hertz theory (John and Sethi, 1993).
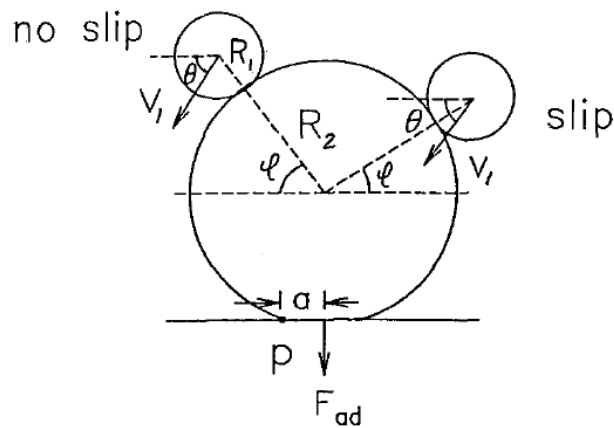
FIGURE 15-OFF CENTRE/OBLIQUE COLLISION. NO SLIP & SLIP (JOHN AND SETHI, 1993)

A momentum balance about point P gives

$$F_{impulse}[\sin\theta(R_2\cos\phi-a)+\cos\theta(R_2\sin\phi+R_2)]=F_a a \tag{5.30}$$

Where F_a is the adhesion force given by equation (4.5). By inserting equation (5.28) and (5.29) it is possible to solve for the velocity, which is the threshold velocity needed to separate particle 2 from the surface. The result is

$$V_{1T} = \left(\frac{6\sigma\pi a R_1 R_2}{m_1(R_1 + R_2)} \right)^{5/6} (2\rho k_p)^{1/3} [-\cos(\phi+\theta)]^{-1/6} \left(\sin\theta \left(\cos\phi - \frac{a}{R_2} \right) + \cos\theta(\sin\phi + 1) \right)^{-5/6} \quad (5.31)$$

Equation (5.31) is the no slip-situation.

For the slip situation the threshold velocity is

$$V_{1T} = \left(\frac{6\sigma\pi a R_1 R_2}{m_1(R_1 + R_2)} \right)^{5/6} (2\rho k_p)^{1/3} [\cos(\theta-\phi)]^{-1} \left(\cos\phi - \frac{a}{R_2}\sin\phi \right)^{-5/6} \quad (5.32)$$

John et.al. (1993) did some calculations with equation (5.31) and (5.32) with the following data:

$R_1 = 1.5\mu m$

$R_1 = 4.3\mu m$

$\sigma = 80.9\,\text{erg}/\text{cm}^2$ (1 erg = 10^{-7} J)

$\rho = 1.35\,\text{g}/\text{cm}^3$ for both particles

By setting $\theta = 57°$ they tried to find the minimum impaction velocity which resulted in resuspension. The no slip situation required a minimum threshold velocity of 0.12 m/s which was found at $\phi = 62.5°$. The slip required a higher threshold velocity of 0.17 m/s, which was found at $\phi = 28.5$. Compared to the threshold velocity associated with the vertical collision, which was 3.9 m/s, it is clear that oblique collisions are more effective when it comes to resuspension.

In chapter 7 a parameter study will be preformed to see how different variables such as radius, density, surface energy etc. affect the threshold velocities.

5.6. PARTICLE IMPACTION WITH POWDERY LAYER

The next topic is powdery layer. What happens when a dusty layer is hit by an impacting particle? In the previous chapter the collision of a single particle hitting another single resting particle was examined, Abd-Elhady (2004, 2005, 2006) took this knowledge a bit further and investigated how a layer exposed to both a shear and impaction, will behave.

To avoid particulate fouling with shear stresses, Abd-Elhady defines a critical flow velocity at which the particle stick to the surface. Small particles require a higher critical flow velocity

than larger particles do, this is supported by both theoretical and experimental arguments (Abd-Elhady et al., 2004). figure 16 gives the critical velocity for different particle sizes
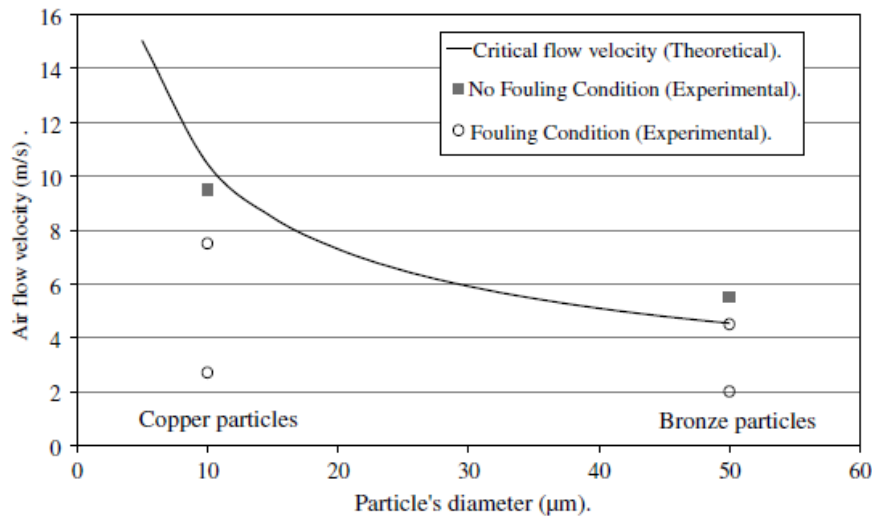
FIGURE 16-CRITICAL FLOW SPEED FOR DIFFERENT PARTICLES SIZES (ABD-ELHADY ET AL., 2004)

The experiment by Abd-Elhady had a particle distribution ranging from 1 to 20 μm and surprisingly no particles smaller than 10 μm settled on the tube. The assumption is that these were removed by bigger impacting spheres. This lead to a lower critical velocities for the smallest (<10 μm) particles than figure 16 indicates. In the conclusions Abd-Elhady et.al. (2004) admits that knowledge regarding how different particle sizes interact, is limited. The effect caused by particle impaction onto a powdery layer is nor understood, but was later investigated by Abd-Elhady himself in 2006. The 2006-paper by Abd-Elhady is the background for this chapter.

5.6.1. THE SIMULATION SETUP

A 20x20xN bed of particles with equal material and diameter was laid down on a steel surface. Where N was the number of particles in the height, and was set equal to 1, 2, 3, 5 and 10. For the data reported in Abd-Elhady (2006) N=3, the porosity 0.4 and the particle material was copper. All the particles had a diameter of 50μm.

The impacting particle hit the bed particle at three different angles (90˚, 80˚ and 70˚) and at different velocities starting from 0.025 m/s and increased to 2m/s with a step of 0.025 m/s. The angle of impact is indicated at figure 17. The computer simulation represents a time difference of 3μs real time and required 2.4 hours of computation time for N=3. The computational time grew fast and reached 10.4 hours for N=10. With a time difference of only 3μs, the effect of gravity is neglectable.

48
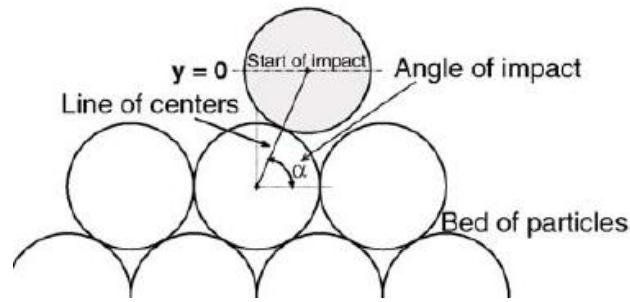
FIGURE 17-50MICROMETER COPPER PARTICLE IMPACTING A POWDERY LAYER (ABD-ELHADY ET AL., 2006)

5.6.2. DISPLACEMENT

If the particle has too little inertia upon impact, it will stick due to reasons already discussed. For greater velocities it will rebound and resuspend already fouled particles. From figure 19 page 50 it can be seen that the particle stick if the particle is below 0.05m/s if the angle of impact equals 90˚. If the angle of impact is 80˚ or 70˚ the particle stick at velocities below 0.1 and 0.15 m/s, respectively. This is shown through the displacement which equals

$$\delta = (R_1 + R_2) - |\vec{r}_1 - \vec{r}_2|$$ (5.33)

figure 18 explains equation (5.33)
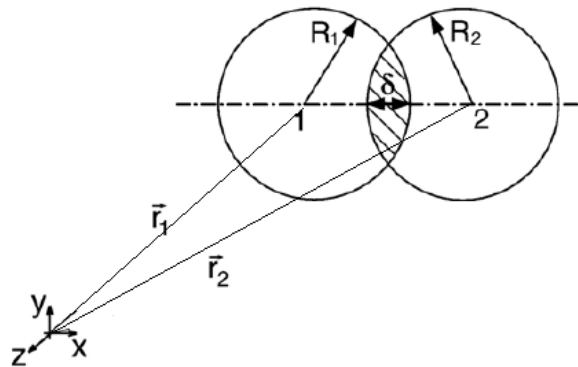
FIGURE 18-PARTICLE DISPLACEMENT (ABD-ELHADY ET AL., 2006)

Sticking occurs if the displacement is zero after the collision.

49
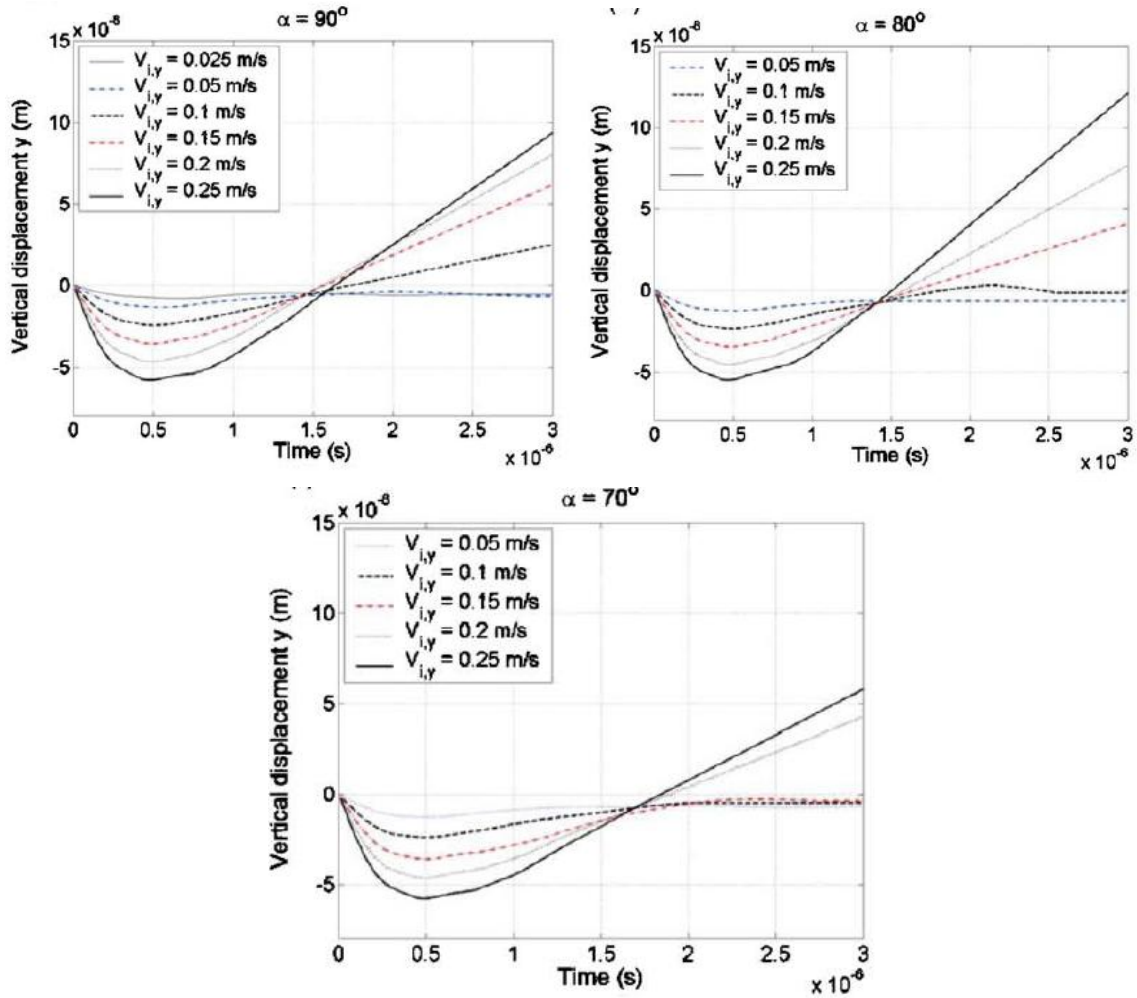
FIGURE 19-DISPLACEMENT FOR A 50MICROMETER PARTICLE HITTING A 20X20X3 BED OF PARTICLES (ABD-ELHADY ET AL., 2006)

5.6.3. EJECTION TIME

The ejection time, i.e. the time needed for an incoming particle to rebound, is roughly 1.5µs for all situations in figure 19. N=3 for all the plots in figure 19, and the ejection time was found to be independent of incoming velocity and angle of impact. It is however dependent on the number of layers, particle diameter and material properties. A thick layer will dampen the incoming particle more effectively and thereby increase the ejection time. Abd-Elhady (2006) reports that the ejection time is related to the number of beds as

$$t_{ejection} = C_1 \cdot N^{C_2} \ [\mu s] \tag{5.34}$$

Where C is some constant which varies with the diameter and material properties. See table below for the constants.

TABLE 3-CONSTANTS FOR DIFFERENT MATERIALS AND PARTICLE SIZES (ABD-ELHADY ET AL., 2006)

	C_1	C_2
Copper		
d=25µm	0.63	0.46
d=50µm	1.06	0.51
d=100µm	1.92	0.51
Steel		
d=25µm	n/a	n/a
d=50µm	0.3	0.5
d=100µm	n/a	n/a

From Table 3 it is usually assumed that C_2=0.5 forcing the ejection time to have square root dependency on the number of layers.

$$t_{ejection} = C_1 \sqrt{N}$$
(5.35)

Equation (5.35) gives an error of maximum 4% compared to the simulated results.

The ejection time is important because it gives an indication of the impulse force exerted by the incoming particle. This force is given by the linear momentum divided by the ejection time, see equation (5.28).

5.6.4. THRESHOLD VELOCITIES

The threshold velocities needed to cause rebound were 0.05, 0.1 and 0.15 m/s for 90˚, 80˚ and 70˚, respectively. But this is only the rebound limit, and no resuspension of already attached particles occurs at these velocities. In other word the velocity must be increased further to achieve the self cleaning effect which is wanted for heat exchanger. Fortunately 0.15 m/s is not a high velocity when regarding heat exchangers, so the outlook at this point is quite optimistic.

Abd-Elhady et.al. have done both theoretical (Abd-Elhady et al., 2006) and experimental (Abd-Elhady and Rindt, 2003) tests to resuspend particles from a powdery layer by impaction. A resuspended particle was photographed right after impaction, see figure 20. The picture it says two rebounds, which is the total number of particles leaving the surface after collision, i.e. the incoming particle plus a previously attached particle.
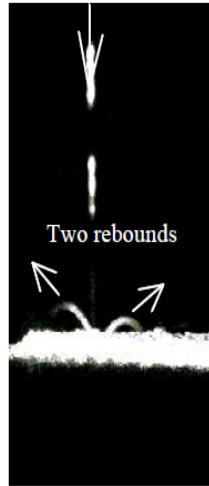
FIGURE 20-PARTICLE HITTING A BED. INCOMING VELOCITY 1.3 M/S. TWO RESUSPENSIONS (ABD-ELHADY AND RINDT, 2003)

By simulating impaction with a powdery layer at different velocities, Abd-Elhady (2006) presented a figure which described how many particles which detached as a function of the incoming velocity.
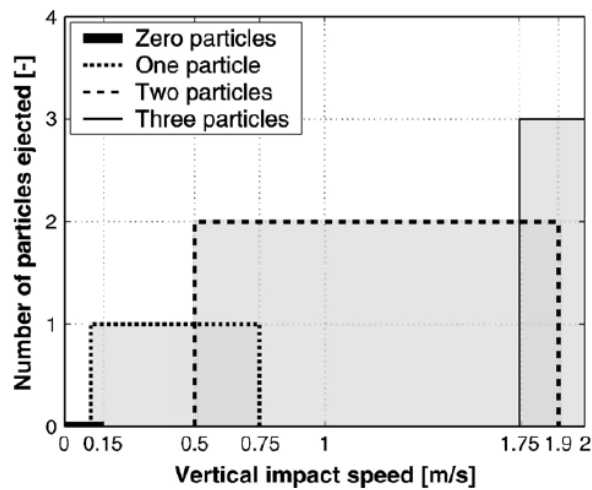
FIGURE 21-NUMBER OF DETACHED PARTICLES GIVEN AS FUNCTION OF INCOMING VELOCITY (ABD-ELHADY ET AL., 2006)

The simulated results do not deviate much from experimental data. The experimental results are given in figure 22.
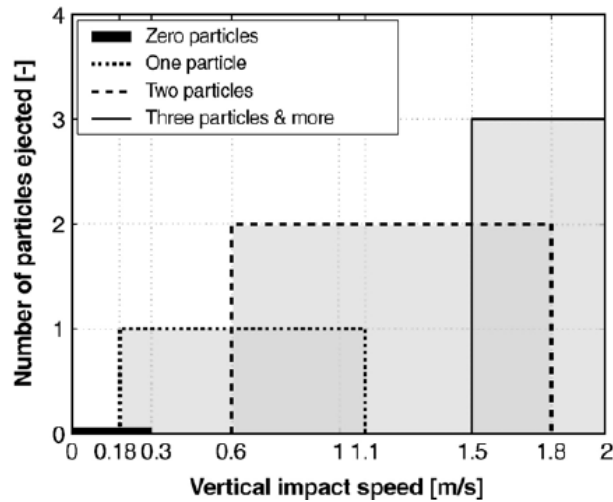
FIGURE 22-NUMBER OF DETACHED PARTICLES GIVEN AS FUNCTION OF INCOMING VELOCITY, EXPERIMENTAL VALUES (ABD-ELHADY ET AL., 2006)

The overlapping areas are explained by difference in impact angles.

The table below compares the simulated and experimental results.

TABLE 4-THEORETICAL AND EXPERIMENTAL THRESHOLD VELOCITIES

	Simulation	Experiment
Sticking velocity	0.15 m/s	0.3 m/s
1 particle rebound	0.1 m/s	0.18 m/s
2 or more particle rebound	0.5 m/s	0.6 m/s

5.7. RESUSPENSION OF DEPOSITED PARTICLE BY DRAG AND AEROSOL COLLISION

The results by Marshall (2007) were also presented in chapter 5.1, and the reader should be familiar with some of the conclusions from that paper. Two of the most important notes in Marshall's conclusion are:

- Particle lift off is not directly related to fluid forces, but to collision and adhesion to a passing particle or aggregate

- The capture for the smallest particles is governed by interaction between aggregates in the flow and aggregates attached to the wall. Meaning that the smallest particles are transported to the wall not as single particles, but as aggregates.

Based on Marshall's computations it is not sufficient to look at a single particle attached to the wall. The powder-layer simulation by Abd-Elhady is a more realistic approach, but the effect of a resting aggregate is still to be highlighted.

The oxford dictionary defines an aggregate as "a structure formed from by particles loosely compacted together." Note that the definition does not demand a specific structure, so an aggregate is a randomly composed structure. Loosely compact means that the building blocks are not sintered together.

Before the collision model is presented, a closer look on how small particles behave inside a channel is in order. Marshall presented the adhesion parameter, see equation(5.2), which indicates how particles position themselves in a channel flow; a big adhesion parameter gives high concentration of particles close to the wall, and these particles are likely to form aggregates. See figure 8 on page 34. Although Marshall's computation was with laminar flow, which is not the case for most heat exchangers, the effect of aggregate concentration close to the wall is considerable. A turbulent flow on the other hand, would cause rapid mixing, and therefore reverse the effect of the adhesion parameter.

figure 23 shows the particle concentration and the accompanying velocity profile for two different adhesion parameters.
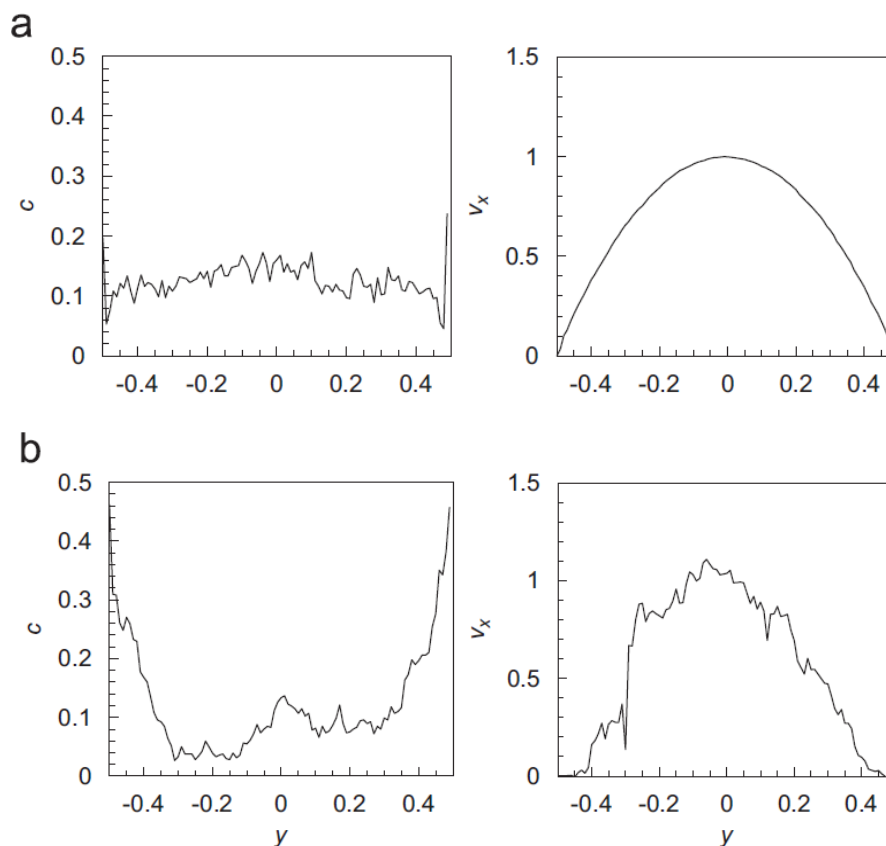
FIGURE 23-PARTICLE CONCENTRATION AND VELOCITY PROFILES FOR DIFFERENT ADHESION PARAMETERS, 1.5 (TOP) AND 150 (BOTTOM) (MARSHALL, 2007)

54

A low adhesion parameter will distribute the particles uniformly across the flow channel, and a high parameter will concentrate the particles in the near wall area. The latter will increase the formation of aggregates and also influence the velocity profile (Marshall, 2007), as figure 23 indicates.

In the reentrainment model soon to be presented, the surface is assumed smooth. The contact between the resting aggregate and surface is determined by the separation distance between of the primary particles and the surface. The primary particles, which make up the aggregate, are all spherical and the aggregate is characterized by a diameter $D_{ag} = k_0 D_p$ where D_p and k_0 is the diameter of the primary particle and a model constant, respectively. k_0 indicates how big the aggregate is compared to the primary particles. The aggregate is assumed to be small and thereby completely inside the viscous sublayer, further the sublayer is described purely as a shear flow and is undisturbed by both the aggregate and outer flow turbulence (Theerachaisupakij et al., 2003).

The collision is so-called centered collision, i.e. the direction of the incoming particle is parallel to the normal vector of impact. The model also assumes that this direction is parallel to the line connecting the two mass centers. The latter is of course always true for a spherical particle, but needs to be defined here because the target is an aggregate.
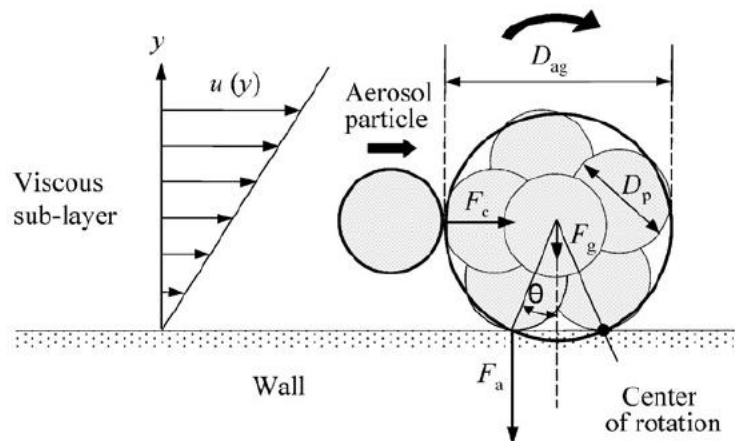
FIGURE 24-SINGLE PARTICLE HITTING AN AGGREGATE (THEERACHAISUPAKIJ ET AL., 2003)

There are in total 4 forces on figure 24; gravity, adhesion, collision and drag. To analyze the resuspension a moment balance will be set up around the point "centre of rotation".

5.7.1. ACTIVE FORCES

This chapter will present the forces which are active in the model; the forces are also indicated on figure 24.

5.7.1.1. ADHESION

The moment caused by adhesion is counter clockwise and given by

$$M_A = F_A D_{ag} \sin \theta \qquad (5.36)$$

Where F_A is the adhesion force. Generally equation (4.5) is used for the adhesion force, but Theerachaisupakij et.al. (2003) used the Hamaker constant instead. The review paper by Ziskind (2006) discusses the Hamaker constant and the method by Theerachaisupakij (2003) is in line with Ziskind's discussion. The adhesion force is given by

$$F_a = \frac{1}{12} A D_p L_e^{-2} \qquad (5.37)$$

Where A is the Hamaker constant and L_e is the separation distance between the particles and the wall. Most solids and liquids have Hamaker constant in the range $(0.4 - 4) \times 10^{-19} \text{J}$ (Ziskind, 2006) and in the present model $A = 2 \cdot 10^{-19} \text{ J}$ (Theerachaisupakij et al., 2003).

5.7.1.2. GRAVITY

The gravity also causes a counter clockwise moment and is given by

$$M_g = \frac{1}{2} F_g D_{ag} \sin \theta \qquad (5.38)$$

The gravity moment is small compared to the adhesion moment, actually two orders of magnitude less, thus it is neglected in the further analysis. The relative importance of gravity compared to the adhesion is shown in figure 25.
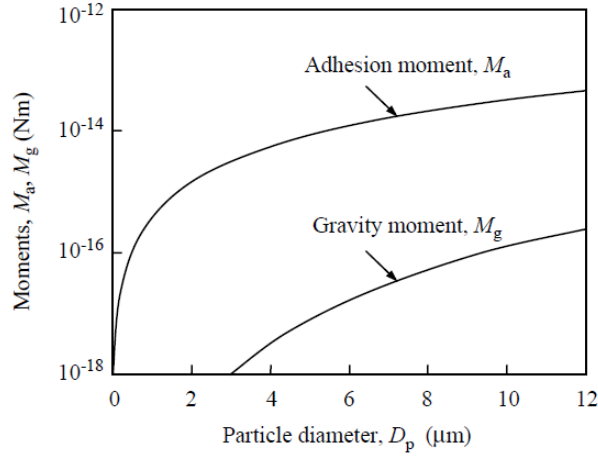
FIGURE 25-GRAVITY AND ADHESION MOMENT (THEERACHAISUPAKIJ ET AL., 2003)

5.7.1.3. DRAG (AERODYNAMIC FORCE)

The moment caused by the shear flow is approximately

$$M_d \approx \frac{15\pi}{16} \tau_w D_{ag}^3 \tag{5.39}$$

Where τ_w is the wall shear due to the shear flow, and is given by

$$\tau_w = 3.96 \cdot 10^{-2} \rho_f \upsilon_f^{1/4} D_t^{-1/4} \overline{u}^{7/4} \tag{5.40}$$

Theerachaisupakij et.al. (2003) do not include any discussion about this expression in their paper, and further investigation should focus on the validity of equation (5.40). For now, however, it will be used as given in the original model. The experimental data in Theerachaisupakij (2003) did deviate slightly from the theoretical values, but they gave the same trends. This gives equation (5.40) some reliability.

However, if equation (5.40) should fail, the error will not be transmitted into the parameter study in chapter 7 nor into the programmed models in chapter 6.2.3, because there the shear drag is neglected. The only resuspension force considered there is the collision force.

In equation (5.40) υ_f and ρ_f is the kinematic viscosity and density of the fluid, respectively, and D_t is the external diameter. $\overline{u}$ is the averaged velocity in the channel.

57

5.7.1.4. COLLISION (IMPULSE FORCE)

The collision moment is given by

$$M_c = \frac{1}{2} F_c D_{ag} \cos\theta \qquad (5.41)$$

Theerachaisupakij (2003) only looks at the maximum collision force. This force is the one which could cause an inceptive rotation for the aggregate. As discussed earlier, once an inceptive motion is started the particle is assumed to be resuspended. The maximum collision force is given by

$$F_c = 1.12 k^{-2/5} m^{3/5} D^{1/5} v^{6/5} \qquad (5.42)$$

Where v is the collision velocity which equal to the air flow in the height of impact. To find this velocity the law of the wall (chapter 2.2.9) is a possible method. k equals the left hand side of equation (5.8), that is $k = (1-v_1^2)/E_1 + (1-v_2^2)/E_2$, m and D is the weighted mean of mass and diameter, respectively, both given by $m_1 m_2/(m_1 + m_2)$ and $D_1 D_2/(D_1 + D_2)$. 1 and 2 refer to the colliding particle and target aggregate, respectively.

5.7.2. MOMENTUM BALANCE

The gravity is already neglected because it is two orders of magnitude less than the adhesion force for a certain particle size, which leaves only the adhesion to withstand the sum of drag and collision force. Is it possible to neglect either the moment caused by drag or collision? It actually depends on the average fluid velocity and size of the particles. This is illustrated in figure 26. In region 1 the drag is dominating compared to the collision, and in region 2 the collision moment is largest.

58
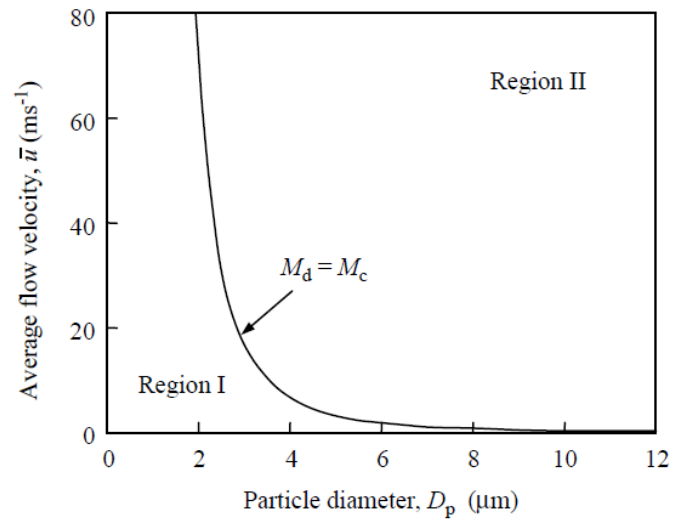
FIGURE 26-RELATIVE IMPORTANCE OF AERODYNAMIC AND COLLISION MOMENTS (THEERACHAISUPAKIJ ET AL., 2003)

figure 27 is the same as figure 26, but zoomed in for particles larger than 5µm.
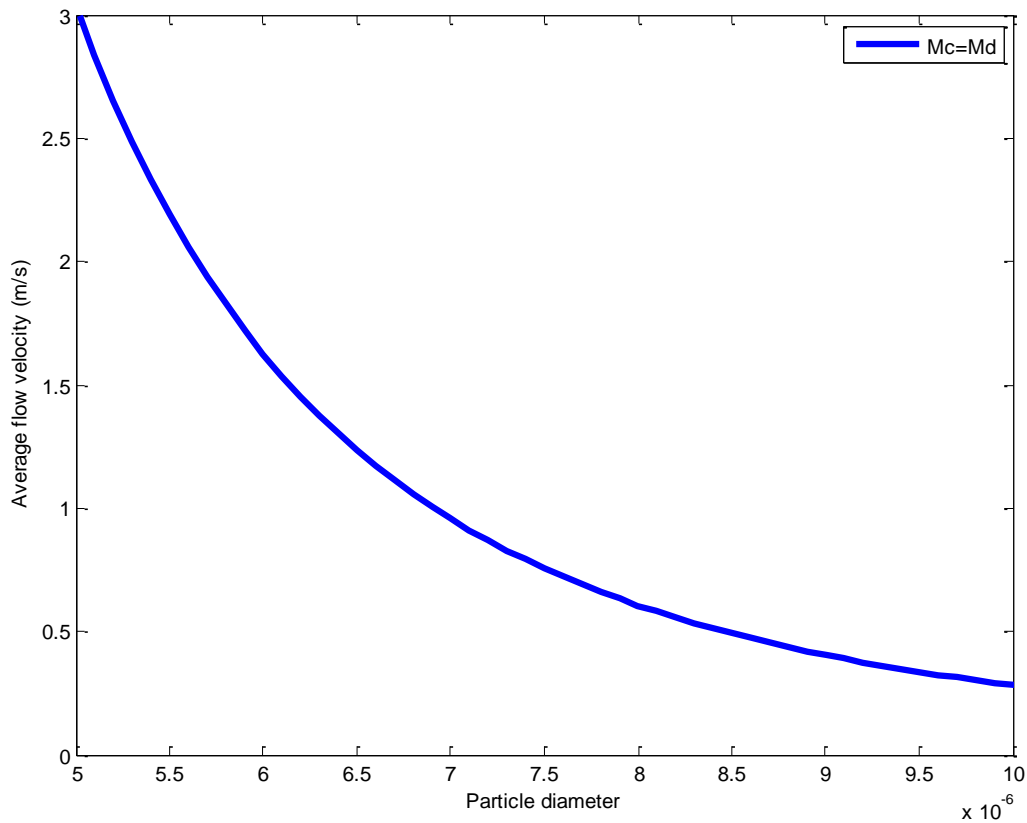
FIGURE 27-RELATIVE IMPORTANCE OF AERODYNAMIC AND COLLISION MOMENTS. THEY ARE EQUAL ON THE BLUE LINE

From figure 26 and figure 27 it is reasonable to assume that for particles larger than 5μm, the collision moment is the most significant resuspension mechanism since the velocities easily reach values greater than the blue line. In *"Appendix 3 – Hydrodynamic moment to collision moment"* the reader will find a colourplot which visualizing the ratio between collision momentum and hydrodynamic at different fluid velocities.

The graphs above are based upon the following physical constants

TABLE 5-CONSTANTS USED IN MATLAB-SIMULATIONS

A	2×10^{-19} J	Hamaker constant
D_t	7.8×10^{-3} m	Channel diameter
K	0.1 Pa	$(1 - v_1^2)/E_1 + (1 - v_2^2)/E_2$
K_0	2	Ratio between incoming particle and resting particle
L_e	5.5×10^{-9} m	Space between particle and surface

tanθ	0.3	
ν$_f$	1.55×10^{-5} m^2/s	Fluid kinematic viscosity
ρ$_f$	1.18 kg/m^3	Fluid density (air)
ρ$_p$	4000 kg/m^3	Particle density (Alumina)
Φ	0.25	Particle packing fraction

Note that the graphs only discuss the *ratio* between the collision and hydrodynamic moment, and nothing is said about whether or not a collision leads to resuspension. The way to quantify this is to look at the balance between the combined drag and collision moment to the adhesion moment:

$$\frac{M_d + M_c}{M_a} \tag{5.43}$$

The resting particle/aggregate will resuspend if the ratio is larger than one. But if the velocities are above the blue line in figure 27 than M_d could be neglected. In equation (5.43) the different moments are as follows:

Combining equation (5.36) and (5.37) gives

$$M_a = 0.0833 A L_e^{-2} k_0 \sin \theta D_p^2 \tag{5.44}$$

Equation (5.39) and (5.40) gives

$$M_d = 0.117 \rho_f \upsilon_f^{1/4} D_t^{-1/4} k_0^3 D_p^3 \bar{u}^{7/4} \tag{5.45}$$

Equation (5.41) and (5.42) gives

$$M_c = 0.00343 \upsilon_f^{-9/10} D_t^{-3/10} k^{-2/5} \rho_p^{3/5} \phi^{3/5} (1+k_0^3 \phi)^{-3/5} (1+k_0)^{-1/5} \cos \theta D_p^{21/5} \bar{u}^{21/10} \tag{5.46}$$

For derivation of equation (5.46) the reader is referred to (Theerachaisupakij et al., 2003).

5.7.3. STATISTICAL TURBULENCE

In this chapter statistical turbulence will be introduced to the model by Theerachaisupakij (2003) presented in the previous chapter. The turbulence will be described by what is known as the turbulent intensity, which is the RMS-value of the fluctuating component given as a percentage of the average velocity, or

$$\frac{u_{RMS}}{\bar{u}} = \text{constant} \qquad\qquad (5.47)$$

Where $u_{RMS} = \sqrt{\overline{u'^2}}$ is the fluctuating RMS-value in the streamwise direction. Similar expressions are possible for the two other dimensions. This turbulent intensity will be introduced into equation (5.46) and the model.

Klebanoff (1995) have measurements of the turbulent intensities for all three dimensions. His results indicate that all the intensities vary from zero at the wall to about 10% at the inner part of the boundary layer. See figure 28.
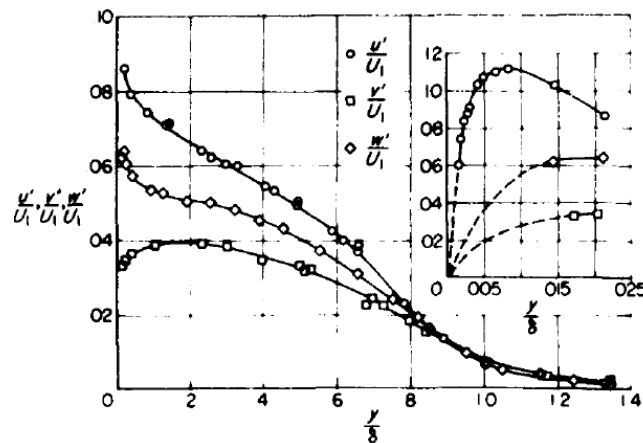
FIGURE 28-TURBULENT INTENSITIES FOR A FREE TURBULENT SHEAR FLOW (KLEBANOFF, 1955)

figure 28 also shows that the turbulent intensity is less for the y and z direction than for the stream wise direction. Before the turbulence is introduced into the model, the static critical flow velocities for different particle sizes are calculated and plotted in figure 29. The physical data used in the calculations are the same as those given in Table 5.
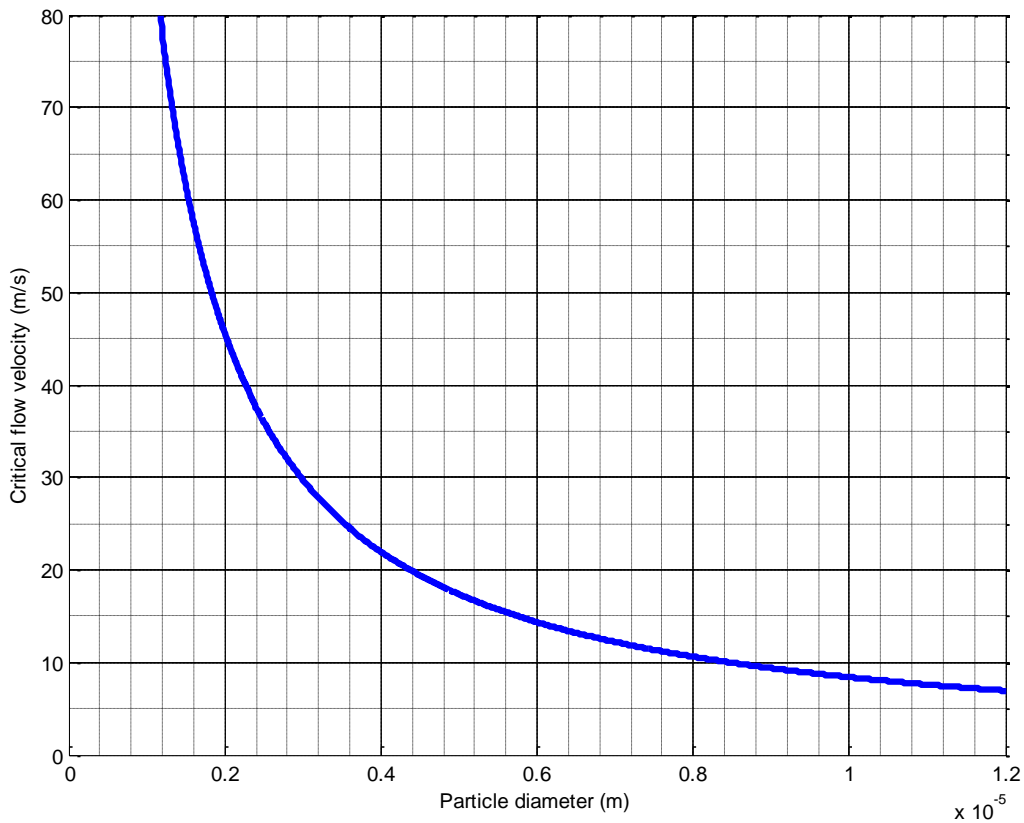
FIGURE 29-CRITICAL AVERAGE FLOW VELOCITY FOR REENTRAINMENT BASED ON PURE COLLISION-ADHESION MOMENT BALANCE (THEERACHAISUPAKIJ ET AL., 2003)

To show the effect of turbulence, two selected particle diameters, say 5μm and 10μm, will resuspend if the flow velocity is larger than 17.4 m/s and 8.4 m/s, respectively. In a real flow, however, a smaller *average* velocity will at some periods of time have instantaneous velocities higher than the critical. This results that a 10μm-particle may resuspend even if the average velocity is less than 8.4 m/s. Likewise the instantaneous velocity will sometimes be less than 8.4 m/s even when the average is larger. To simulate this turbulent effect it is assumed that the turbulence is normally distributed around the average. The standard deviation is represented as the turbulent intensity, i.e. 10% of the average for the streamwise component.

Statistical turbulence is another way of solving the closure problem of turbulence. Previously only the mean averaged quantities were considered. Statistical analysis highlights properties related to the fluctuations which is lost in time averaging, such as frequency, space-time correlations and interactions between the different fluctuations, e.g. the Reynolds stresses (White, 2011a). More information about statistical turbulence is available in Tenneks and Lumley (1972).

63

A justification to the choice of a normal distribution as the PDF (probability density function) for the velocity is important. First of all the normal distribution is well known to most engineers, and secondly easily implemented into computer codes since most common high-order programming languages (e.g. MATLAB) have pre-installed packages to handle a normal distribution. When deciding which PDF to implement the programmer/engineer should anyway have some measuring data from the flow itself, because in some situations the normal distribution is a bad choice. The central moments will decide whether or not a Gaussian/normal distribution is good or bad for a statistical description of a turbulent flow, and the method of revealing the central moments will be discussed briefly on the following pages. The discussion about statistical turbulence is also available in the literature, and the writer recommends the textbook by Tennekes and Lumley (1972) for first time readers.

Let's assume the signal $u = \bar{u} + u'$ is measured with a high frequent device, e.g. a hot wire, over a time period of T. Then sometimes the signal is inside the interval Δu, and the total fraction of time the signal is inside Δu is

$$\frac{1}{T}\sum_i \Delta t_i \tag{5.48}$$

Where Δt_i is the time the signal is inside that particular interval. From statistical theory the probability of finding u in one particular interval is

$$B(u) \cdot \Delta u = \lim_{T \to \infty} \frac{1}{T}\sum_i \Delta t_i \tag{5.49}$$

Where $B(u)$ is the probability density. The mean velocity is given by

$$\bar{u} = \int_{-\infty}^{\infty} u B(u) du \tag{5.50}$$

A common procedure is to subtract the mean from the signal, and then get the fluctuation

$$u' = u - \bar{u} \tag{5.51}$$

The first central moment is

$$\int_{-\infty}^{\infty} u' B(u) du \equiv 0 \tag{5.52}$$

The second central moment is known as the variance

$$\int_{-\infty}^{\infty} u'^2 B(u) du = \overline{u'^2} = \sigma^2 \tag{5.53}$$

64

The observant reader will recognize the variance as the square of the standard deviation, i.e. the RMS-value discussed in equation (5.47). The standard deviation also represents the width of the probability density. Further, the variance is not affected if the PDF is unsymmetrical about the mean (Tennekes and Lumley, 1972)

The third central moment is on the other hand affected by unsymmetrical PDFs, and is given by

$$\int_{-\infty}^{\infty} u'^3 B(u) du = \overline{u'^3} \tag{5.54}$$

If the PDF is symmetrical about the mean, then $\overline{u'^3} = 0$, which is the case of a Gaussian/normal distribution. A frequently reported statistical parameter is the *skewness* $S = \overline{u'^3}/\sigma^3$. A positive skewness indicates that the PDF is skewed in the negative direction of the mean.

The firth central moment is

$$\int_{-\infty}^{\infty} u'^4 B(u) du = \overline{u'^4} \tag{5.55}$$

The flatness, frequently named kurtosis, is defined by $F = \overline{u'^4}/\sigma^4$. The flatness value is large if the probability function has thick 'tails', i.e. the probability to find values far away from the mean is big.

For a normal distribution: $S = 0$ and $F = 3$

The discussion about central moments is important because if the skewness and flatness of a signal is known, a standard PDF could be selected with some quantitative basis. But for now it is assumed a normal distribution for the velocity, and the discussion about central moments is left with this discussion.

5.7.4. STATISTICAL COLLISIONS

Lets again use the situation in figure 24 on page 55. A MATLAB-code is developed which calculates the probability that a collision has high enough velocity to resuspend the target particle, given an average flow velocity and particle diameter. E.g. what is the probability for a resuspension for a 5μm particle if the average velocity is 15 m/s? The answer is about 20%, see figure 30. The moment balance is purely based on collision and adhesion, so the shear drag is neglected $M_d = 0$ in equation (5.43). For a 5μm particle the critical average velocity was 17.4m/s, and if the turbulence is assumed normally distributed about the average it follows that in 50% of the collisions will lead to resuspension if the average velocity is 17.4

m/s. Below a plot of the resuspension fraction for a 5μm and 10μm is given as a function of the average flow velocity. Again the data in Table 5 is used in the calculations and the resuspension fraction is defined as

$$R_f = \frac{\text{number of resuspension}}{\text{number for collisions}}$$

(5.56)
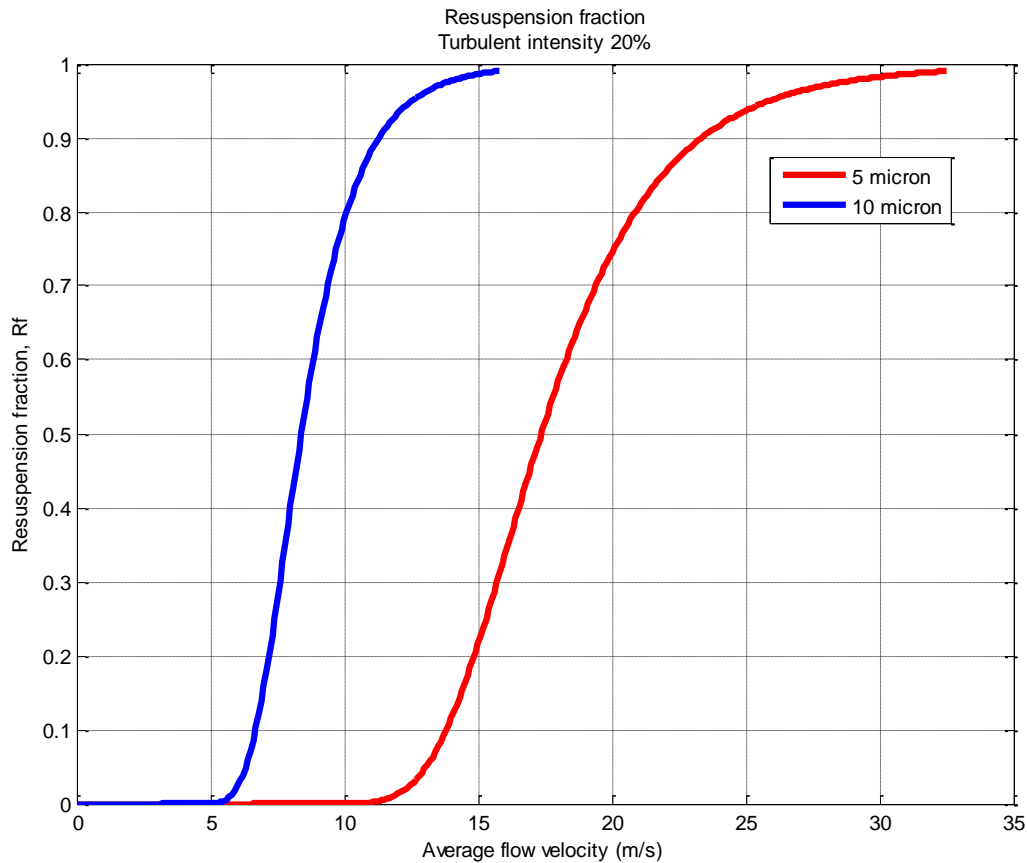
FIGURE 30-RESUSPENSION FRACTION FOR DIFFERENT PARTICLE SIZES

The turbulence intensity in figure 30 is 20%, which is twice the RMS-value suggested by Klebanoff (1955). A turbulent intensity at 40% has been reported (Hinze 1975). A higher intensity only gives a wider distribution of the PDF, but the flatness is still 3 as discussed earlier. In plain text this simply means that the turbulence force big fluctuations for the velocity. If a lower RMS-value is selected, the curves in figure 30 would have been steeper.

The computer code behind figure 30 is quite simple and will be presented here

TABLE 6-COMPUTER CODE WITH STATISTICAL TURBULENCE

```
% Physical constants should be placed here.
D_p = 10*10^-6;
U_crit = ucrit(D_p,A,D_t,k,k_0,z_e,theta,v_kin_f,rho_f,rho_p,phi);
u = 0;
frekvens = 0;
```

```
turb_intensity = 0.2;
j=1;
while j<=length(u) && frekvens(j)<0.99
    j=j+1;
    u(j)=u(j-1)+0.01;
    frekvens(j) = 1-sannsynlighet(U_crit,u(j),turb_intensity*u(j));
end
length(u);
length(frekvens);
plot(u, frekvens,'b')
hold all
```

```
function out = sannsynlighet( x,mu,sigma )
out = 0.5*(1+erf((x-mu)/(sigma*sqrt(2))));
end
```

```
function U_crit = ucrit(D_p,A,D_t,k,k_0,z_e,theta,v_kin_f,rho_f,rho_p,phi)
U_crit = 4.57*A^(10/21)*z_e^(-
20/21)*v_kin_f^(3/7)*D_t^(1/7)*k^(4/21)*rho_p^(-2/7)*phi^(-2/7)*k_0^(-
32/21)*(1+k_0^3*phi)^(2/7)*(1+k_0)^(2/21)*(tan(theta))^(10/21)*D_p^(-
22/21);
end
```

The first script defines a particle diameter and calculates the required critical average flow velocity, e.g. 5µm gives 17.4 m/s for the data used in Table 5. The initial average velocity and resuspension fraction (called `frekvens` in the code) are both set to zero. The while-loop calculates the resuspension fraction for all velocities up to the point where the resuspension fraction is 0.99.

The function `sannsynlighet` returns the cumulative density function for a normally distributed density, i.e. the probability to have the value `x` or lower, given a mean of `mu` and variance `sigma`.

The function `U_crit` returns the critical average velocity at which resuspension will happen if a collision takes place.

In figure 30 the resuspension fraction is plotted against the absolute velocity. An attempt to make the results universal is done by nondimensionalizing the velocity by the critical velocity, or

$$\Theta_u = \frac{u}{u_{crit}} \tag{5.57}$$

And the result is that the resuspension fraction is independent of the particle diameter when plotted against the nondimensional velocity.

Resuspension fraction vs. nondimensional velocity
Turbulent intensity 20%
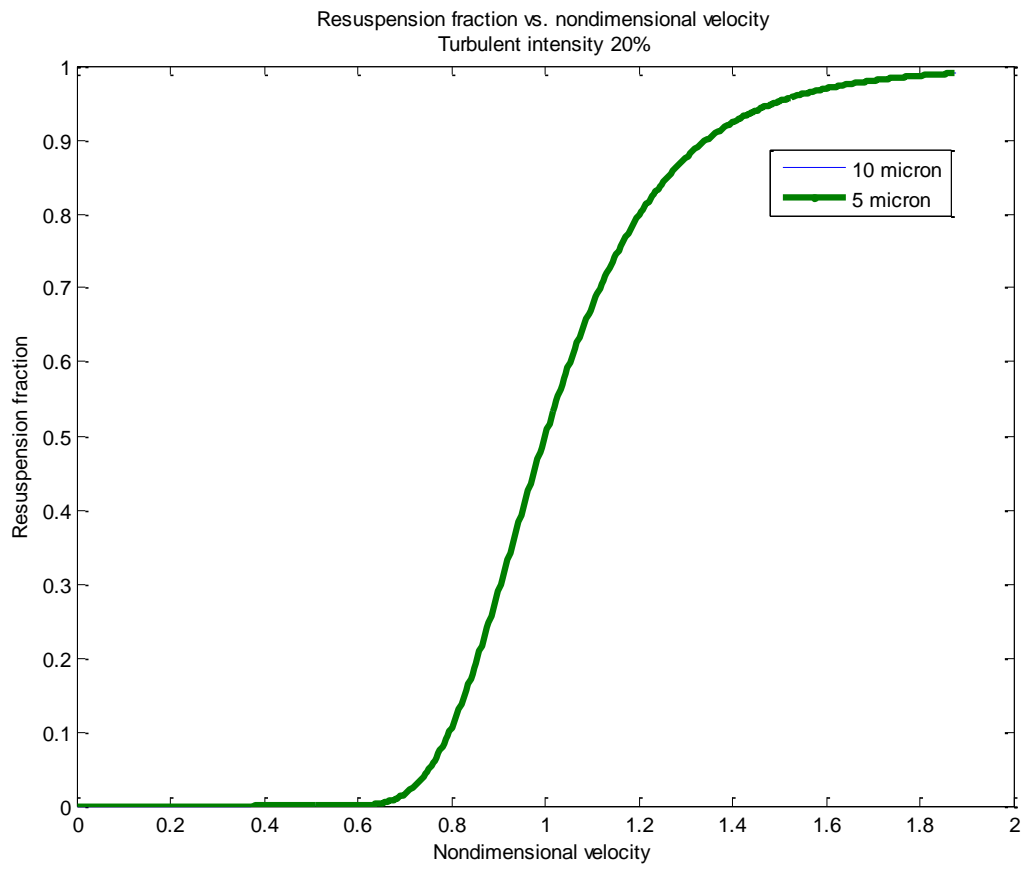
FIGURE 31-RESUSPENSION FRACTION VS. NONDIMENSIONAL VELOCITY FOR 10 AND 5 MICRON. TURBULENT INTENSITY OF 10%.

The effect of changing turbulent intensity is illustrated in figure 32.

Resuspension fraction for different turbulent intensities
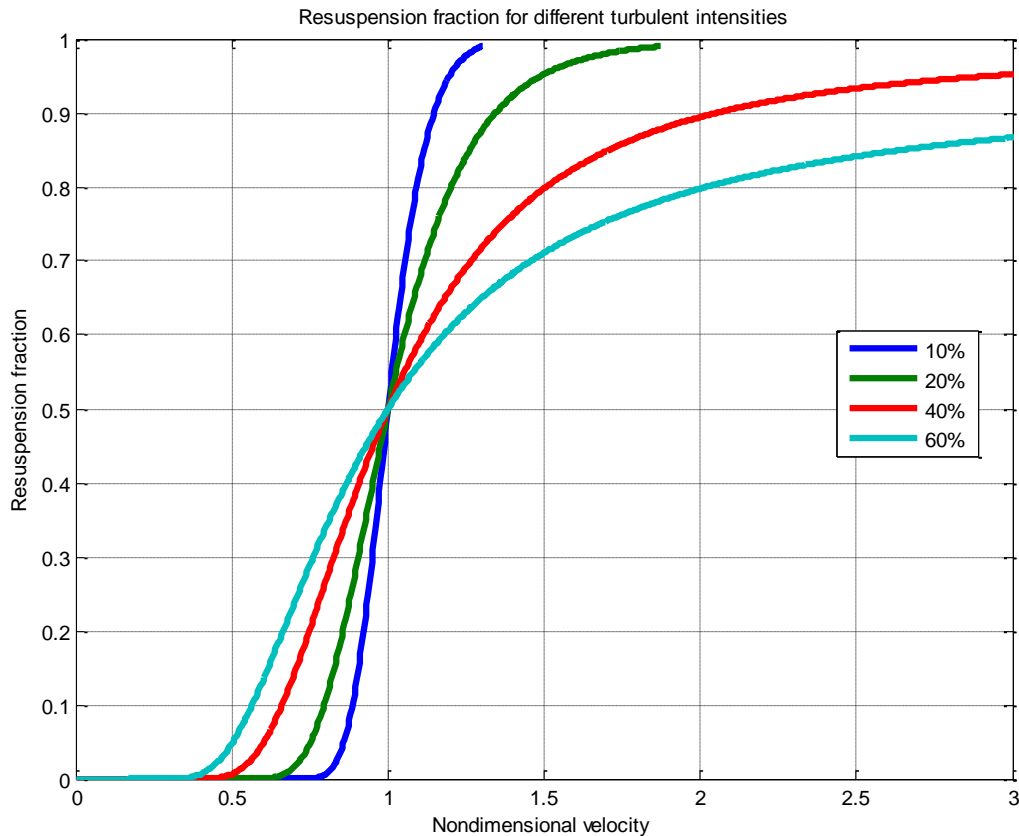
FIGURE 32-THE EFFECT OF TURBULENT INTENSITY UPON THE RESUSPENSION FRACTION

As can be seen from the figure above the resuspension fraction is 50% when the average velocity equals the critical velocity regardless of the turbulent intensity. At this velocity the incoming particle causes enough momentum to resuspend the target in 50% of the time, the reason is of course that the normal distribution is symmetrical about the mean. Increased intensity allows resuspension at a lower average velocity, e.g. if the intensity is 40% the resuspension fraction is about 20% when the average velocity is 75% of the critical velocity, whereas the corresponding resuspension fraction is 0% for an intensity of only 10%. This result is interesting when regarding heat exchangers, because in such equipment low velocities are wishful in order to avoid vibration problems (Næss, 2011), but low velocities also give low turbulent intensities, so there is a tradeoff between the avoidance of vibration and high turbulence.

To visualize how the turbulence intensity affects a turbulent signal, let's say the velocity, a small computer code was written in MATLAB to illustrate the effect. The fluctuating RMS-value was set equal to the intensity times the average and 4 simulations were carried out for two different intensities, 10% and 20% respectively. The result is plotted in figure 33.

69
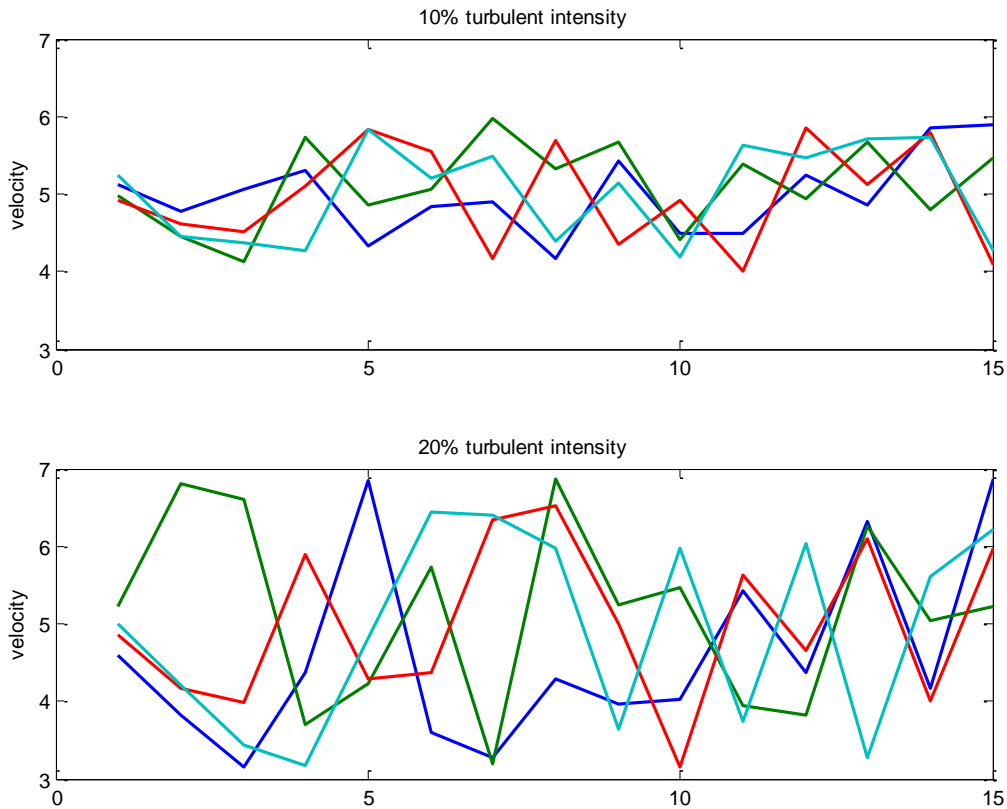
FIGURE 33-10% AND 20% TURBULENT INTENSITY. INSTANTENIOUS VELOCITIES, 5M/S AVERAGE

The RMS-value of the fluctuating equals 10% and 20% of the mean, and in the simulations the RMS-value is multiplied with 2 in order to cover 95% of the total spread of a normal distribution. That is twice the standard deviation.

6. MODEL IMPLEMENTATION

In this chapter three different collision models will be implemented. All the models have been presented previously, so the new information in this chapter is the MATLAB-version which the writer has implemented based on the different papers. The reason to implement the models into MATLAB-codes is to be able to carry out a parameter study. Parameters such as particle size, surface energy, Hamaker constant and mechanical constants (including the Young's modulus) will be studied chapter 7.

Differences in both the models themselves and results will be highlighted and discussed shortly.

The MATLAB-coding will be given in plain text, that way further parameter study and re-testing of the results is possible.

6.1.   DIFFERENCES BETWEEN THE MODELS

The three models implemented were the perpendicular collision/vertical (#1 in figure 34) and off-centre, or oblique, collision (#2) by John et.al. (1993) and the aggregate collision (#3) by Theerachaisupakij et.al. (2003). The different collisions are sketched in figure figure 34
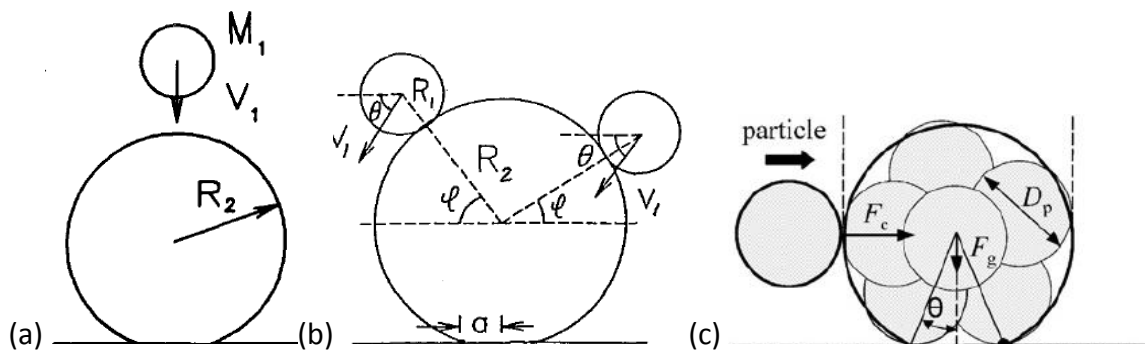
FIGURE 34-THE IMPLEMENTED MODELS. FROM LEFT MODEL #1, MODEL #2 AND MODEL #3. (JOHN AND SETHI, 1993, THEERACHAISUPAKIJ ET AL., 2003)

TABLE 7-DIFFERENCES BETWEEN THE IMPLEMENTED MODELS

	#1	#2	#3
Year of publish	1993	1993	2003
Active forces	Adhesion Collision/impulse	Adhesion Collision/impulse	Adhesion Gravity (neglected) Collision/impulse Hydrodynamic drag (not studied)

71

Adhesion	$F_a = \dfrac{3}{2}\sigma\pi r_p$	$F_a = \dfrac{3}{2}\sigma\pi r_p$	$F_a = \dfrac{1}{6}Ar_p L_e^{-2}$
Collision	$F_{impulse} = \dfrac{m_1 v_1}{\Delta t}$	$F_{impulse} = \dfrac{m_1 v_1}{\Delta t}$	$F_c = 1.12k^{-2/5}m^{3/5}D^{1/5}v^{1/6}$ See equation (5.42) for description
Resuspension mechanism	Lift off	Rolling	Rolling
Resuspension criteria	Particle #2 must have kinetic energy after collision which exceeds the surface energy. The energy is transferred from particle #1 during the collision. Criteria: Incoming velocity must be above a *threshold velocity*	The collision torque during the collision must exceed the adhesion moment. The torque is given by the incoming velocity which in turn gives the maximum of the impulse force. The torque is based on this. As the torque is larger than the adhesion moment, the inceptive rolling motion starts. Resuspension is thereby assumed. Criteria: Incoming velocity must be above a *threshold velocity*	Collision moment must exceed the adhesion moment. Once that happens an inceptive rolling motion starts and the resuspension is assumed to happen. Criteria: Average flow velocity must be above a critical velocity.
Statistical	No. Possible to use statistical techniques for the adhesion parameter. Further work.	No. Possible to use statistical techniques for the adhesion parameter. Further work.	Yes. Turbulent statistics was implemented by the writer. Not in the original paper.

Where σ (surface energy), A (Hamaker constant), L_e (separation distance), Δt (collision time) given by Hertz theory

In model #3 both the gravity and hydrodynamic forces were neglected. The gravity was neglected because of the unimportance of this force; it was two orders of magnitudes less

than the adhesion. The hydrodynamic force was neglected because it is outside the scope of this thesis; however it should be included in simulation studies in the future because it is a dominating force.

Model #1 and #2 both considers one particle hitting another particle, while the target particle in model #3 is an aggregate. Aggregates will form on a heat exchanger surface if given enough time. Aggregates may also sinter, i.e. a type of melting and so-called neck-formation between the particles. Once this happens, separation is almost impossible by particle impaction (Abd-Elhady et al., 2007). Removal of sintered particles must be done with mechanical cleaning.

Model #2 allows changes in the incoming angle while #1 and #3 are static in the sense that they assume a vertical and horizontal angle of attack, respectively. This makes model #2 more realistic but harder to handle in MATLAB because the user needs to make sure that the input angles are physically reasonable.

Despite the differences between the models, the writer is under the impression that all the models combined cover a broad range of thinkable collisions in a heat exchanger; the vertical collision happens if a particle is thrown perpendicular towards a wall by an external eddy. The collision could also be oblique, and this is handled with model #2. A resuspended particle could also hit a neighboring particle after resuspension; this is most likely to happen with a horizontal angle. The aggregate-model is sort of a special case, but it is the only model of the three presented, which correlate the resuspension criteria to the free flow outside the boundary layer. Model #1 and #2 focuses on the critical impact velocity only, and not the velocity in the free stream.

Previous work has shown that rolling is the dominating resuspension mechanism. Direct lift off requires drastically higher impaction velocities and is often neglected due to this fact. The lift off-model is anyway included because the impaction velocities related to direct lift off is not frightfully high compared to velocities in a heat exchanger. E.g. the critical velocity in John et.al. (1993) was found to be 3.9 m/s.

Model #3 was originally not included with turbulent statistics. This was however implemented alongside with the programming done here. Turbulent statistics is not possible to implement in model #1 and #2 directly because neither of them regards fluid flow, only collision, and in future implementations statistical turbulence should however be introduced to these models as well. It is also possible to introduce statistical behavior to the adhesion, but in this thesis the adhesion is assumed static.

Note that model #1 and #2 uses the surface energy, whereas model #3 uses the Hamaker constant. The differences between the surface energy and Hamaker constant were discussed in chapter 4.

6.2. CODING

All the coding was done in MATLAB version 7.11.0 (2011b) available through the NTNU Software distribution.

6.2.1. MODEL #1

The first model required two .m-files. Generally the model runs equation (5.26) for different input parameters.

TABLE 8-COMPUTER CODE MODEL #1

```
function VT1 = vertical_plot(R2,R1)
%different physical properties is placed here
VT1 = vertical(rho1,rho2,R1*10^-6,R2*10^-6,y,kp,ks);
End
```
```
function VT1 = vertical(rho1,rho2,R1,R2,y,kp,ks)
K=4/(3*pi*(kp+ks));
a = ((6*y*pi*R2^2)/K)^(1/3);
VT1 = 1.63 * (1 + (rho2/rho1)*(R2/R1)^3) * (R2^-(5/6)) * (y^5/(rho2^3 *
K^2))^(1/6);
end
```

The code is constructed such a way that the operator calls the function `vertical_plot(R2,R1)` where R2 and R1 are the radius of the target particle and incoming particle in micrometers, respectively. All mechanical constants must be typed into the script pre-hand of the function call.

6.2.2. MODEL #2

The second model consists of two .m-files and is divided into *"no slip"* and *"slip". No slip* means that there is no motion perpendicular to the line of centers, and *slip* means that the particles may slide during collision. The "no slip" and "slip"-calculations use equation (5.31) and (5.32), respectively. Both situations have been implemented into MATLAB, but in order to save space only the "no slip" collision will be presented and discussed.

TABLE 9-COMPUTER CODE MODEL #2

```
function VT1 = noslip(R1, R2, theta, phi)
%different physical properties is placed here
M1 = rho1 * (4/3)*pi*R1^3;
K = 4 / (3*pi*(kp + ks));
a = ((6*y*pi*R2^2)/(K))^(1/3);

A = ((6*y*pi*a*R1*R2)/(M1*(R1+R2)))^(5/6);
B = (2*rho1*kp)^(1/3);
C = (-cosd(phi+theta))^(-1/6);
D = (sind(theta)*(cosd(phi)-a/R2) + cosd(theta)*(sind(phi)+1))^(-5/6);
```

```
VT1 = A*B*C*D;

end
```

The second .m-file is a plotting script which plots the threshold velocity for different attack angles. From the first .m-file it was observed that the threshold velocity was dependent on the collision angle, and by acknowledging that this angle is sort of a random variable, the minimum threshold velocity was found by calculating the threshold velocity for all possible collision angles given R_1, R_2 and θ (the velocity angle).

TABLE 10-COMPUTER CODE MODEL #2 PLOTTING

```
%different physical properties is placed here
VT1 = noslip(rho1,rho2,R1,R2,y,kp,ks,phi,theta);
j=1;
while phi(j)<=100
    phi(j+1)=phi(j)+1;
    VT1(j+1)=noslip(rho1,rho2,R1,R2,y,kp,ks,phi(j+1),theta);
    j=j+1;
end
figure(1),clf
plot(phi,VT1)
```

6.2.3. MODEL #3

The third model balances gravity, adhesion, collision and hydrodynamic drag and assumes that once an inceptive motion has started, the aggregate will resuspend. Only the static model will be presented here, the turbulent statistics which the writer has implemented alongside the original model was presented in chapter 5.7.4. Further the gravity and hydrodynamic forces is neglected due to reasons already discussed.

TABLE 11-COMPUTER CODE MODEL #3

```
FUNCTION U_CRIT = COLLDRAGDYNDRAG(D_P)
%INPUT, MATERIAL AND MECHANICAL PROPERTIES
U_CRIT = 4.57*A^(10/21)*Z_E^(-
20/21)*V_KIN_F^(3/7)*D_T^(1/7)*K^(4/21)*RHO_P^(-2/7)*PHI^(-2/7)*K_0^(-
32/21)*(1+K_0^3*PHI)^(2/7)*(1+K_0)^(2/21)*(TAN(THETA))^(10/21)*D_P^(-
22/21);
END
```

The function `colldragdyndrag` returns the critical average flow velocity at which a collision is capable to resuspend an attached aggregate. The aggregate is composed of spheres of equal size as the incoming particle, and is described by the diameter ratio `k_0` being the diameter of the aggregate to the primary particle. The aggregate is also defined by a packing density, i.e. the number of particle to the occupied volume.

7. PARAMETER STUDY

In this chapter studies the effect of some of the parameters in each model. The effect is quantified through the uncertainty, or sensitivity, for each studied variable. The sensitivity is, which you will see shortly, dependent on the initial values of the system. For example the change in threshold velocity for a 1μ-particle colliding with a 4μ-particle, is dramatic if the incoming particle's size is changed to 2μm instead. The change in threshold velocity regarding that particular situation, is larger than if the incoming particle had been changed from 2μm to 4μm while the target particle was constant at 8μm, despite the fact that the relative change is the same. The reason is of course that the adhesion is relatively more important for a 4μ-particle than an 8μ-particle when relating it to the relative mass of each size. The adhesion is proportional to the radius while the mass is proportional to the radius cubed.

The uncertainty is calculated by the following formula

$$\omega = \sqrt{\sum \left(\frac{\partial DV}{\partial \chi} \Delta \chi \right)^2} \qquad (7.1)$$

Where ω is the uncertainty, DV indicates dependent variable and χ is the parameter. The dependent variable could be either the threshold velocity (model #1 and #2) or the free stream velocity (model #3).

The parameter study presented here has unfortunately no experimental support. The laboratory work which should have been finished within the hand-in-date was delayed. The wind tunnel section is finished and up and running at the time of writing, but a fouling experiment is out of reach before the hand-in-date.

7.1. MODEL #1

The material properties given in John et.al. (1993) will form the basis of this parameter study. That means that one variable will be changed sequentially in order to give the reader a fully picture of the physical importance of each parameter. This way of performing the parameter study was agreed between the writer and his supervisor, and therefore covering point 3 in the problem description; "defined in cooperation with the department". After the study of one parameter, that particular parameter will be set back to its initial values before a new parameter is changed. The initial (base) values for each simulation for both model#1 and model #2 are shown in Table 12.

TABLE 12-INITIAL VALUES MODEL #1 AND #2

Surface energy	0.00809 J/m^2
k_p	2.42E-10 m^2/N
k_s	1.43E-10 m^2/N
R1	2 μm
R2	4 μm
ρ1	1350 kg/m^3
ρ2	1350 kg/m^3

With these settings the threshold velocity is 1.49 m/s.

7.1.1. EFFECT OF RADIUS

The threshold velocity seems to decrease as the target particle gets bigger. This is due to the relative importance of the adhesion to the mass of the particle. The adhesion is linear to the radius whereas the impaction force is linear to the mass, which again is a function of the radius cubed. The threshold velocity also decreases when the size of the incoming particle increases, this is physically obvious.

Using equation (7.1) for each target size (4, 8 and 16 μm) gives an uncertainty of 9.4, 5.3 and 3.0, respectively. Again the uncertainty confirms that change in incoming radius is more important for small particles.

TABLE 13-PARAMETER STUDY EFFECT OF RADIUS

	$R_2 = 4$ μm	$R_2 = 8$ μm	$R_2 = 16$ μm
$R_1 = 0.25R_2$	10.82 m/s	6.07 m/s	3.40 m/s
$R_1 = 0.5R_2$	1.49 m/s	0.84 m/s	0.47 m/s
$R_1 = R_2$	0.33 m/s	0.19 m/s	0.10 m/s
$R_1 = 2R_2$	0.18 m/s	0.11 m/s	0.06 m/s
ω	9.4	5.3	3.0

7.1.2. EFFECT OF DENSITY

Also for the density the sensitivity decreases for increasing parameter. The threshold velocity's sensitivity to the density is however less compared to the sensitivity regarding radius. The reason is again found in the relative importance between the adhesion force and mass; the adhesion is independent of the mass, while the impaction force increases with the mass/density.

TABLE 14-PARAMETER STUDY EFFECT OF DENSITY

	$\rho_2 = 600$ kg/m^3	$\rho_2 = 1200$ kg/m^3	$\rho_2 = 1800$ kg/m^3
$\rho_1 = 0.5\rho_2$	4.24 m/s	3.00 m/s	2.45 m/s
$\rho_1 = \rho_2$	2.25 m/s	1.58 m/s	1.30 m/s
$\rho_1 = 2\rho_2$	1.25 m/s	0.88 m/s	0.72 m/s
ω	2.2	1.6	1.3

7.1.3. EFFECT OF K$_P$

The mechanical constants are given by equation (5.8), but John et.al. (1993) uses a slightly different form of the equation by multiplying the right hand side with $3\pi/4$. The expression for E^* is therefore

$$E^* = \frac{4}{3\pi(k_p + k_s)} \tag{7.2}$$

Where $k_j = (1-v_j^2)/\pi E_j$, and v_j and E_j is the poission ratio and Young's modulus, respectively. The poission and young's modulus are only indirectly studied by changing the two different k_j parameters.

TABLE 15-PARAMETER STUDY EFFECT OF MECHANICAL CONSTANTS

	Threshold velocity
$k_p = 0.25k_{ps}$	1.21 m/s
$k_p = 0.50k_{ps}$	1.32 m/s
$k_p = 1.00k_{ps}$	1.49 m/s
$k_p = 1.50k_{ps}$	1.64 m/s
$k_p = 2.00k_{ps}$	1.76 m/s
ω	0.3

Where k_{ps} is the standard value given in the paper, $2.42\cdot10^{-10}$ m^2/N.

The effect of k_p is little significant since the sensitivity in the threshold is only 0.3, which is about one order of magnitude less than the sensitivity connected to the radius and density.

The sensitivity connected to k_s is even less, only 0.16. The calculations for this one is left out here in order to save space, but it is possible to reproduce the data by putting the initial values into the MATLAB-script and performing the same parameter change as in Table 15.

7.1.4. EFFECT OF SURFACE ENERGY

The sensitivity towards the surface energy is about the same as the density. The effect of surface energy is compared with the effect of the Hamaker constant in chapter 7.3.1, and the relation between these two was presented in chapter 4.

TABLE 16-PARAMETER STUDY EFFECT OF SURFACE ENERGY

	Threshold velocity
$\sigma = 0.25\sigma_s$	0.47 m/s
$\sigma = 0.50\sigma_s$	0.84 m/s
$\sigma = 1.00\sigma_s$	1.50 m/s
$\sigma = 1.50\sigma_s$	2.10 m/s
$\sigma = 2.00\sigma_s$	2.67 m/s
ω	1.12

Where σ_s is the standard value given in the paper, 0.0809 J/m^2.

7.2.   MODEL #2

Model #2 is based on the same theory as model #1 is, therefore the parameter study for radius, density, mechanical constants and surface energy will not be repeated here. Here the effect of impaction angle and velocity angle will be highlighted.

The impaction angle is where the collision takes place on the target particle. The velocity angle is the angle at which the impacting particle travels. See figure 15 page 46. The impaction angle and velocity angle is given the symbols ϕ and θ respectively.

Another difference between model #1 and #2 is that the model #2 calculates the required velocity to initiate rolling of the target particle, while model #1 calculates direct lift off. Rolling is a much easier resuspension mechanism because the adhesion force must not be exceeded directly, only the moment about the contact point must be exceeded.

The parameter study will only include the *no slip*-situation from figure 15. This might seem a bit extreme, but the writer is under the impression that the difference between the perfect slip and no-slip is neglectable. This is also illustrated in the original paper by John et.al. (1993) where the models are presented. The minimum threshold velocities for the "no slip" and "slip" were 0.12 m/s and 0.17 m/s, respectively.

The procedure for the parameter study is that all the physical constants are set equal to those listed in the original pape, see table Table 12, except the radii which are set equal to 4 and 2 μm for the target and incoming particle, respectively. This procedure is the same as used for model #1. Then the velocity angle, θ, will be varied from 0 to 80 and for each velocity angle the threshold velocity will be calculated for each possible impaction angle.

The best way to represent the results is by a graph because the tabulated results will require too much space. In Table 17 however, the minimum threshold velocity is given for different velocity angle.

7.2.1. EFFECT OF VELOCITY AND IMPACTION ANGLE
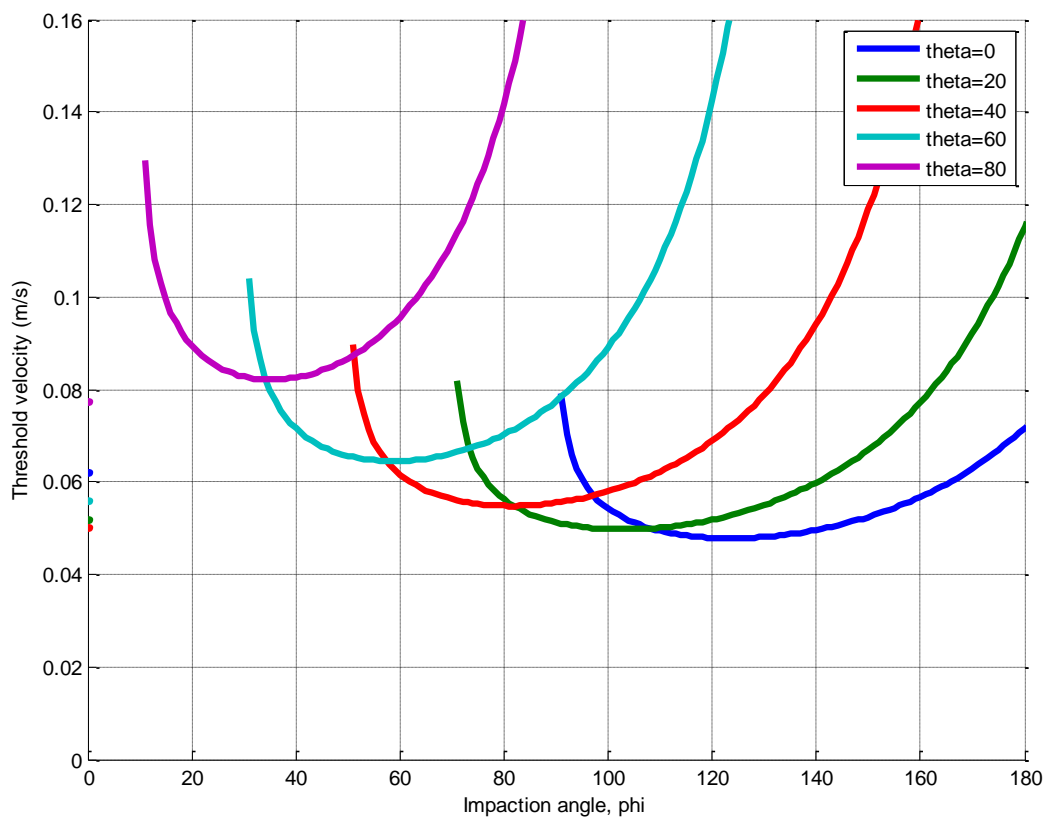
FIGURE 35-EFFECT OF VELOCITY AND IMPACTION ANGLE, MODEL #2

As can be seen from figure 35 the effect of increased velocity angle is that the bucket-graphs become thinner. The minimum value on the graphs also increases with increasing velocity angles.

In Table 17 the minimum threshold velocities are given for different velocity angles.

TABLE 17-PARAMETER STUDY EFFECT OF VELOCITY ANGLE (MINIMUM THRESHOLD VELOCITY)

θ (velocity angle)	Minimum threshold velocity	ϕ (impaction angle)

0˚	0.0478 m/s	122˚
20˚	0.0501 m/s	110˚
40˚	0.0548 m/s	82˚
60˚	0.0645 m/s	59˚
80˚	0.0821 m/s	35˚

The sensitivity related to the velocity angle is 0.02, in other words insignificant. This is also illustrated in Table 17 where the threshold velocity is only increased by a factor of 2 by varying the velocity angle 80˚. In other words a small change in the velocity angle does not affect the minimum required velocity for resuspension.

For $\theta = 0$ (that's a horizontal collision) the minimum threshold velocity is found at $\phi = 122$ (that's on the upper right section of the sphere on figure 34b, remember that the no-slip is the considered collision in this parameter study.) For $\theta = 20°$ the minimum threshold velocity is found at $\phi = 110°$, the rest is given in Table 17.

figure 35 illustrates the effect of a changing impaction angle too. The curves are wide buckets implying that a small change in ϕ doesn't change the threshold velocity much.

The fact that the threshold velocity is not very sensible to the velocity angle or the impaction angle is good news, this way it is possible to set a minimum required impaction velocity at which all impaction lead to resuspension. By setting this required velocity to, let's say, 0.2 m/s, it is very likely that any impaction will lead to resuspension. The values described here are of course only valid for 4µm (target) and 2µm (impactor) particles, and physical properties listed in Table 12. Any change in any of the physical values and sizes much be considered, and the effects of these changes were studied in the previous parameter study.

7.2.2. DECOMPOSITION OF THE INCOMING VELOCITY

The simulation are referred to the no-slip condition, as already discussed, which is the left hand side of the figure 15 page 46. In Table 18 the velocity is decomposed horizontal and vertical components.

TABLE 18-DECOMPOSED MINIMUM THRESHOLD VELOCITY

θ	Horizontal velocity component (m/s)	Vertical velocity component (m/s)
0	0.0478	0
20	0.0471	0.0171
40	0.0420	0.0352
60	0.0320	0.0559
80	0.0143	0.0809

The interesting thing now is to calculate the moment caused by each component about point P in figure 15. For this two extremes cases are considered, $\theta = 0$ and $\theta = 80$. The contact time is given by equation (5.29) for these collisions the contact time is $7.3049 \cdot 10^{-12}\,\text{s}$ and $6.859 \cdot 10^{-12}\,\text{s}$, respectively. The impulse for each component is calculated by equation (5.28) and tabulated in Table 19.

TABLE 19-DECOMPOSED IMPULSE FORCES

θ	Horizontal impulse (N)	Vertical impulse (N)
0	$2.9587 \cdot 10^{-4}$	0
80	$9.4269 \cdot 10^{-5}$	$5.333 \cdot 10^{-4}$

It is also possible to obtain these impulse forces by just decomposing the total impulse force. For $\theta = 0$ the moment arm is 7.39μm, for $\theta = 80$ the moment arms are 3.27μm and 6.29μm for the vertical and horizontal force, respectively. This results in the following moments

TABLE 20-DECOMPOSED MOMENTS

θ	Horizontal moment (Nm)	Vertical moment (Nm)
0	$21.86 \cdot 10^{-10}$	0
80	$5.93 \cdot 10^{-10}$	$17.43 \cdot 10^{-10}$

The sum of the moments is $21.86 \cdot 10^{-10}\,\text{Nm}$ and $23.36 \cdot 10^{-10}\,\text{Nm}$ for $\theta = 0$ and $\theta = 80$, respectively. A difference of 6.9% is observed.

This small decomposition has revealed that collision for both $\theta = 0$ and $\theta = 80$ causes roughly the same rolling moment on the target particle, which of course is suspected because each collision needs to counteract the same adhesion moment.

7.3.   MODEL #3

Some parameter study in model #3 has already been reported in chapter 5.7.4 the effect of a varying turbulent intensity, see figure 32. This will not be repeated here.

The parameter study of model #3 will uncover the effect of a changing Hamaker constant, which is related to the surface energy through equation (4.1), the packing fraction and the separation distance.

In the original paper these values were set equal to $2 \cdot 10^{-19}\,\text{J}$, 0.25 and $5.5 \cdot 10^{-9}\,\text{m}$, respectively. The Hamaker constant is for most solids and liquids between $(0.4 - 4) \cdot 10^{-19}\,\text{J}$ (Ziskind, 2006) and the separation distance is a parameter which varies greatly between different materials. The packing fraction is the total volume of the aggregate divided by the

combined volume of the primary particles. The packing fraction may be understood as an aggregate density.

All the other parameters will be held constant during the simulation study. The tube diameter is set to 10cm; this simulates a realistic tube flow. The primary particle diameter is set to 10μm and held constant. The remaining parameters are equals those given in the paper (Theerachaisupakij et al., 2003).The turbulent intensity is 10%.

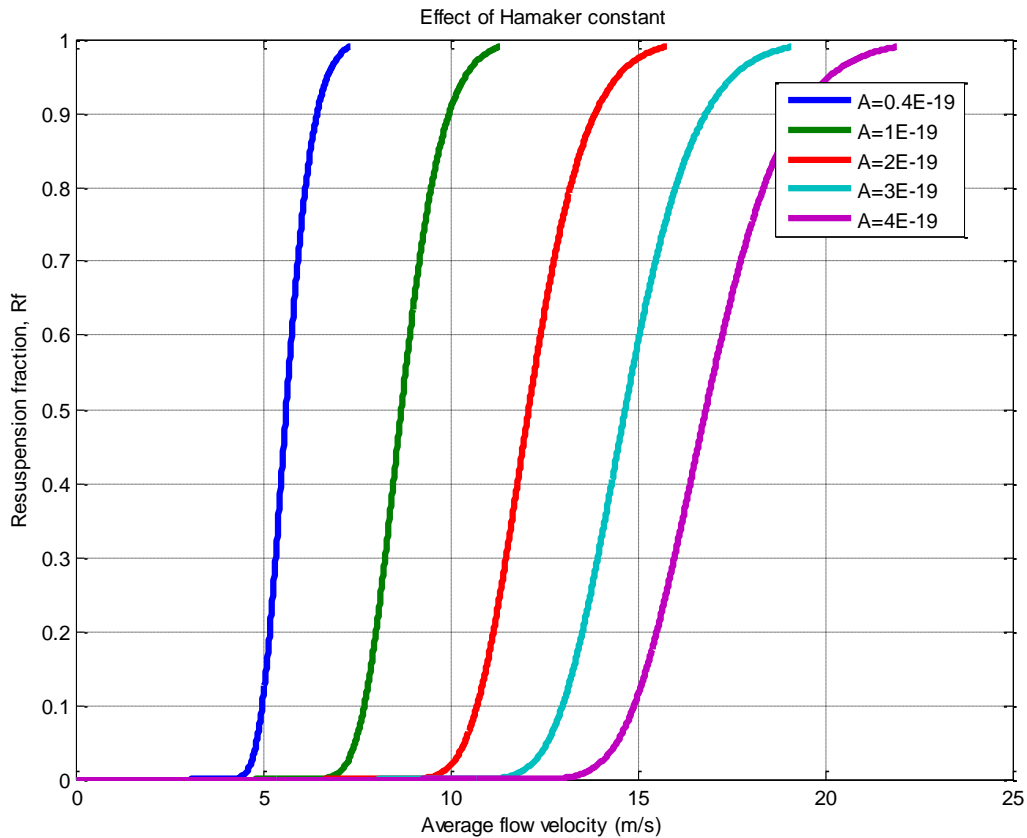### 7.3.1. EFFECT OF HAMAKER CONSTANT

FIGURE 36-RESUSPENSION FRACTION FOR DIFFERENT HAMAKER CONSTANTS

The critical average flow velocities, at which the resuspension fraction equals 0.5, are given in Table 21.

TABLE 21-PARAMETER STUDY EFFECT OF HAMAKER CONSTANTS

Hamaker constant (J)	Average flow velocity (m/s)
0.4E-19	5.62
1.0E-19	8.69
2.0E-19	12.09

3.0E-19	14.67
4.0E-19	16.82
ω	5.7

A sensitivity of 5.7 is quite near the sensitivity observed for the surface energy observed during the parameter study of model #1.

7.3.2. EFFECT OF SEPARATION DISTANCE

The effect of separation distance is such that the required flow velocity increases sharply as the distance decreases. The standard separation distance given in the paper by Theerachaisupakij (2003) is 5.5nm. By putting this distance to 2nm the required fluid velocity increases with the factor of 2. See table below.

TABLE 22-PARAMETER STUDY EFFECT OF SEPARATION DISTANCE

Separation distances (nm)	Average flow velocity (m/s)
2.0	31.68
3.0	21.53
4.0	16.37
5.0	13.23
6.0	11.12
ω	11.99

A sensitivity of 11.99 is the highest observed sensitivity during the parameter study.

7.3.2.1. COMMENTS ON THE SEPARATION DISTANCE

The separation distances above are in the nanometer-magnitude, which is too big for real situations. Theerachaisupakij et.al. (2003) write that their standard separation distance of 5.5nm is the *effective* separation distance without any further explanation for what that means. This is the background for the selected interval in Table 22.

Table 22 indicates that a decreasing separation distance gives a higher required free stream velocity; the reason is that the adhesion forces, or the Van der Waals forces, decrease with the separation distance squared (Ziskind, 2006). Hence a small separation distance implies that the aggregate sticks better. To illustrate the importance of the separation distances, two very small distances were selected of respectively 8Å (ångström) and 4Å, and tested

with model #3. 1Å is equivalent to 0.1nm, or 10^{-10}m. These separation distances required an average free stream velocity of 75m/s and 147m/s, respectively.

Real separation distances are in the range of about 5Å (Næss, 2011), one order of magnitude less than the separation distances regarded in the parameter study, so the unanswered question is what *"effective separation distance"* means? One possibility lies in the fact that the attached particle is not a sphere, but an aggregate. This yields that 2, 3 or maybe 4 primary particles are actually in contact with the surface – with a separation distance in the order of 5Å, while the other primary particles are not in touch with the surface. However, the aggregate are usually bigger than these primary particles alone and thus the *effective* adhesion force is less than the hydrodynamic length indicates. The writer has not been able to investigate this issue in full, so in future studies further investigations regarding the separation distance is suggested.

7.3.3. EFFECT OF PACKING FRACTION

Increasing packing fraction decreases the velocity, as seen in Table 23. The velocity doesn't change significantly however, and a sensitivity of 1.62 is observed. The packing fraction is sort of a constant property for a specific material once it is compressed together, thus it is reasonable to assume that the packing fraction is relatively constant.

TABLE 23-PARAMETER STUDY EFFECT OF PACKING FRACTION

Packing fraction	Average flow velocity (m/s)
0.10	13.57
0.25	12.09
0.50	11.47
0.75	11.25
1.00	11.13
ω	1.62

This leads to a sensitivity of 1.62.

7.4. COMMENTS ON THE PARAMETER STUDY

The parameter study supports the statement in the beginning of this chapter: The sensitivity is dependent on the initial value of the whole system. Take the radius for instance; a 4μ-target particle has a sensitivity of 9.4 towards the radius of the incoming particle, while the sensitivity for a 16μ-target particle is only 3.0.

Regarding the mechanical constants for both the surface and particles, a sensitivity of 0.3 and 0.16 was observed.

The parameter study for model #2 reveals that the velocity angle, θ, gave a sensitivity of 0.02 for the minimum threshold velocity. Further the effect of impaction angle, ϕ, was observed to be limited too. The threshold velocity plotted against the impaction angle gave what is known as bucket-graphs with small changes over a wide range of possible angles.

The Hamaker constant illustrated its importance during the parameter study of model #3, where the required average flow velocity increased from 5.6 m/s to 16.8 m/s by changing the constant from $0.4 \cdot 10^{-19}$ J to $4 \cdot 10^{-19}$ J. This range was chosen because it is the Hamaker-interval at which most fluids and solids are. The sensitivity regarding the Hamaker constant was 5.7.

The separation distance showed great importance. This parameter, which is the distance between two bodies in contact, was studied in the range of 2nm to 6nm. The average flow velocity required for resuspension fell from 31.7m/s to 11.1 m/s during this interval. This gives a sensitivity of 11.99, the highest reported in this parameter study.

7.5. CONCLUSIONS PARAMETER STUDY

This parameter study has revealed the effect of the parameters studied. The sensitivity which is calculated for each parameter must not be understood as a universal measure, since it is dependent on the initial values selected prior to each study. The sensitivity tells something about the change in the dependent variable given those initial values. The choice of standard initial values makes it possible to comparing the effect of one parameter to another within the same model. However, caution should be exercised when comparing across models. Further the sensitivity should be used together with the tabulated values of the dependent variable to give a fully picture of the parameter effect.

The most important parameters are radius, separation distance and Hamaker constant. A change in one or more of these parameters will have a dramatic effect on the dependent variable. The separation distance was only studied between 2 and 6nm. Further work should answer if this interval is enough, or if another interval should be investigated. The separation distance used by referred paper for model #3 was 5.5nm, but real separation distances are typically one tenth of this value.

8. EXPERIMENTAL WORK

A wind tunnel was build at the Department of Energy and Process Technology (NTNU) by post.doc. Muyiwa Sam Adaramola and prof Erling Næss, with the purpose to study particulate fouling inside heat exchangers. One of the objectives in this thesis was to participate in this test rig. Due to time delays the fouling experiments was yet to start by the hand in time of thesis, so only the initial phase of the test rig was studied by the writer.

Before the upstart of the test rig no information about the flow rate or flow velocities at different fan speeds were known, and needed to be examined. The working fluid was ambient air sucked from outside, through a heating battery (capable of heating the air up to 400˚C), through the tunnel section and released through a chimney. The flow rate was measured by an orifice plate and a u-tube manometer, and compared with a grid-mapping by a pitot tube.

Two different orifice plates were tested, with opening of 75mm and 100mm. The first test was 75mm which lead to too high pressure drops, and thereby low velocities, hence the larger 100mm plate was installed. The pressure drop decreased and allowed a higher velocity through the tunnel section. The latter is important in order to resuspend attached particles, either by hydrodynamic drag or particle collision.

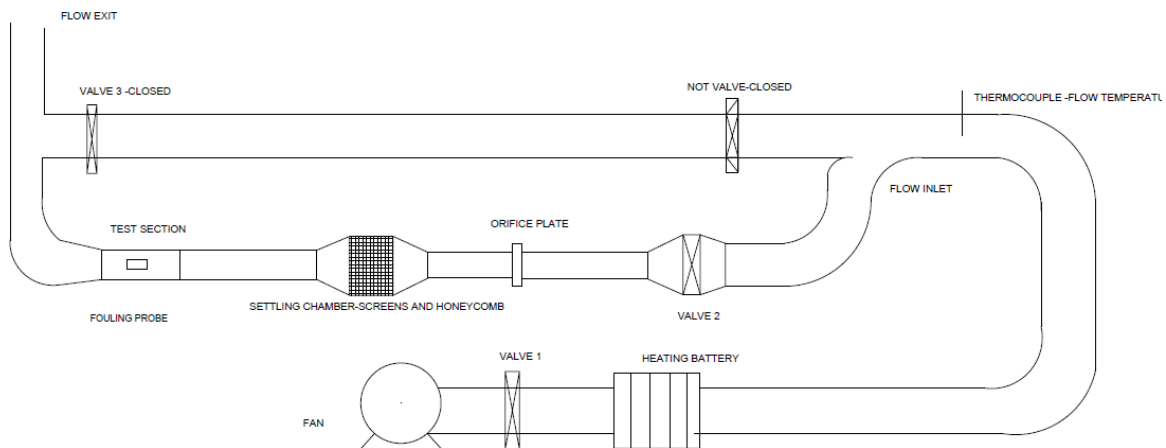## 8.1.   THE WIND TUNNEL AND THE EXPERIMENTAL PROCEDURE

FIGURE 37-FLOW DIAGRAM WIND TUNNEL (NÆSS, 2011)

The main focus will be on the test section (where the pitot tube was placed), control speed of the fan (controlled by an external computer) and the orifice plate, with the u-tube manometer. The ambient temperature was monitored by an external thermometer in the laboratory.

89

When mapping the grid-velocities the fan speed was set to 2000RPM regardless of the opening diameter of the orifice plate. And when measuring the free stream velocity the fan speed was set to 750RPM and increased to 2500RPM in a 250RPM-stepwise procedure. Then the speed was reduced, stepwise again, to validate the measurements. No significant differences were observed.

The flow rate was calculated by the u-tube manometer and by integrating the grid-velocity over the tunnel section.

8.1.1. PITOT TUBE

The local velocity was measured by a pitot (static) tube. The working principle of the pitot tube is assumed known for the reader, otherwise a solid description is available in the literature (White, 2011b). The pitot tube measures the difference between static and total pressure, the latter being the static pressure plus the dynamic pressure. By subtracting these, the dynamic pressure is available through reading from a liquid column. The column was tilted so the effective gravity was reduced by 1/10, making the reading more accurate.

The local velocity is then given by

$$u = \sqrt{\frac{gH}{5}\frac{\rho_{pitot}}{\rho_{air}}}$$

(8.1)

Where g (m/s^2) is the gravity constant, H (m) is the reading and ρ is the density. The pitot fluid was denatured alcohol (Norwegian: rødsprit) with density 800 kg/m^3.

The air density was calculated by the ideal gas law

$$\rho_{air} = \frac{p_{ambient}}{RT}$$

(8.2)

Where R is the gas constant, 286.9 J/kgK for air, and T is the absolute temperature in Kelvin.

8.1.2. THE ORIFICE PLATE

The orifice plate is inserted into the wind tunnel in order to measure the volumetric flow. The working principle is that the plate forces a pressure drop which depends on the flow rate. This pressure drop is measured by a u-tube manometer water column, and back-calculations give the flow rate.

The plate is simply a blocking in the tunnel with a known opening diameter. The ratio $\beta = d_2 / d_1$ is a key parameter in the calculations. d_1 and d_2 is the diameter of the channel and opening hole of the orifice plate, respectively.

The flow rate is given by (White, 2011b)

$$Q = CA_2 \sqrt{\frac{2\Delta p}{\rho_{air}(1-\beta^4)}} \qquad (8.3)$$

Where C is the discharge coefficient which accounts for losses, Δp is the reading from the u-tube manometer, A_2 is the area of the opening diameter and ρ_{air} is calculated by equation (8.2). The discharge coefficient generally depends on both the diameter ratio β and the Reynolds number, but 0.6 could be chosen as a standard value (EngineeringToolbox, 2011).

8.2.   VELOCITY PLOTS

Below the contour plots of the velocities for different orifice plates and positions are given. The contour plots are generated with MATLAB based on the velocity grid mapping done with the pitot tube. The plots show that the velocity is well distributed across the channel, meaning that the flow is turbulent. Based on the grid mapping of the velocity the flow rate was calculated and compared to the measurements done by the u-tube manometer, see Table 26 on page 97.

8.2.1. 2000 RPM, 75MM, DOWNSTREAM

Flow field
75mm orifice plate
2000 RPM
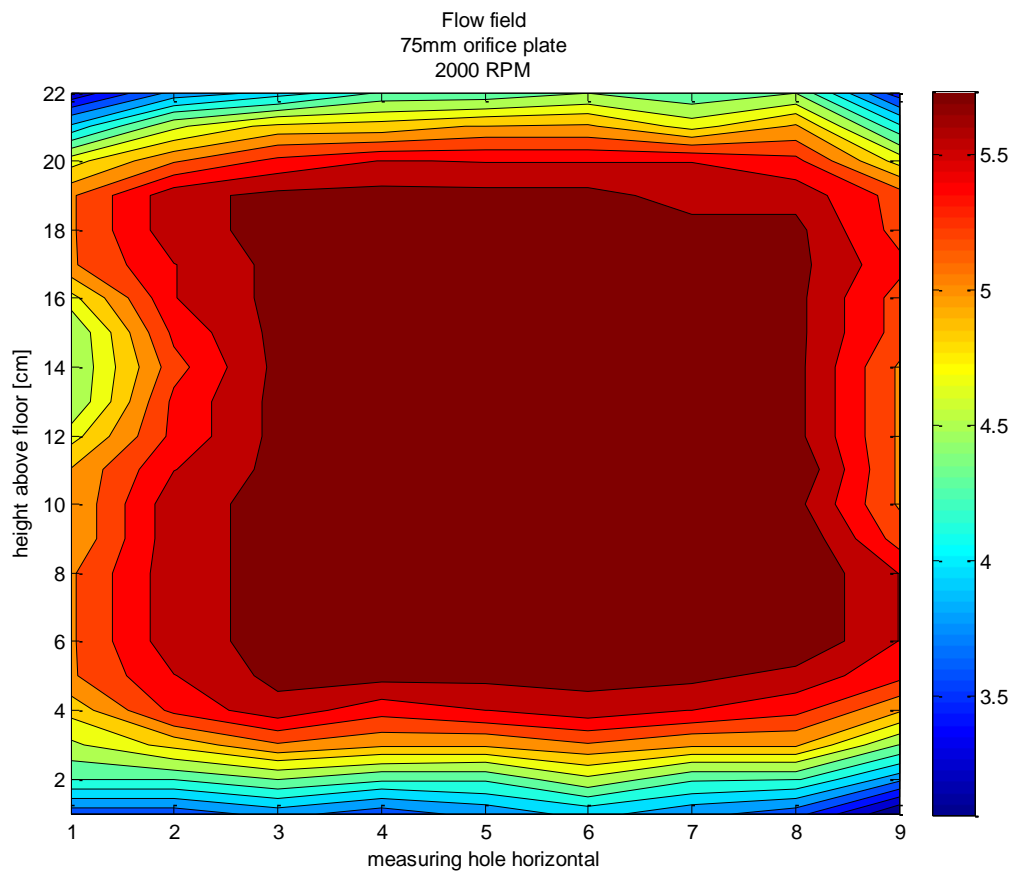
FIGURE 38-VELOCITY PLOT. 2000 RPM, 75MM, DOWNSTREAM

8.2.2. 2000 RPM, 100MM, DOWNSTREAM
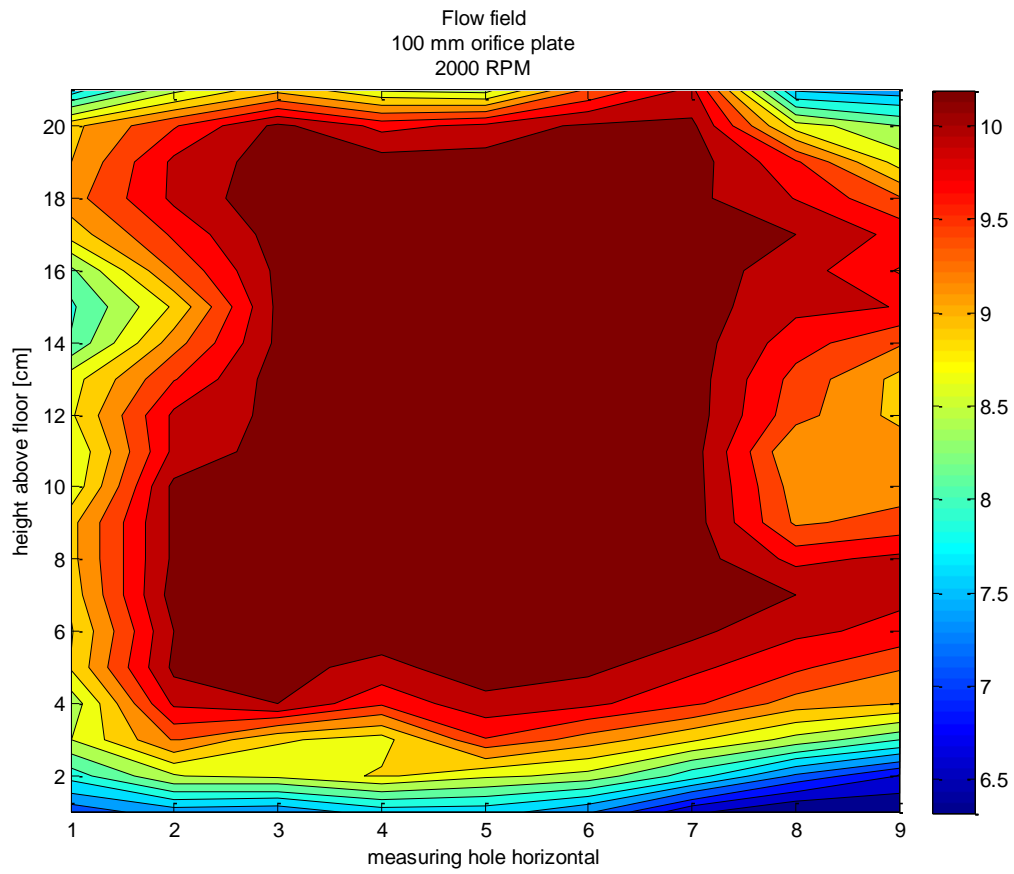
FIGURE 39-VELOCITY PLOT. 2000 RPM, 100MM, DOWNSTREAM

8.2.3. 2000 RPM, 75MM, UPSTREAM

Flow field
75mm orifice plate
2000 RPM
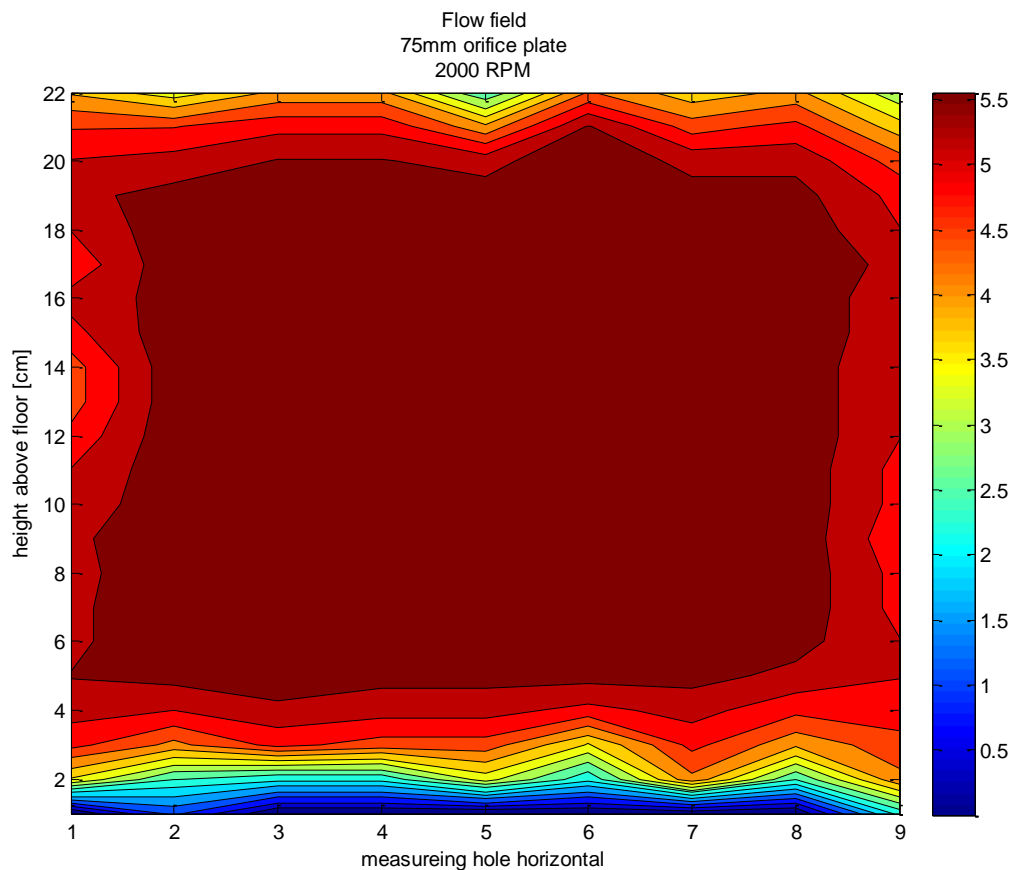
FIGURE 40-VELOCITY PLOT. 2000 RPM, 75MM, UPSTREAM

8.2.4. COMMENTS

There are differences between the three different plots which are worth mentioning. First, the downstream plots show that the boundary layer is more developed than the upstream plot. Upstream the flow field is much more distributed over the whole channel. Second, the near floor region upstream is located in a wake caused by some edge in the wind tunnel. This is no problem regarding the fouling probe further downstream, but some effort should be made to even this edge down. Last, the downstream plots reveal a low velocity area on the left hand side about 14-15 cm above the floor in both the 75mm and 100mm plots. What kind of obstacle which causes this is unknown, and a closer look inside the tunnel is suggested before doing fouling experiments because this area could intrude the fouling probe.

8.3. OPERATING CONDITIONS AT DIFFERENT FAN SPEEDS

During the experiment two different orifice plates were tested; 75mm and 100mm. The effect of these on the flow velocity is illustrated in figure 38 to figure 40. A 100mm-plate gives a lower pressure drop compared to a 75mm plate, and thereby increases the flow speed and volume rates.

8.3.1. FREE STREAM VELOCITY

The velocity was measured in the middle of the channel, i.e. hole nr 5 and about 10cm above the floor. The measured velocities at different fan speeds and orifice plate are as follows

TABLE 24-FREE STREAM VELOCITY AT DIFFERENT FANT SPEEDS

Fan speed	75mm orifice plate Temp/pressure: 20˚C, 1 atm	100mm orifice plate Temp/pressure: 21˚C, 1atm
750	2.28 m/s	3.82 m/s
1000	2.91	5.14
1250	3.87	6.46
1500	4.49	7.60
1750	5.29	8.95
2000	6.09	10.26
2250	6.84	11.50
2500	7.47	12.76
2750	8.26	14.03

8.3.2. FLOW RATE

The flow rate was measured with both the u-tube manometer and calculated by integrating the grid velocity.

TABLE 25-FLOW RATE AT DIFFERENT FAN SPEEDS

Fan speed (RPM)	75mm orifice plate, β=0.375		100mm orifice plate, β=0.5	
	H=X+Y (mm water column)	Q (m^3/s)	H=X+Y (mm water column)	Q (m^3/s)
750	72	0.09	70	0.17
1000	126	0.12	125	0.22
1250	200	0.15	195	0.28
1500	289	0.18	285	0.33
1750	396	0.21	395	0.39
2000	515	0.25	510	0.45
2250	655	0.28	650	0.50
2500	800	0.30	795	0.56
2750	970	0.34	965	0.61

Notice that the water column just happens to be quite equal for both orifice plates. The volume flow is anyway different because both the area in the orifice plate and the beta is different, see equation (8.3).

The way the grid mapping was done was to divide the wind tunnel into 9 vertical and 21 horizontal points, and measure the local velocity at each point. The distance between each vertical point is 2cm, and the distance between the boundary holes and the walls is 3 cm. figure 41 shows the setup.
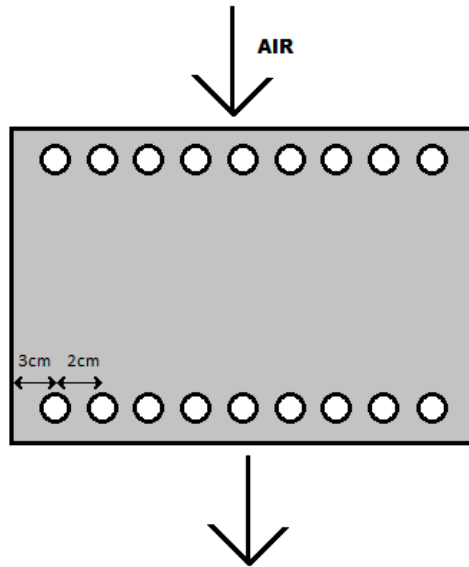
FIGURE 41-DRILLED HOLES IN THE WIND TUNNEL, UPSTREAM AND DOWNSTREAM

Therefore the velocity values of hole number 1 and 9 was multiplied by 4 cm, and the others with 2 cm. The total width of the channels was thereby secured, i.e. 4x2+7x2=22 cm. The pitot tube was lowered 1 cm for each measurement, and therefore each row was multiplied with 1 cm. The volume flows calculated here is for 2000 RPM.

The flow rate calculations based on velocity integration gives

TABLE 26-FLOW RATE BASED ON VELOCITY MAPPING

Fan speed	75mm	100mm
2000	0.253 m^3/s	0.437 m^3/s

The velocity integration and the measurement with the u-tube manometer match remarkably well. A deviation of only 3% is observed for the 100mm orifice plate, and for the 75mm orifice plate they match perfectly.

The fact that two independent measurements give the same value indicates that the results are reliable.

8.4. Sources of uncertainty

Leakages were observed during the experiment, especially when the fan speed was increased above 200RPM and the dynamic pressure inside the channel increased. At 2000RPM, however, the leakages were unnoticeable. The leakages were observed in the corners of the test section. No attempt was done to indicate how much these leakages affected the flow rate.

While moving the pitot tube the clip, which held the pitot tube stable, broke. This forced manually holding of the pitot tube while doing readings. The pitot tube was however remarkably stable, and the angle was checked before each reading. The pitot tube needs to be parallel to the flow, and a deviation of 5˚ or more will give misreading. (White, 2011b) Another source of uncertainty is the metal rod on which the clip was mounted. The rod was marked with cm-interval which was drawn by hand with help of a ruler. During the first measurement, i.e. the "75mm downstream"-measurement, 22 different points in the height direction was possible, while during the second measurement (100mm downstream) only 21 different points were possible. The pitot tube, clip and channel height were the same, so the only possible explanation is that the cm-markings on the metal rod were incorrect.

The atmospheric pressure was just measured once. The mercury barometer was not calibrated, so the decision to use the standard atmospheric pressure was taken. Under normal weather conditions the atmospheric pressure does not deviate more than 1% from the standard atmosphere. The use of 1atm for the pressure does not affect the density significantly.

8.5. FUTURE EXPERIMENTS

As mentioned earlier, the velocity grid mapping and velocity measurements at different fan speed are just the startup experiments for an ongoing labwork regarding particulate fouling and avoidance of such. In the following time further work will take place on this lab setup

First, separate the available particles into size classes. This is important because different mechanisms regarding fouling depends on the size of the particles, e.g. the transport to the wall, adhesion forces (equation (4.5)), collision forces all depend on the size of the particles. The particles could be classified into the following classes:

Class 1 <1μm

Class 2 <20μm

Class 3 <100μm

Class 4 >100μm

The particles could also be classified according to their relaxation time, and then figure 4 on page 8 may become handy. Either way, the big particles should be classified in an own class. The big particles are those who could be inserted into the flow and cause resuspension due their impaction properties; given momentum they are able to penetrate a boundary layer and hit the attached particles underneath. The latter has been pointed out many times throughout this report.

The separation of particles will be done with the help of a particle impactor. The impactor fractionize the particles into classes according to their hydrodynamic characteristics.

FIGURE 42-PARTICLE IMPACTOR. WORKING PRINCIPLE
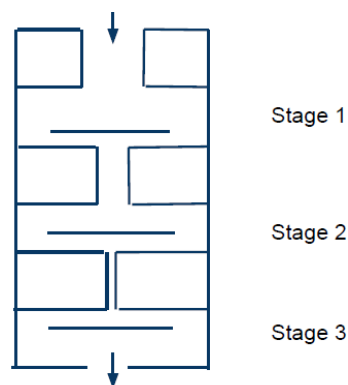
At stage 1 the jet is relative slow and only the biggest particles will escape the flow and hit the collector. This is because the biggest particles have the required inertia to escape the flow. After stage 1 the jet increases in velocity, this gives the particles higher linear momentum than in stage 1, and the next class of particles are able to escape the flow and hit

99

the collector. The sequence is repeated in stage 3. figure 42 only shows 3 stages, but real particle impactors may have additional stages.

Second, after the particles have been introduced into the wind tunnel, the distribution needs to be investigated. A uniform concentration is wishful. To measure the distribution an isokinetic sampling a possible technique. If the velocity into the measuring tube is higher than the free stream velocity, it will suck more particles and measure a higher concentration than the real value. To ensure isokinetic sampling an external pump needs to be installed which controls the suction. A procedure for isokinetic sampling is given in (Temu, 1998).

Third, after the particles are inserted and a uniform distribution ensured, the fouling test may start. The first test could be a qualitative experiment. Different heat exchanger surfaces (tube, flat plate, oval tubes etc.) could be mounted in the wind tunnel and the fouling build-up monitored by photography for different fan speeds and particle concentrations.

Fourth, the effect of thermophoresis needs to be examined; the air needs to be heated and the heat exchangers cooled. One hypothesis is that the fouling rate will increase in the presence of a temperature gradient towards the cold surface. Such increase has been observed in the heat exchanger at Årdal (Næss, 2011)

Last, when the cooled surface is completely covered with particles, the particle concentration could be increased together with the flow velocity. Bigger particles could also be inserted. This way the combined effect of increased shear stress and particle impaction onto a foulded heat exchanger can be tested experimentally. The fouling layer could be measured with the heat flux or more qualitatively by photography. Another way is to measure the weight of the heat exchanger before and after the increase in velocity and particle concentration.

9. DISCUSSION

Fouling of heat transfer equipment in general is an issue for industry worldwide, and especially for metallurgical industries particulate fouling is a concern. The technical consequences are reduced heat transfer and increased pressure drop. The direct economical costs are hard to quantify on a global scale, but Temu (1998) suggested that in Britain the direct cost was somewhere between £200 and £500 million in 1978. This estimate is based on energy and production losses, maintenance and capital costs, while indirect costs were not included. This founds the motivation for this thesis.

The reduced heat transfer must be compensated by increased use of external heating and cooling, while the additional pressure drop requires more pumping power. Both result in increased power consumption and increased environmental emissions. For instance in oil refineries worldwide 88 million tons of increased CO_2-emissions is suggested as a reasonable number (Müller-Steinhagen, 2009).

The chapter about turbulent flows is included to support the talk about what forces and mechanisms that are accelerating particles in flows. Small particles (relaxation time less than 1) will follow any streamline with ease, since they lack the required inertia to escape these. Big particles however (relaxation time larger than 10, typically) are able to escape. This is how the hypothesis about particle resuspension by particle impaction came about; big particles which escape the flow may be sent on a collision course towards a fouling layer and, if the velocity, angle and other conditions are fulfilled, resuspend attached particles. One assumption used in the impaction models, is that once the target particle is set into motion, it will resuspend. The only question left is what force is needed to put the target particle into motion.

The answer to what causes particle acceleration is still open, but it seems that the particles need to pick up their momentum from outside the boundary layer *and* that the near wall fluid is not able to accelerate particles, only decelerate them. The same talk reviled that in order for a particle to be accelerated by and simultaneously be able to escape the eddy, the relaxation time of the particle must be in the same range as the relaxation time of the eddy. The diameter of the particles will then have a square root dependency on the diameter of the eddy, see equation(3.11). This is anyway only an order of magnitude-estimates, but it was concluded that the acceleration finds place outside the boundary layer.

The forces which hold a particle attached to a surface were considered in chapter 4. There are two different ways these forces are quantified: through the Hamaker constant or the surface energy. While the Hamaker constant is a fundamental material property which regards the van der Waals forces between molecules (Visser, 1988), the surface energy is a situation dependent property. Both values need to be calculated if bodies of different

materials make contact. The correlations for surface-surface interactions are given in equation (4.3) and (5.22) for the Hamaker constant and surface energy, respectively.

In this thesis the adhesion forces were treated static; given by the particle size and Hamaker constant/surface energy, only. However, in reality, adhesion forces are highly dependent on the surface roughness as well (Ziskind, 2006). The roughness on the other hand, is a random variable across the surface, and then the adhesion force should also be a random variable. This issue is anyway outside the scope of this thesis, but for future particle resuspension-models it should be considered implemented.

Collision theory was first regarded in chapter 5. The only deformation considered in this thesis is the elastic deformation. In an elastic deformation, which not only is reversible, all the energy is recycled when the deformation is reversed. An elastic deformation is then analogous to a perfect spring. In reality few collisions are perfectly elastic, and plastic deformation should be considered also in collision theories. Unfortunately, plastic deformation complicates the mathematics considerably, see for instance (Thornton and Ning, 1998), and the benefit of including plastic deformation in the models considered in this thesis is limited. The big question in this thesis is whether or not an incoming particle is capable of resuspend the target particle, and the answer is governed by factors such as momentum, angle and adhesive properties, not whether or not the deformation is elastic or plastic.

Even though the collisions are assumed elastic in this thesis, energy is lost during the collisions due to adhesive forces. These forces need to be exceeded by the rebound energy of any particle, and if not, the particle will stick. This is why incoming particles must have a higher velocity than a certain threshold velocity.

A energy budget for any collision was given in equation (5.12) and the rebound velocity after the surface energy was subtracted, is given in equation (5.17). These equations are valid for an elastic-adhesive sphere hitting a plane wall. In chapter 5.5.1 the theory was extended to include a collision between two elastic-adhesive spheres. The discussion in chapter 5.5.1 is only valid for so called perpendicular collisions, which are rare situation in heat exchangers. The most plausible place for such collisions is at stagnation points, for instance on the front side of a tube, so this model only covers a fraction of possible collisions.

This required another extension of the model, and so called off center collisions were considered in chapter 5.5.2. Off centre collisions, or oblique collisions, could cause resuspension by rolling. This is contrary to the perpendicular collision which only could resuspend particles by direct lift off. Rolling is initiated whenever the adhesive moment is exceeded by the collision moment generated. The collision moment is a direct consequence of the impulse which stops the incoming particle. The impulse is proportional to the momentum, i.e. velocity times the mass, thus a higher mass or velocity will generate a bigger

collision moment. Again it seems that big particles are the ones which could trigger resuspension by impaction the easiest.

Another observation is that resuspension by rolling is much easier than direct lift off. The threshold velocity which causes lift off was 3.9 m/s while the equivalent threshold velocity for an oblique collision was 0.12 m/s, that is 32 times less. These calculations are based upon the physical data given in John et.al. (1993).

The third and last model implemented considers an aggregate which is hit by a single particle. The reason to look at such collisions is because attached particles often are adhered together as well, as Marshall (2007) pointed out. The downside associated with this model is that the collision is assumed horizontally, and it is not possible to simulate oblique collisions directly. In that case, the model needs to be modified. No such attempt has been done during this thesis, but is suggested as future work.

On the upside this model do illustrates what happens with a newly resuspended aggregate, namely that it could bounce into another attached aggregate. As pointed out numerous times, the rolling is the likeliest resuspension. Rolling will set attached particles into a horizontal movement, and this is exactly analogous to the collision in model #3.

The parameter study in chapter 7 has already been discussed in chapter 7.4. The effect of various parameters was quantified through the sensitivity, but the sensitivity is dependent on the initial values of the particular model, and it is questionable if the sensitivity is comparable across different models as well. Anyway, the parameter study showed that some parameters are more important than others. Among the most significant variables were radius and density of the incoming particle, both these increase the momentum of the particles, and thus the impulse developed in a collision. The Hamaker constant and the separation distance were also significant parameters, both affecting the adhesion force.

Surprisingly the mechanical constants, including the young's modulus and poission ratio, didn't have much effect on the threshold criteria.

The separation distance used in the parameter study was in the range from 2nm to 6nm. This is too big compared to real separation distances which are typically 0,5nm, or 5Å. The separation distance was however discussed comprehensively in chapter 7.3.2 on page 85, so the reader is referred back to that chapter. In future modeling, however, the issue with the separation distance should be investigated further.

The experimental work which was planned to be a part of this thesis was delayed due to different reasons. First, it took a longer period of time to build the wind tunnel than first anticipated. Second, the fouling experiment which of course requires particles was not possible to carry out since the metal particles hadn't arrived the laboratory before hand in.

Even if they had been, the particle impactor was not up and running at the time of writing. So classification of particles was not possible.

A defined task in the problem description is that the writer should participate in the calibration of the test rig, which he did. The operating conditions of the fan speed were examined, and both flow speed and flow rate were documented with a pitot tube and u-tube manometer, respectively. Also, the velocity distribution was examined to make sure that the flow was fully turbulent – which it was, but also to verify that the flow rate was measured correctly with the u-tube manometer. The difference in flow rate between the calculations based on the velocity mapping and u-tube manometer was 3%, in other words the measurements are trustworthy.

During this grid-mapping measurement, some strange areas in the cross section were documented. For instance in the downstream plots (figure 38 and figure 39), a low velocity area is present. These areas should be double-checked before the startup of any fouling experiment since they may interact with the test probe.

10. CONCLUSIONS

A literature study has been performed with emphasis on models for particle removal by impaction; the studied models are presented in chapter 6. Both qualitative experiments and quantitative studies have been inspected.

The model by Abd-Elhady (chapter 6.6) was considered too complicated for MATLAB implementation, but experimental data by the same researcher (chapter 6.6.4.) indicates that if a copper particle of 54μm hits a powdery with a velocity of 0.6m/s or higher it will, not only rebounce, but resuspend at least 1 other particle.

The three models which were implemented (chapter 7) were quite simple and easy to implement. However, they cover a broad range of possible collisions; perpendicular, oblique to horizontal collisions. One of the objectives of this thesis was to gain knowledge about the requirements behind a resuspension caused by impacting particles. This objective has been fulfilled by the literature and parameter study (chapter 8), where different parameters and their effect on the threshold velocities was studied. It is hard to draw general conclusions from the parameter study since it considered specific particle properties. A perpendicular collision needs a velocity of about 10 m/s if $R_1 = 1\mu m$ and $R_2 = 4\mu m$, but this threshold velocity decreases sharply with the incoming particle's size. It also decreases if the target particle is bigger and the relative size of the hitting particle still is 25% of the target size. An oblique collision has lower threshold velocities because of the different resuspension mechanism; a perpendicular collision resuspend particles by direct liftoff, while an oblique collision only has to exceed the adhesion moment. It is difficult to quantify the ratio between these two resuspension mechanisms because it depends on size, material and impaction and velocity angles (see chapter 8.2), but the ratio could be as high as 1-2 orders of magnitude, i.e. a factor 10-100.

Note that the threshold velocity refers to the required velocity upon impact, not the free stream velocity. Model #3 does however relate the criteria to the free stream, but it does so by assuming a linear velocity profile close to the wall. This is okay for average values, but instantaneous velocity profiles are not necessarily linear when regarding turbulent flows.

Even though all the reported threshold velocities and resuspension criteria in this thesis only apply for the underlying simulations, and not in general, the study can together with the model presentation and MATLAB-implementations, be helpful to predict how particles of other material and sizes will behave.

From the parameter study it is worth mentioning that the particle size, density and surface energy are all important parameters which affect the threshold velocity significantly. The separation distance has already been discussed comprehensively both in chapter 8.3.2. and in the discussion, and in future modeling some attention should be earmarked to this

parameter. Statistical turbulence was also implemented in model #3 by the author, and the results from this exercise were successful; due to turbulent intensity, resuspension started below the required threshold value. For instance, if the intensity was 40% then 2 out of 10 collision would cause resuspension even though the average velocity was 75% of the required threshold velocity. It is therefore concluded that high turbulent intensity is beneficial and helps cleaning the heat transfer surface.

None of the models have been retested experimentally, but in their accompanying journal papers some experimental results are given. Although the reported experiments deviate slightly from the calculations, they are all in agreement.

The thesis has also presented a short discussion about which fluid movements that are capable of accelerate particles transverse to the main flow, e.g. towards the walls in a tube. In general the eddies must be bigger than the particle size, otherwise they lack the required momentum to accelerate the particle. Equation (3.11) gives a square root dependency between the particle and eddy diameter. The particle cannot be too small either, because then it won't escape the eddy. Chapter 4.5 argues that the Stokes number must be about 1 in order to secure both acceleration and particle escape; i.e. the relaxation time of the particle must equal the relaxation time of the eddy. The discussion in chapter 4.5 concludes that the only place particle acceleration can happen is outside the boundary layer.

11. FURTHER STUDY

Suggestions for further studies and work have been mentioned throughout the thesis, the most important, in the writer's opinion, will be repeated here.

- Only elastic deformations have been considered in this thesis. Real particles will however undergo plastic deformation if the forces applied exceed the material yield stresses. This is obviously important for spherical particles since after such deformation, they will be nonspherical. And previous studies have shown that nonspherical particles behave differently regarding deposition and resuspension (Hammersgård, 2011).

- The three models implemented consider perpendicular/vertical, oblique and horizontal collisions. A coherent model should be developed which considers all these different collisions. This model should also consider particle collision with a powdery layer. The simulation code by Abd-Elhady is potentially useful in that matter. His theory is however quite sophisticated and requires high computational time. To do such collision-simulation on a personal computer is a time consuming task, and external CPU-time should be considered.

- Turbulence seems to affect the resuspension, see chapter 6.7.4. Higher turbulent intensity will cause resuspension at lower velocities than low-turbulent flows do. The statistical description of turbulent flows presented and implemented in model #3 in chapter 6.7. is very simple, and in future modeling more accurate procedures should be considered. Data acquisition from Direct numerical simulations (DNS) or Large eddy simulation (LES) could be fed into the turbulent model in order to predict the randomness related to the instantaneous velocity distribution.

- In this thesis, and many journal papers cited here, a particle is assumed to resuspend whenever it starts to move. The assumption is that when particle motion starts the contact area shrinks, and thereby the adhesion moment is reduced. Closer investigation is suggested to verify this assumption. Such investigation could also revile if particles re-settle after resuspension, and if so, more effort should be focused on preventing this re-settling.

APPENDIX 1 – THRESHOLD VELOCITY FOR DIFFERENT SIZE PARTICLES

Here equation (5.26) will be derived in details.

$$\frac{1}{2}m_2(V_{2,in}^2 - V_{2,out}^2) = W_S \tag{12.1}$$

Where W_S is the energy lost in the collision due to adhesion forces and surface energy. The reboud velocity is set to zero in order to find the threshold velocity.

The target initial velocity is given by (5.23) which is the velocity just after the incoming particle has rebounded. Inserting into equation (12.1) gives

$$\frac{1}{2}m_2\left(\frac{2m_1}{m_1 + m_2}\right)^2 V_1^2 = W_S \tag{12.2}$$

The bodies are assumed perfect spheres with uniform density, so equation (12.2) can be rewritten into

$$\frac{16\pi}{6}R_2^3\rho_2\left(\frac{R_1^3\rho_1}{R_1^3\rho_1 + R_2^3\rho_2}\right)^2 V_1^2 = W_S \tag{12.3}$$

Where the mass has been substituted with $(4/3)\pi R^3\rho$. Rearranging and solving for V_1

$$V_1^2 = W_S\frac{6}{16\pi}\frac{1}{R_2^3\rho_2}\left(\frac{R_1^3\rho_1 + R_2^3\rho_2}{R_1^3\rho_1}\right)^2 \tag{12.4}$$

Where $W_S = 7.09\left(\frac{\sigma^5 R^4}{E^{*2}}\right)^{1/3}$

$$V_{1T} = 0.92\left(1 + \frac{R_2^3}{R_1^3}\frac{\rho_2}{\rho_1}\right)\left(\frac{\sigma^5}{\rho_2^3 R_2^5 E^{*2}}\right)^{1/6} \tag{12.5}$$

APPENDIX 2 – VORTEX STRETCHING

The vorticity is the curl of the velocity, or

$$\omega = \nabla \times \vec{V} \qquad (12.6)$$

The vortex stretching mechanism is important when it comes to maintaining and produceing vorticity in turbulent flows. The vortex stretching mechanism is not given in the Navier-Stokes equation directly, one needs to take the curl of these equations to uncover the vorticity. Only the left hand side is given here, but this is sufficient to illustrate the vortex stretching

$$\nabla \times \left(\frac{\partial \vec{V}}{\partial t} + \vec{V} \cdot \nabla \vec{V} \right) =$$

$$\frac{\partial \nabla \times \vec{V}}{\partial t} + (\vec{V} \cdot \nabla)(\nabla \times \vec{V}) - (\nabla \times \vec{V}) \cdot \nabla \vec{V} + (\vec{V} \cdot \nabla)(\nabla \times \vec{V}) = \qquad (12.7)$$

$$\frac{\partial \omega}{\partial t} + (\vec{V} \cdot \nabla)\omega + (\vec{V} \cdot \nabla)\omega - \omega \nabla \vec{V}$$

The last term in equation (12.7) is known as the Vortex Stretching term (Pope, 2000). To illustrate that the vorticity is dependent on all three dimensions, let first component (x-component) of the last term reads

$$\left(\frac{\partial w}{\partial y} - \frac{\partial v}{\partial z} \right) \frac{\partial u}{\partial x} + \left(\frac{\partial u}{\partial z} - \frac{\partial w}{\partial x} \right) \frac{\partial u}{\partial y} + \left(\frac{\partial v}{\partial x} - \frac{\partial u}{\partial y} \right) \frac{\partial u}{\partial z} \qquad (12.8)$$

By inspecting (12.8) it comes clear that the vortex stretching is dependent of all dimensions. In other words the turbulence is 3 dimensional and the vorticity can only be maintained by a 3 dimensional flow. Equation (12.8) only shows the first component (x-direction), but the y- and z-component also depends on all three dimensions.
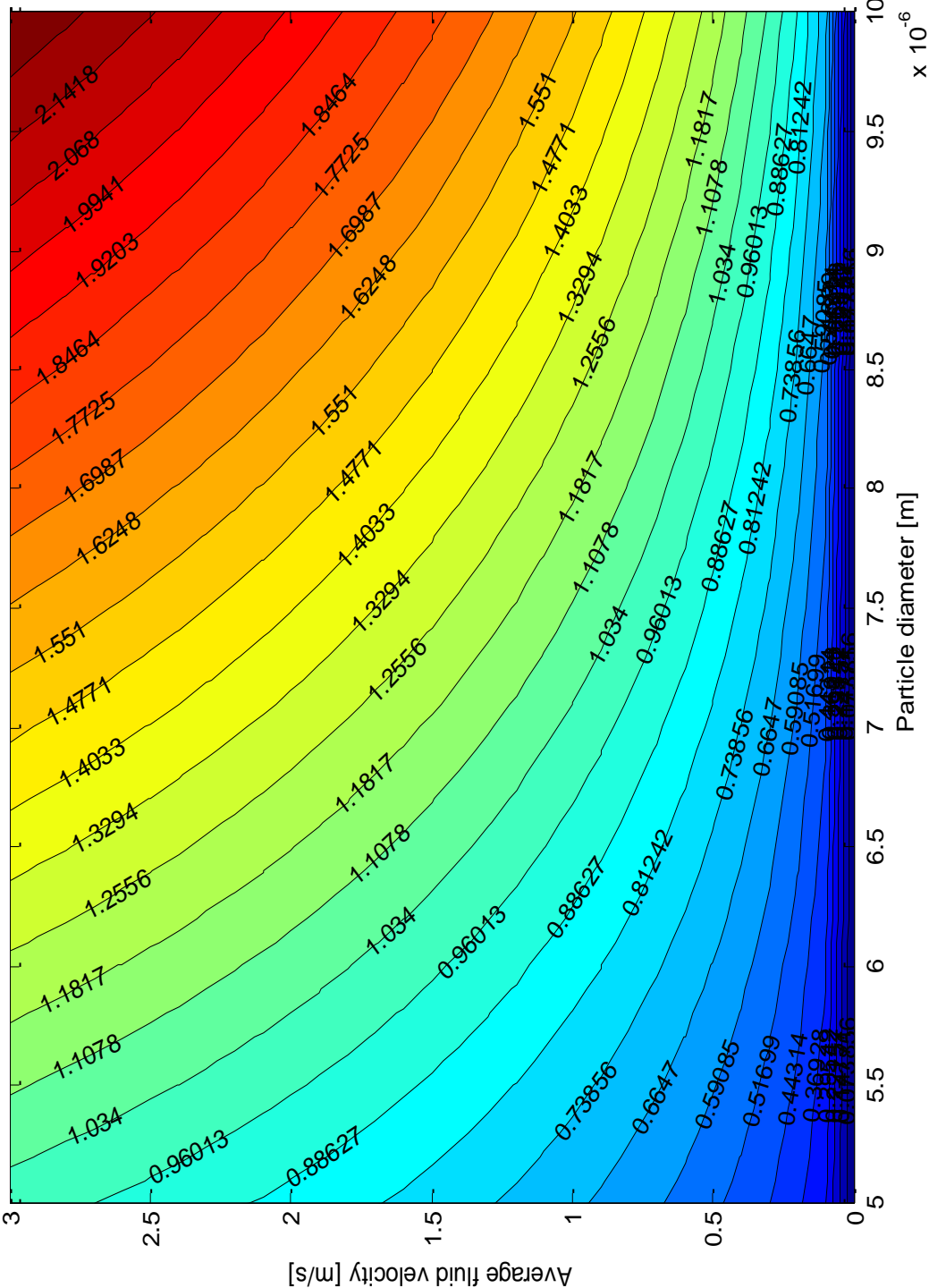
Appendix 4 – Ploting code

```
hold all
% all material properties is put here
VT1 = noslip(rho1,rho2,R1,R2,y,kp,ks,phi,theta);
j=1;

while phi(j)<=180
    phi(j+1)=phi(j)+1;
    if isreal(noslip(rho1,rho2,R1,R2,y,kp,ks,phi(j+1),theta))
        VT1(j+1)=noslip(rho1,rho2,R1,R2,y,kp,ks,phi(j+1),theta);
    else
        VT1(j+1) = NaN;
    end
    j=j+1;
end

plot(phi,VT1)
```

REFERENCES

ABD-ELHADY, M. S., CLEVERS, S. H., ADRIAANS, T. N. G., RINDT, C. C. M., WIJERS, J. G. & VAN STEENHOVEN, A. A. 2007. Influence of sintering on the growth rate of particulate fouling layers. *International Journal of Heat and Mass Transfer,* 50**,** 196-207.

ABD-ELHADY, M. S. & RINDT, C. C. M. 2003. Removal of Particles from a powdery fouled surface due to impaction. *ECI Conference on Heat Exchanger Fouling and Cleaning: Fundamentals and Applications.* Santa Fe.

ABD-ELHADY, M. S., RINDT, C. C. M., WIJERS, J. G. & VAN STEENHOVEN, A. A. 2006. Modelling the impaction of a micron particle with a powdery layer. *Powder Technology,* 168**,** 111-124.

ABD-ELHADY, M. S., RINDT, C. C. M., WIJERS, J. G., VAN STEENHOVEN, A. A., BRAMER, E. A. & VAN DER MEER, T. H. 2004. Minimum gas speed in heat exchangers to avoid particulate fouling. *International Journal of Heat and Mass Transfer,* 47**,** 3943-3955.

ANDERSSON, H. 1988. Turbulence modelling - Lecture notes (not published).

ANDERSSON, H. 2010. Turbulent fluid flow - lecture notes (not published). NTNU.

BEAL, S. K. 1978. Correlations for the sticking probability and erosion of particles. *Journal of Aerosol Science,* 9**,** 455-461.

BIASI, L., DE LOS REYES, A., REEKS, M. W. & DE SANTI, G. F. 2001. Use of a simple model for the interpretation of experimental data on particle resuspension in turbulent flows. *Journal of Aerosol Science,* 32**,** 1175-1200.

BOTT, T. R. 1994. *Fouling of Heat Exchangers*, Elsevier Science.

EAMES, I. & DALZIEL, S. B. 2000. Dust resuspension by the flow around an impacting sphere. *Journal of Fluid Mechanics,* 403**,** 305-328.

EINSTEIN, A. 1956. *The Theory of Brownian Movement,* New York, Dover.

ENGINEERINGTOOLBOX. 2011. *Orificle nozzle venturi* [Online]. Available: http://www.engineeringtoolbox.com/orifice-nozzle-venturi-d_590.html [Accessed 8. june 2011].

EPSTEIN, N. 1983. Thinking about Heat Transfer Fouling: A 5x5 matrix. *Heat Transfer Engineering,* 4**,** 43-55.

EPSTEIN, N. 1988. Particulate fouling of heat transfer surfaces: mechanisms and models. *In:* MELO, L. F. (ed.) *Fouling Science and Technology.*

ERTESVÅG, I. S. 2000. *Turbulent strøyming og forbrenning: frå turbulensteori til ingeniørverkty,* Trondheim, Tapir akademisk forl.

GOLFWRX.COM. 2011. Available: http://www.golfwrx.com/forums/uploads/monthly_07_2009/post-28008-1247591563-1_thumb.jpg [Accessed].

GUHA, A. 2008. Transport and deposition of particles in turbulent and laminar flow.

HAMMERSGÅRD, A. 2011. Mechanisms of Particle Deposition and Removal (Not published). NTNU.

HAUGEN, N. E. 2011. *RE: Personlig samtale under veiledning, SINTEF.*

HINZE, J. O. 1975. *Turbulence,* New York, McGraw-Hill.

IBRAHIM, A. H., DUNN, P. F. & BRACH, R. M. 2003. Microparticle detachment from surfaces exposed to turbulent air flow: controlled experiments and modeling. *Journal of Aerosol Science,* 34**,** 765-782.

JOHN, W., FRITTER, D. N. & WINKLMAYR, W. 1991. Resuspension induced by impacting particles. *Journal of Aerosol Science,* 22**,** 723-736.

JOHN, W. & SETHI, V. 1993. Threshold for resuspension by particle impaction. *Aerosol Science and Technology,* 19**,** 69-79.

KIM, J., MOIN, P. & MOSER, R. 1987. Turbulence statistics in fully developed channel flow at low Reynolds number. *Journal of Fluid Mechanics,* 177**,** 133-166.

KLAREN D.G. 2005. Cost savings for 'zero-fouling' crude oil preheaters. *Hydrocarbon processing,* 84**,** 6.

KLEBANOFF, P. S. 1955. Characteristics of turbulence in a boundary layer with zero pressure. NACA.

MARSHALL, J. S. 2007. Particle aggregation and capture by walls in a particulate aerosol channel flow. *Journal of Aerosol Science,* 38**,** 333-351.

MIT OPEN COURSEWARE 2008. Transport Processes in the Environment.

MÜLLER-STEINHAGEN, H. 2009. Heat Exchangers Fouling: Environmental Impatcs. *Heat Transfer Engineering,* 30.

NATIONALMASTER.COM. *Economy statistics* [Online]. Available: http://www.nationmaster.com/graph/eco_gdp-economy-gdp&date=1978 [Accessed].

NÆSS, E. 2011. *RE: Personlig samtale under veiledning.*

PAPAVERGOS, P. G. & HEDLEY, A. B. 1984. PARTICLE DEPOSITION BEHAVIOR FROM TURBULENT FLOWS. *Chemical Engineering Research & Design,* 62**,** 275-295.

POPE, S. B. 2000. *Turbulent flows,* Cambridge, Cambridge University Press.

STATISTISK SENTRALBYRÅ & KLIMA- OG FORURENSNINGSDIREKTORATET. 2010. Available: http://www.miljostatus.no/no/miljodata/Miljodata/?spraak=NO&dsID=ULKG1&rID=CO2 [Accessed].

TEMU, A. 1998. *Experimental and theoretical study of particle deposition onto a cylinder in cross flow*.

TENNEKES, H. & LUMLEY, J. L. 1972. *A first course in turbulence,* Cambridge, Mass., MIT Press.

THEERACHAISUPAKIJ, W., MATSUSAKA, S., AKASHI, Y. & MASUDA, H. 2003. Reentrainment of deposited particles by drag and aerosol collision. *Journal of Aerosol Science,* 34**,** 261-274.

THORNTON, C. & NING, Z. 1998. A theoretical model for the stick/bounce behaviour of adhesive, elastic- plastic spheres. *Powder Technology,* 99**,** 154-162.

VISSER, J. 1988. Adhesion and Removal of Particles. *In:* MELO, L. F. (ed.) *Fouling Science and Technology.*

WHITE, F. 2011a. *Viscous fluid flow,* New York, McGraw-Hill.

WHITE, F. M. 2006. *Viscous fluid flow,* Boston, McGraw-Hill Higher Education.

WHITE, F. M. 2011b. *Fluid mechanics,* New York, McGraw-Hill.

XU, M. & WILLEKE, K. 1993. Right-angle impaction and rebound of particles. *Journal of Aerosol Science,* 24**,** 19-30.

ZISKIND, G. 2006. Particle resuspension from surfaces: Revisited and re-evaluated. *Reviews in Chemical Engineering,* 22**,** 1-123.